Cyclostratigraphic and lithological characteristics of lacustrine sediments obtained from geophysical downhole measurements and seismic data – Lake Ohrid (North Macedonia/Albania) and Lake Towuti (Indonesia)

Dissertation
zur Erlangung des Doktorgrades
der Naturwissenschaften

vorgelegt beim Fachbereich Geowissenschaften
der Johann Wolfgang Goethe-Universität
in Frankfurt am Main

von
Arne Ulfers
aus München

Frankfurt 2022
(D 30)

vom Fachbereich 11 Geowissenschaften/Geographie der

Johann Wolfgang Goethe - Universität als Dissertation angenommen.

Dekan: Prof. Dr. Jürgen Runge

Gutachter: Prof. Dr. Silke Voigt

Prof. Dr. Andreas Junge

Datum der Disputation: 13.05.2022

TABLE OF CONTENTS

ABSTRACT

As part of two drilling campaigns of the International Continental Scientific Drilling Program (ICDP), several geophysical borehole measurements were carried out by the Leibniz Institute for Applied Geophysics (LIAG) in two lakes. The acquired data was used to answer stratigraphic and paleoclimatic research questions, including the establishment of robust age-depth models and the construction of continuous lithological profiles.

Lake Towuti is located on Sulawesi (Indonesia), within the "Indo-Pacific Warm Pool" (IPWP), a globally important region for atmospheric heat and moisture budgets. The lake exists for approximately one million years, but its exact age is uncertain. We present the first age-depth model for the approximately 100 m continuous sediment sequence from the central part of the lake. The basis for this model is the magnetic susceptibility measured in the borehole and a tephra layer with an age of about 797 ka at 72 m depth. Our age-depth model is inferred from cyclostratigraphic analysis of borehole data and covers a period from 903 ± 11 to 131 ± 67 ka. We suggest that orbital eccentricity and/or changes between global cold and warm periods are responsible for hydroclimatic changes in the IPWP, that these changes affect sedimentation processes in Lake Towuti, and that we can measure and observe this effect in the sediment properties today. Additionally, we created a continuous artificial lithological profile from a series of different borehole data using cluster analysis. This provides information from parts of the borehole where no sediment is available due to core loss.

Lake Ohrid is 1.36 million years old and is located on the Balkan Peninsula on the border between Albania and North Macedonia. The primary hole 'DEEP' in the central part of the lake has been the subject of several investigations, but information about sediments of the marginal locations 'Pestani' and 'Cerava' have not been published yet. In our study, we use natural gamma radiation (GR) measured in the borehole to generate an age-depth model for DEEP. This is performed using the correlation of GR to the global LR04 reference record of Lisiecki and Raymo (2005).

The age information is then transferred via prominent seismic marker horizons to the other two sites, Pestani and Cerava, where it provides the first age-control points for the construction of age-depth models from correlation of GR to LR04. The generated age-depth models are tested using cyclostratigraphic methods, but the limits of this approach are revealed. At DEEP, sedimentation rates (SR) from the cyclostratigraphic method and the correlative approach differ by 2.8 %, at Pestani this difference is 16.7 %, and at Cerava the quality of the data does not allow a reliable evaluation of SR using the cyclostratigraphic approach. We used cluster analysis to construct artificial lithological profiles at all three sites and integrated them into the respective age-depth models. This enables us to determine which sediment types were deposited at what time, and we recognize the change between warm and cold periods in the sediment properties at all three locations. The analyses in this study were all performed on borehole and seismic data and thus do not involve sediment core data. Especially at Pestani and Cerava, new insights into the sedimentological history of Lake Ohrid could be obtained.

In the last part we discuss the occurrence of the half-precession (HP) signal in the European region during the last one million years. The focus is on Lake Ohrid, but a range of other proxies, from the eastern Mediterranean, across the European continent, up to Greenland are analyzed in regards to HP. Applying filters, we focus on the frequency range with a period of 13-8.5 ka and only HP remains in the records. We use correlative methods to determine the clarity of the HP signal in proxies distributed across the European realm. Additionally, we determined the development of HP over time. The HP signal is clearest in the southeast and decreases toward the north. It is further more pronounced in interglacial periods and in the younger part (<621 ka) of most proxies. We suggest that there are mechanisms that transmit the HP signal from its origin near the equator to higher latitudes via different processes. In this context, for instance, the African monsoon, the Nile River and the Mediterranean outflow via the Strait of Gibraltar can be important factors.

ACKNOWLEDGEMENTS

First of all, my special thanks go to Thomas Wonik from the Leibniz Institute of Applied Geophysics (LIAG). He has introduced me to the world of borehole logging and guided me throughout my journey to the present day. He not only provided me with the scientific background, but also backed me up in all aspects that contributed to the success of this dissertation.

Equally, I thank Christian Zeeden. I owe a large part of my understanding of orbital cycles to him. Through his moral support, his creativity and the scientific discussions, the publications in this thesis have improved significantly in quality.

Thomas and Christian proofread this thesis and gave it the final touch. Both of them co-authored all of my publications and without them, this thesis would not have been possible.

My thanks also go to the supervisors at the Goethe University Frankfurt. Both Silke Voigt and Andreas Junge gave me valuable advice regarding the dissertation and especially Silke, as a co-author, motivated me in several phone calls. I am very pleased that they agreed to be my supervisors.

Without measurements, there is no data, and without data, there is no thesis. I am grateful to Thomas Grelle, Jan-Thorsten Blanke and Jens Kuhnisch for collecting the data in the occasionally remotest regions of the world. In this context, I would like to mention Katja Hesse, who patiently explained the principles of downhole logging data processing during my first months at the LIAG.

I would like to express my gratitude to previously unmentioned co-authors. In the Towuti Drilling Project: James M. Russell, Hendrik Vogel and Satria Bijaksana, in the Lake Ohrid project: Bernd Wagner, Sebastian Krastel und Hermann Buness and for the half-precession publication: Mehrdad Sardar Abadi. All of them contributed positively to this dissertation with their input and the constructive discussions.

I would like to thank all colleagues of section S5 "Rock Physics & Borehole Geophysics" and many other members of the LIAG for the friendly and enjoyable working atmosphere in which this thesis could develop. Thanks for all the chats not only on scientific subjects, during lunch breaks, sports breaks, or during several evenings in Hannover.

Finally, I would like to thank my friends and family for their words of encouragement. Especially to my niece and nephew who ‘helped’ me writing this thesis, and to my mother, who always believed in me, remained optimistic and supported me in every situation, whether good or bad.

This study was possible with the financial support of the German Research Foundation (DFG; grant numbers WO672/10-1 and WO672/15-1/2) and with research project funding from the International Continental Scientific Drilling Program.

ABBREVIATIONS

Abbreviation	Meaning	Explanation
BHTV	Borehole Televiewer	Ultrasonic probe imaging the inner wall of a borehole
Cal	Caliper	Diameter of a borehole
Dip	Dip/Inclination	Inclination of the borehole
DLDS	Deep Lakes Drilling System	Assembled barge for drilling operations on lakes
GR	Gamma radiation	Unit is 'gAPI' (= gamma ray unit of the American Petroleum Institute)
HP	Half-precession	Orbital cycle with period of ~12-9 ka
ICDP	International Continental Scientific Drilling Program	
IPWP	Indo-Pacific Warm Pool	Large region in Southeast Asia with warm sea surface temperatures
ka	Kilo-annum	1000 years
LIAG	Leibniz Institute for Applied Geophysics	
Ma	Mega-annum	One million years
mblf	Meters below lake floor	
(M)MS	(Micro)-magnetic susceptibility	Unit is '1E-4SI'
R	Resistivity	Unit is 'Ωm'
Sal	Salinity	Salinity of fluids in a borehole
SBER	Southern Balkan Extensional Regime	Tectonic zone on the Balkan Peninsula
SCOPSCO	Scientific Collaboration on Past Speciation Conditions in Lake Ohrid	ICDP drilling campaign in Lake Ohrid, 2013
SR(s)	Sedimentation rate(s)	Usually in "cm/ka"
TDP	Towuti Drilling Project	ICDP drilling campaign in Lake Towuti, 2015
Temp	Temperature	Temperature in a borehole
Vp	p-wave velocity	Unit is 'm/s'

1. Introduction

1.1 Motivation and scientific goals

Lake environments have received increasing attention in paleoenvironmental studies over the past decades, because they can provide a detailed depiction of the (hydro)climatic evolution in a certain region. Even though the continuous sedimentation of recent lakes rarely extends beyond the Pleistocene, records from lakes are a valuable climate archive (Cohen, 2012; Wilke et al., 2016). Compared to (open) marine environments, sedimentary lake sequences usually exhibit a higher sedimentation rate (SR), which in turn provides high temporal resolution (Melles et al., 2012; Prokopenko et al., 2006; Russell et al., 2020; Stein, 1990). The development of robust age-depth models is essential for the temporal assessment of paleoenvironmental processes sedimentary archives.

The first two publications in this thesis focus primarily on the sedimentological evolution in two lacustrine systems. The investigated lakes are the tropical Lake Towuti on the island of Sulawesi (Indonesia) and Lake Ohrid on the Balkan Peninsula (Albania/North Macedonia).

Both were drilled as part of 'International Continental Scientific Drilling Program' (ICDP). The scientific questions are similar, but the regional setting, the available data and the applied methods are different. The third publication is about half-precession (HP) cycles in Lake Ohrid and their relation to various sedimentary archives in- and around Europe.

Lake Towuti

Did the SR vary over the course of the lake's evolution? To what extent did the SR vary and when did these changes occur? Is there a connection between changes in SR and paleoenvironmental conditions? Is it possible to reconstruct the lithological sequence using geophysical downhole logging data? To answer these questions, it is necessary to first establish a robust age-depth model for Lake Towuti. The presented model is based on the magnetic susceptibility (MS) downhole log from the primary drill site in the central part of the lake, and is anchored to a single tephra layer in the lower part of the borehole. Additionally, a whole suite of geophysical downhole logs is analyzed and a continuous artificial lithology log is created using cluster analysis.

Lake Ohrid

A methodological approach is applied to reconstruct a major part of the sedimentological history of Lake Ohrid. The key question is whether an age-depth model based only on borehole and seismic data can be as accurate as models created from datable core material. Is it possible to use seismic data to transfer age information between the three sites over distances of 5 km and 13 km, respectively? To explain the sedimentary processes at the sites Cerava and Pestani (previously unpublished), is it feasible to use cluster analysis on borehole data and integrate the resulting artificial lithology logs into the age-depth models? The main objective is to precisely determine the age at the main drill site in the central part of the lake using an integrated approach based on geophysical data. The correlation of the downhole gamma radiation (GR) data to the global LR04 benthic stack reference record from Lisiecki and Raymo (2005), in combination with cyclostratigraphic SR estimates, leads to a high quality age-depth model. The next step is to transfer age information via seismic marker horizons to the secondary drill sites and create age-depth models. The integration of the artificial lithology logs allow an initial interpretation of the sedimentological history at both secondary sites Cerava and Pestani. The presented approach can rapidly provide preliminary results on age and sediment type and is particularly useful when datable material is not available.

Half-precession signals in Lake Ohrid and in the European realm

Even though HP is described in several studies, the trans-regional relations of this signal are still poorly understood. The signal appears (to a certain extent) in all examined datasets around Europe, but what are the characteristics and underlying causes for the presence of HP? What are the temporal patterns within one dataset and what are the spatial connections between the datasets? What are the processes that transfer the HP signal between the sites? To address these questions, the HP signal in the records studied must be quantified in order to compare them. Cyclostratigraphic and correlative methods are employed to evaluate the HP signal in each record. Comparison at the European scale indicates a decreasing trend of HP from south to north.

1.2 Orbital forcing

1.2.1 Milanković cycles

Since the description of changes in the Earth's orbital geometry in the 19th century and the discovery of their influence on global climate, lots of progress has been achieved in the field of cyclostratigraphy (Berger, 1988; Hilgen et al., 1995; Hinnov, 2018; Imbrie and Imbrie, 1979; Laskar et al., 2004). The interaction of the astronomical/orbital parameters precession, obliquity and eccentricity are referred to as Milanković cycles (Fig. 1; Milanković, 1941). They are the result of gravitational forces of the planets (eccentricity) and also the Earth-Moon system (precession, eccentricity), and have a direct influence on the quantity and seasonality of insolation the Earth receives, and thus affect climate conditions.

Eccentricity cycles exhibit main periods with 405, 123 and 95 ka, the latter two are often combined to form one 100 or 110 ka component (Fig. 1, top right). Those cycles describe the eccentricity of the Earth's orbit around the Sun and vary between 0 and 0.06 (where 0 would describe a perfect circle). Although the influence of changes in eccentricity on total annual insolation is small (<0.2 %), eccentricity has a direct effect in modulating the amplitude of the precession cycle (Berger, 1988; Imbrie et al., 1993; Weedon, 2003).

Obliquity is described as the tilt of the Earth's rotational axis and has a main period of ~41 ka. The axis is stabilized by gravitational interaction with the moon and varies within 22°-24.5° (Fig. 1, center left; Laskar et al., 1993). The obliquity affects the degree of seasonality, since a greater obliquity causes a higher amplitude of the annual cycle. This effect is strongest at high latitudes (Weedon, 2003).

Precession consists of components with periods between 23-19 ka and is determined by the direction of the tilt of the Earth's rotational axis (Fig. 1, bottom left) and the rotation of the long axis of the Earth's orbit (Weedon, 2003). The effect of precession on seasonal solar insolation is more significant at low latitudes than the effect of obliquity and is of the same order of magnitude in the polar regions (Imbrie et al., 1993).

Even though the periods of orbital cycles change over time, these changes are very slow (Berger et al., 1992; Laskar et al., 2004). In this thesis, only Quaternary sediments are being

considered. For this youngest part of Earth's history, the mentioned changes are negligible and orbital periods are regarded to be constant.

In addition to the main components from Fig. 1, there are harmonics of these orbital cycles. Of particular relevance to this thesis is the HP-cycle, which is a harmonic of the 23-19 ka precession cycles and has a period of 12-9 ka (Berger et al., 1997). The HP signal is assumed to be strongest in the intertropical zone due to the twice-yearly passage of the Sun across the equator (Berger et al., 2006; Short et al., 1991). However, there is still controversy about how HP influences climate and is transferred into geologic records (e.g., De Vleeschouwer et al., 2012; Hinnov et al., 2002).

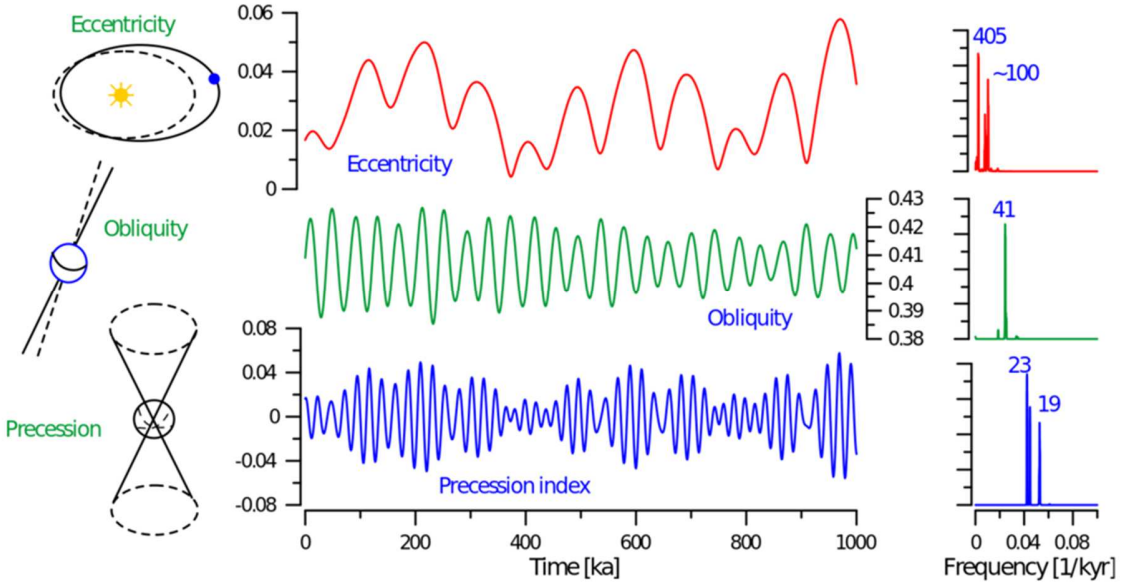

Fig. 1: Geometry of eccentricity, obliquity and precession (left), evolution of orbital parameters over the last 1 Ma in the time-domain (center) and frequency domain (right). The main periodic components are given in thousand years (kyr) in the frequency domain. Figure from cyclostratigraphy.org.

1.2.2 Forcing of sedimentary systems with special emphasis on lake environments

Not only in lake environments, but also in any sedimentary system, several steps affect the process from insolation forcing to the final climatic proxy data (Fig. 2; Meyers, 2017). The change of climate and the sedimentary system are the first responses to insolation and directly affect the deposition. SR may fluctuate, and consequently orbital cycles in the sediment succession will be compressed or stretched out (e.g., Herbert et al., 1994; Meyers

et al., 2001). After deposition, burial and diagenetic processes may modify the nature of the sediments (Meyers, 2017). These include bioturbation, compaction, and the formation or dissolution of minerals (e.g., Anderson, 2001). The latter often depends on the redox state of bottom waters, which (in lakes) is usually controlled by primary productivity and/or lake level fluctuations (e.g., Vuillemin et al., 2016).

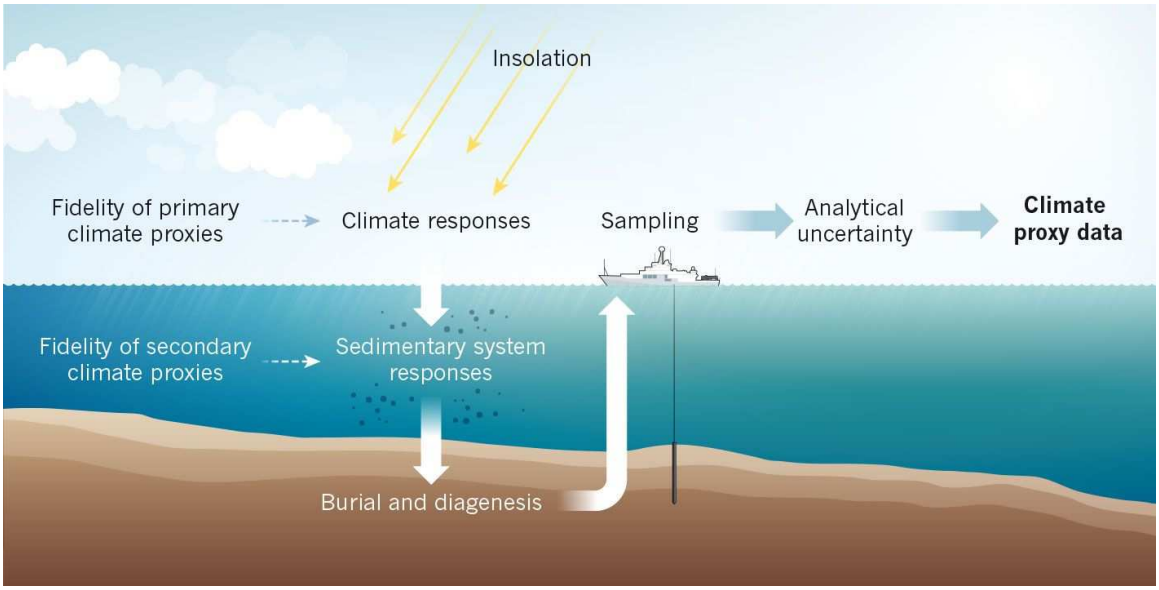

Fig. 2: From insolation to climate proxy data. Note the various factors, which influence the climate proxy data, also after sampling/measurements are completed. From Meyers (2017).

Lake deposits contain material largely derived from the catchment area, and therefore provide a unique perspective on the history of the lake in terms of local paleoclimate conditions (O'Sullivan and Reynolds, 2004; Wilke et al., 2016). Combining paleoecological information from several lake records provides the opportunity to reconstruct continental and global climatic changes (Wilke et al., 2016).

Sedimentation in lakes, unlike in many other depositional systems, is usually rapid and relatively continuous. As a result, lakes are excellent subjects to obtain high-resolution records of climate history (e.g., Cohen, 2012). To cover the longest possible time interval, lakes which are particularly ancient are selected for deep drilling programs. Most of these lakes are located in tectonic basins, or are the result of volcanic activity or a meteorite impact (e.g., Cohen, 2012; Koeberl et al., 2007; Zolitschka et al., 2009).

However, several aspects need to be considered, prior to conducting paleoclimatic investigations in a lacustrine environment and are typically avoided during site selection. All types of gravity induced flows, such as turbidites or slumps, complicate paleoclimatic analyses as they are not part of the pelagic sedimentation and contain (from a geological point of view) no time (Cohen, 2012; Lindhorst et al., 2012). Likewise, (undetected) hiatuses are not ideal in a sedimentary sequence as a certain (often-unknown) piece of the record is missing (Cohen, 2012).

The optimal sedimentary sequence for paleoclimate investigations in lakes extends far back in time, has no hiatuses or slump deposits, and exhibits SR providing high stratigraphic resolution, thus preserving orbital cycles in good quality.

1.3 Principals of geophysical downhole logging

1.3.1 Technical aspects

Usually, borehole measurements are carried out from the bottom to the top of the hole. In unstable formations, such as the mostly unconsolidated lake sediments, the drill pipes are pulled successively and the logging is conducted in open borehole sections of typically several tens of meters in length (exception is GR, see below). This method is more time-consuming than logging the entire open borehole in one run, but it prevents the borehole from collapsing, thus making it inaccessible for further logging or, even worse, probes from being buried. There are several reasons to include borehole logging in (paleoclimatic) drilling projects. Even though downhole geophysical logs do not provide direct access to physical rock/sediment samples, they do provide properties related to porosity, lithology, and the presence and characteristics of fluids (Ellis and Singer, 2007).

As the cable is pulled up the borehole, the depth of the working tool is measured with special equipment (Rider and Kennedy, 2011). Typically, these depth measurements are the most accurate depth data in drilling projects, and composite sediment cores are consequently adjusted to the depth measured from logging. The fact that the drilled holes in lake drilling projects are almost exactly vertical implies that the measured depth is equal to the depth below the sediment surface (thereafter referred to ‘meters below lake floor’ = mblf).

Borehole logging tools are used to measure long intervals within a borehole, which ensures a continuous recording of the sediment properties. Depending on the depth of the borehole and the selected length of the intervals for open hole measurements, only a few intervals have to be spliced together to generate a complete record over the entire depth. Overlap of the individual intervals prevent information from being lost and guarantee continuity. In comparison, sediment core sections are only 1 or 1.5 m in length, which consequently leads to more splice junctions. As this alone is a factor of uncertainty, core sections are often not complete as material is lost during the drilling operation. Conversely, it is possible that the core material expands due to pressure relief and gas release and thus increases in length (e.g., Friese et al., 2017; Lovell et al., 1998; Wagner et al., 2009). Regardless which of these effects occur in the sediment core, the depth measured from the composite core record will not equal the continuity and the depth precision of the logging depth. Downhole logging is often the only information available in areas of reduced core recovery and by extrapolating the lithology from the borehole data, information deficits can be bridged (e.g., Brewer et al., 1998).

In lake drilling projects, the borehole measurements are conducted immediately after drilling. It cannot be avoided that borehole fluids may interact with the borehole wall and affect the physical properties of the sediments/pore fluids in close proximity. The data measured in the borehole are nevertheless collected under the best possible in-situ conditions of the sediments (e.g., Ellis and Singer, 2007; Wonik and Olea, 2007).

In comparison, the drilling process itself and the subsequent pulling out of the hole may already disturb core material. The cores are then transported over long distances and re-stored several times. Due to these processes, for instance, shaking of the samples can change the porosity and in-situ properties are no longer given. However, with regard to the in-situ conditions in the drilled hole, the geometry of the borehole needs to be considered. The washout of certain areas can result in voids and instead of sediment properties, it is mainly the fluid filling the void that is characterized by the downhole tools. Misinterpretations can be avoided by a quality control of the individual logs under consideration of caliper logs.

In comparison, the resolution of core material is much higher (sub-cm investigations are common) than that of downhole logging tools (mostly in the 10-20 cm range; see below).

All the features from this chapter should be considered when interpreting borehole data and the differences to the core material should be taken into account. Downhole logging data can answer many (paleo)geoscientific questions on their own and additionally complement core data. This has been successfully demonstrated in lake drilling projects by Baumgarten et al. (2015) and Baumgarten and Wonik (2015).

1.3.2 Downhole logging properties and probes

The downhole logging tools employed by the Leibniz Institute for Applied Geophysics (LIAG) and relevant for this thesis are listed in Table 1.

The natural GR (including its spectral components U, Th, K) can be measured through the drill pipe. This is why GR is typically measured in one run as the first parameter in a logging campaign. The vertical resolution is determined by the bismuth germinate crystal in the probe, the logging velocity and the formation characteristics. In this case, the used probe has a vertical resolution of 15-20 cm. GR may reflect detrital clastic content, while spectral component ratios (U, Th, K) may provide a more specific indication about different clay mineral types (Quirein et al., 1982; Rider and Kennedy, 2011).

MS is measured in open hole conditions and is dependent on the mineral assemblage of diamagnetic, paramagnetic and ferromagnetic minerals as e.g. magnetite, Fe-oxides or biotite (Buecker et al., 2000; Stage, 1999). The vertical resolution of the probe is ~20 cm. The micro-susceptibility tool (MMS) is used for the same purpose, but its resolution is as low as ~2 cm. MMS measurements are time-consuming and therefore only performed in short intervals of particular interest.

The ‘Dual Laterolog Sonde’ measures resistivity (R) and is sensitive to porosity and texture of the formation in the open hole. The ‘Rshallow’ data is acquired in proximity to the borehole wall and can be affected by fluid/mud intrusion to the formation, while the ‘Rdeep’ has a penetration depth of 30-100 cm (e.g., Buecker et al., 2000; Rider and Kennedy, 2011). The used ‘Dual Laterolog Sonde’ provides a vertical resolution of 10-15 cm.

The acoustic velocity of the p-wave (Vp) is determined in open hole conditions using the sonic tool. Like R, the Vp is sensitive to porosity and texture of the sediments (Buecker et al., 2000). Vp can be used to estimate the porosity of sediments, but this is not always possible in highly unconsolidated sediments such as those found in lacustrine environments (Erickson and Jarrard, 1998). The vertical resolution of the sonic tool is approximately 20 cm.

The borehole diameter (Cal) and the borehole inclination (Dip) are determined with the 'Dipmeter ADIP A21' tool from Antares company. The geometry of the borehole and enhanced caliper can affect all other measured properties and need to be considered when interpreting borehole measurement data.

Acoustic imaging in the open borehole (BHTV) provides a 360° view of the borehole wall. The resolution of this tool is within the mm-scale, but logging is time-consuming and usually only short intervals of particular interest are recorded (Rider and Kennedy, 2011).

The salinity and temperature of the borehole fluid may indicate fluid intrusion from the formation into the hole. The geothermal gradient in lake drilling projects is usually low, since the reached depths are only a few hundred meters.

Table 1: Downhole logging tools used in the lake drilling projects by the LIAG.

Downhole logging tool	**Measured parameter**	**Abbreviation**
Spectral Gamma Ray Sonde SGR 70, Type 1419, Antares	Natural gamma radiation, U-, Th-, K-concentration	GR
Susceptibility Sonde, Type 1108, Antares	Magnetic susceptibility	MS
Dual Laterolog Sonde, Antares	Resistivity (Rdeep & Rshallow)	R
Sonic Sonde, Antares	Acoustic velocity (vp)	Vp
BHTV - FAC40 Televiewer, ALT	Acoustic imaging of borehole-wall	BHTV
Dipmeter ADIP A21, Antares	Caliper, orientation of borehole	Cal; Dip
Micro-susceptibility instrument, Type 1121, Antares	Magnetic susceptibility	MMS
Salinity/temperature Sonde, Antares	Salinity and temperature of borehole fluid	Temp/Sal

1.4 Lake Towuti

1.4.1 Geological and climatic setting

Lake Towuti is located on the island of Sulawesi in the western Pacific near the equator (2.75°S, 121.5°E; Fig. 3). With an elevation of 318 m above sea level, it is the downstream end of the Malili Lake System and is connected by surface outflow to upstream Lakes Matano and Mahalona. The only outlet from Lake Towuti is the Larona River to the west. With a size of 560 km^2, it is the largest lake of the Malili Lake System and has a maximum water depth of 203 m (Haffner et al., 2001; Lehmusluoto et al., 1995; Russell et al., 2020).

Sulawesi is characterized by volcanic and tectonic activity and an entire system of strike-slip faults transects the island (Fig. 3a). The Malili Lake System is between two of those major faults, the Matano, and Lawanopo Fault. Rotational movement and northward drift of eastern Sulawesi result in lateral and vertical motion along the Matano Fault. The (sub)basins formed through this process contain the Malili Lakes (Hall and Wilson, 2000; Hamilton, 1979). Tectonic processes are one factor of uncertainty in paleoenvironmental investigation as they are disconnected from past climatic conditions, but may still influence sedimentation processes in Lake Towuti (Russell et al., 2020).

The region between the Matano and Lawanopo Faults is largely dominated by ophiolites consisting of mafic and ultramafic rocks (Fig. 3a; Kadarusman et al., 2004; Monnier et al., 1995). Such lithology is also characteristic on the small-scale geological map of the area around Lake Towuti (Fig. 3b). The predominant rock types in the direct catchment area of the lake are (un)serpentinized peridodite and undefined ultramafic rock. Only small areas in the southeast and to the north contain limestone and/or metasediments, and some riverbeds contain Quaternary alluvium (Costa et al., 2015). The erosion of this material has a direct influence on sediment composition delivered to the lake. The major part of the sediments derives from the northern Mahalona River, which is merged upstream with the Lampenisu River (Fig. 3b). This material is rich in Mg and serpentine. More felsic material enriched in K, kaolinite, and quartz is from the Loeha River in the east. Smaller rivers in the northeast and southwest supply sediments enriched in Fr, Cr, and Ni, likely derived from topsoil erosion (Goudge et al., 2017; Hasberg et al., 2019; Morlock et al., 2019; Sheppard et al., 2019).

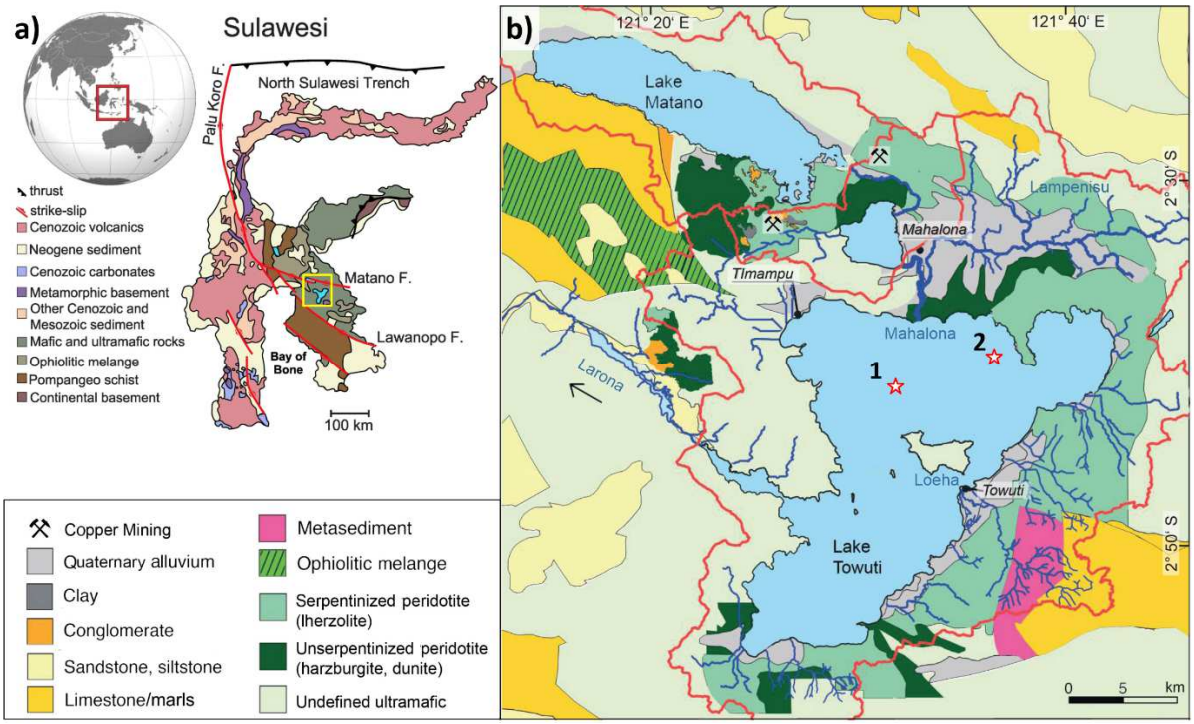

Fig. 3: Setting of Lake Towuti on the island of Sulawesi. **a)** Location of Sulawesi and geologic overview. Several strike-slip faults transect the island. The yellow square highlights the position of the Malili Lake System. On the macro scale, mafic and ultramafic rocks characterize this region. **b)** Geologic map of the Malili Lake System including Lake Matano, Lake Mahalona and Lake Towuti. The only outflow from Lake Towuti is the Larona River towards the west. Red lines around the lakes mark their catchment areas. The major inflow is from the Mahalona River, but several smaller rivers contribute additional water and sediment. Stars indicate drill sites. Figures modified from Costa et al. (2015) and Russell et al. (2020).

The climate on Sulawesi is tropical and humid with an average rainfall of 2700 mm/year at the elevation of Lake Towuti (Hendon, 2003). Temperature and precipitation are largely determined by the Indo-Pacific-Warm Pool (IPWP). It is the largest contiguous area with sea surface temperatures of ~28 °C on Earth, and is therefore a major source of atmospheric heat and moisture (An, 2000; De Deckker, 2016). The size and location of the IPWP is governed by the coupled interactions between the Australian-Indonesian winter and summer monsoons, the El Niño Southern Oscillation and the position of the Intertropical Convergence Zone (Aldrian and Dwi Susanto, 2003; Yan et al., 1992).

1.4.2 The ICDP Towuti Drilling Project

The Towuti Drilling Project (TDP) addresses several interdisciplinary objectives. One of the major goals is to understand environmental and climatic changes with regard to the IPWP over multiple glacial-interglacial cycles during the mid- to late Pleistocene (Russell et al., 2020, 2016).

Several endemic species inherit Lake Towuti. Research also focuses on how geological and environmental changes affect the evolution of these organisms (Stelbrink et al., 2014). A further objective is to examine the geomicrobiological and biogeochemical processes in the metal-rich, ultramafic lake environment (Friese et al., 2021; Vuillemin et al., 2016).

In order to evaluate the potential of Lake Towuti for reaching the main objectives and to identify the most suitable drill sites for the TDP, a series of pre-site surveys was necessary. Between 2007 and 2013, both single channel and multichannel seismic data was recorded on a dense grid across the lake. The seismic data reveal two major sedimentary units. Unit 1 is characterized by horizontally, well-stratified sediments and ranges from the lake bottom to about 100 mblf, Unit 2 varies in thickness between a few tens to about 150 m and consists of discontinuous, sub-parallel layers. Beneath Unit 2 is the basement rock, which is interspersed with numerous faults (Russell and Bijaksana, 2012; Russell et al., 2016). The second part of the pre-site surveys was completed in 2010, when eleven shallow sediment cores (7-19.8 m) were recovered with piston corers. The one located closest to the later main borehole of the deep drilling campaign (Fig. 3b; Site 1) indicates a continuous succession for the last ~60 ka, with a SR of ~5.5 cm/ka. From this short core, responses to global climate variability were inferred, i.e., evidence for drier regional climate conditions during the last glacial maximum as compared to the interglacial periods thereafter or before (Russell et al., 2014; Vogel et al., 2015; Wicaksono et al., 2015).

The ICDP deep drilling campaign of the TDP started in May 2015 at Site 1 in the northern central basin of Lake Towuti (Fig. 3b). Drilling operators deployed an assembled barge, the ICDP 'Deep Lakes Drilling System' (DLDS) and used a drill string with a diameter of 122.6 mm (66 mm core diameter) for drilling. Three coring techniques were employed: Hydraulic piston corer for soft sediments, 'Alien' rotating corer for more resistant lithologies, and 'Extended Nose Corer' which turned out to be a poor choice, as it resulted in major core loss (Russell et al., 2016).

Site 1 is located in the northern central basin. It is the primary hole of the campaign and provides a "master record" of Lake Towuti's history (Fig. 3b). Six holes were drilled at this location to provide a complete composite record. Site 2 is in the deepest part of the lake (~200 m water depth) within the distal area of the Mahalona River (Fig. 3b). The aim is to investigate lake-level

changes and/or major changes in the hydrological connection between Lake Towuti, Mahalona, and Matano. At Site 2, three holes were drilled. Site 3 was originally planned in the southern basin to provide a record unaffected by the Mahalona River. Due to long transit times combined with equipment failures, it was relocated to the west of Site 1. Two holes were drilled at Site 3. The TDP recovered ~1018 m of sediment core in total, with an average core recovery of 91.7 %. The deepest hole is 175 mblf covering the entire sedimentary infill reaching close to the bedrock (Russell et al., 2016; Vogel et al., 2015).

Geophysical downhole logging was conducted by the LIAG. Various sediment/fluid properties were measured in two boreholes from Site 1 and in one from Site 2 using a series of downhole probes. These included natural GR (with the spectral components U, Th, K), MS, R, Vp, Temp/Sal, caliper and dip of the borehole. To avoid borehole collapse, drill pipes were pulled out successively for downhole measurements. Subsequently, the parts of the upper and lower sections were merged to obtain continuous datasets.

1.4.3 Lithology and sediment description

The pre-site seismic surveys have demonstrated that two separate units overlie the basement. Russell et al. (2020) interpret the lithified, mafic conglomerate at the base of the TDP Site 1 to reflect local bedrock.

The sediments of Unit 2 are deposited on top of the bedrock and represent a mixture of lacustrine, fluvial, and terrestrial environments. It is interpreted as a pre-lacustrine facies with the initial stage of subsidence of the Towuti Basin. The grain size of the material reaches from silt to gravel with a clay content of less than 50 %. Most of the succession in Unit 2 is composed of mafic minerals, but there are interspersed layers of felsic material. Since the only source of felsic material is to the east (Fig. 3b), the alternation of these two mineral groups in the sediments suggests motion of the intrabasinal faults. Changes of sediment type due to tectonic activity make it difficult to extract a robust paleoclimate record from Unit 2. The boundary between Unit 2 and overlying Unit 1 delineates the permanent transition to lacustrine conditions and the formation of Lake Towuti (Russell et al., 2020, 2016).

Unit 1 sediments are interpreted as lacustrine facies in a persistent lake environment. The material is fine-grained with clay contents between 60-90 % by volume. Three main litho-types can be classified based on differences in color, structure, siderite, and TOC content: green clays, red sideritic clays, and diatomaceous ooze. The clay types are suggested to reflect climate-induced lake-level fluctuations and mixing of the water body. The diatom layers are indicative for phases of increased primary production. In addition to the main types, several tephra layers and turbidite deposits are found in the Unit 1 sediments. These event layers typically reach only a few centimeters in thickness, but at Site 2, turbidites sourced from the Mahalona River are common and increase in thickness (up to 50 cm). For paleoclimatic investigations, the nearly 100-m-thick Unit 1 at Site 1 provides the best conditions as it is a continuous lacustrine sequence reflecting orbital driven climate change and contains minor amounts of event layers (Costa et al., 2015; Russell et al., 2020, 2016; Ulfers et al., 2021).

1.5 Lake Ohrid

1.5.1 Setting and hydrology of Lake Ohrid

Lake Ohrid is located on the Balkan Peninsula on the border between North Macedonia and Albania (41.0°N, 20.7°E; Fig. 4). It is 693 m above sea level, covers an area of 358 km^2 and has a maximum depth of 293 m. The main outlet of the lake is the river Crni Drim in the north; inflows are the river Sateska in the northeast and the river Cerava in the south. However, it is not rivers but karst springs that contribute the most to the Lake Ohrid's water inflow (Matzinger et al., 2006; Wagner et al., 2014).

Lake Ohrid is situated within the Dinarides-Albanides-Hellenides mountain range, which itself is part of the 'Southern Balkan Extensional Regime' (SBER; Fig. 4). The SBER resulted from a change in the rollback of the Hellenic slap and caused an E-W extension of the southern Balkan region (Fig. 4b). The subsequently formed active graben system is characterized by an alternating sequence of approximately N-S oriented mountain ranges and valleys, of which some accommodate lakes (Fig. 4a; Burchfiel et al., 2008; Hoffmann et al., 2010; Lindhorst et al., 2015). The initial opening of the Ohrid Basin as a pull-apart basin occurred during a transtensional phase in the late Miocene (Burchfiel et al., 2008; Reicherter et al., 2011). The

faults within the lake are considered active faults as they offset the youngest observed strata. The interpretation of the seismic profiles indicates that the Lake Ohrid Basin is still in extension today (Lindhorst et al., 2015).

The relatively plain areas north and south of the lake are mainly composed of Tertiary and Quaternary fluvial deposits. On the lake's sides are mountain ridges with an altitude of up to 2300 m above sea level. The Mokra Mountains in the west consist mostly of Triassic carbonites and Jurassic ophiolite, while the Galičica Mountains in the east are dominated by Triassic carbonates (Fig. 4c; Hoffmann et al., 2010; Jozja and Neziraj, 1998; Reicherter et al., 2011).

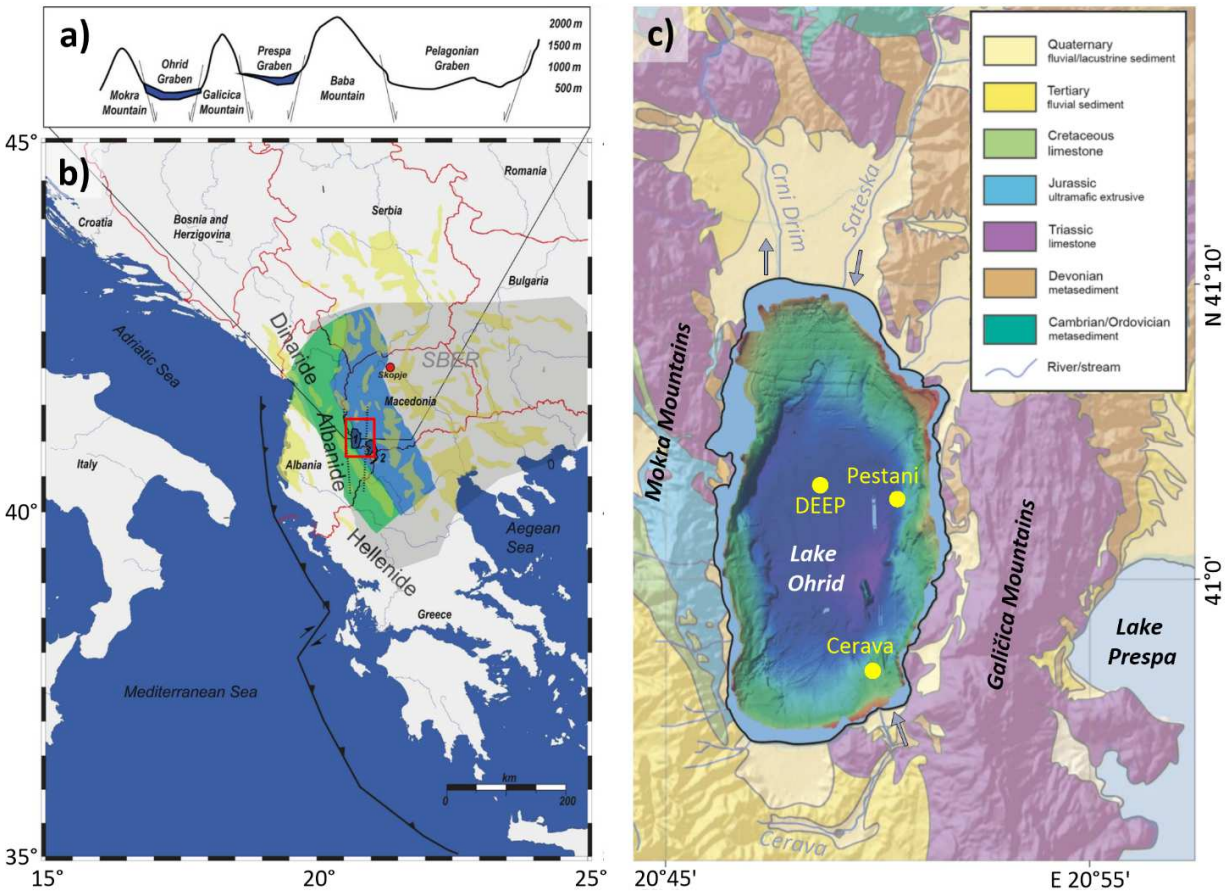

Fig. 4: Location of Lake Ohrid and surrounding geology. **a)** Profile from west to east through the tectonically active graben system with alternating mountain ridges and basins. The Ohrid Basin is the youngest of these basins and is still active today. **b)** Overview of the Balkan Peninsula with the location of Lake Ohrid within Dinarides-Albanides-Hellenides mountain range. Area shaded in grey is the Southern Balkan Extensional Regime (SBER). The content of the red square is detailed in c) and marks the position of Lake Ohrid (modified after Lindhorst et al., 2015). **c)** Bathymetric map of Lake Ohrid and geologic map of the surrounding region. The ICDP drill sites are highlighted in yellow. Main river inflow and outflow are marked by arrows. Note Lake Prespa in higher altitude to the east. Galičica Mountains range consisting of Triassic limestone is separating the lakes, but water flows through a karst system from Lake Prespa into Lake Ohrid (modified from Wagner et al., 2019).

A karst system supplying several sub-lacustrine and surface springs is the main contributor, accounting for about 55 % of the water input to Lake Ohrid. Most of the springs are located on the eastern shore, as the karst water originates via the outflow from Lake Prespa and from precipitation in the Galičica Mountains (Fig. 4c). Lake Prespa is located ~155 m above Lake Ohrid towards the east of the Galičica Mountains and does not have a surface outflow (Matzinger et al., 2006; Wagner et al., 2017). The karst aquifer provides Lake Ohrid with Ca^{2+} and HCO^{3-} ions and filters particulate matter (H. Vogel et al., 2010). The remaining 45 % of the water inflow to Lake Ohrid is from direct precipitation or from river tributaries, of which the river Sateska in the northeast contributes 15 % of the total water inflow. Water leaves Lake Ohrid to 60 % by surface runoff via the river Crni Drim in the north and to 40 % by evaporation (Matzinger et al., 2006; Popovska and Bonacci, 2007).

Due to the location of the lake in a relatively sheltered basin at high altitude and the proximity to the Adriatic Sea, modern climate in the Lake Ohrid area is dominated by both Mediterranean and continental conditions. The region receives the highest amounts of precipitation in winter and the lowest in summer, when conditions are relatively dry. The average annual precipitation amounts to 800-900 mm (Matzinger et al., 2006; Popovska and Bonacci, 2007; Watzin et al., 2002).

1.5.2 The ICDP deep drilling campaign

Several features make Lake Ohrid an excellent location for the successful investigation of various research questions. The 'Scientific Collaboration on Past Speciation Conditions in Lake Ohrid' (SCOPSCO) is centered around four primary objectives: (1) The determination of the absolute age of the lake which includes its early history of and the formation of the Ohrid Basin. (2) Unraveling the regional seismotectonic history, including the effects of major earthquakes and associated mass-wasting events. (3) Obtaining a continuous record of Quaternary volcanic activity and climate change in the central northern Mediterranean. (4) Investigations on how geological events influence the evolution of the numerous endemic species in Lake Ohrid (Wagner et al., 2014).

A number of pre-site surveys was carried out prior to the deep drilling campaign. Between 2004 and 2009 hydro- and seismoacoustic measurements were conducted using different equipment configurations. A grid of multichannel seismic profiles with a length of more than 500 km was collected. Interpretation of these data revealed a thick undisturbed sediment sequence in the central area of the basin. The only problem are strong multiple reflectors which blur the lower part of the sedimentary sequence (Lindhorst et al., 2015, 2012; Wagner et al., 2008).

Simultaneously, short cores were extracted from the upper sediment layers with gravity and piston corers. These include a core with a length of about 10 m from the western part and a core with a length of 1.6 m from the central part of the basin (located close to the later DEEP site). Analyses of those short cores revealed the potential to reproduce climate variability over a long period of time using climate-sensitive proxies in sediments from Lake Ohrid (H. Vogel et al., 2010; Wagner et al., 2010, 2014). Based on the seismic surveys and the short sediment cores, five drill sites were originally planned and ultimately four were drilled. Three of them are relevant for this thesis: the 'DEEP', 'Pestani' and 'Cerava' site.

In March 2013, the ICDP drilling campaign started and by May a total of ~2100 m of sediment cores were drilled from Lake Ohrid. Drilling operations were carried out using the DLDS. All holes were drilled with a diameter of 149 mm and water based mud (Baumgarten et al., 2015; Wagner et al., 2014).

The "DEEP" site is located in the center of the lake at a water depth of 243 m (Fig. 4c). From the pre-site surveys, a continuous, undisturbed, thick sedimentary sequence was expected. Six holes were drilled and a maximum depth of 569 mblf was reached with a composite recovery of 95 %. Preliminary results from the drilling operations found that the upper ~430 m consist of hemipelagic sediments, while sediments below are from a shallow water facies (Wagner et al., 2014).

The "Pestani" site is located on the eastern side of the central basin at a depth of 262 m (Fig. 4c). The objective of this hole was to retrieve the sediments directly above the basement in a depth of about 200 mblf. A single hole was drilled to a depth of 194.5 mblf with a core recovery of 91 %. The preliminary core description shows fine-grained hemipelagic sediments in the

upper ~150 mblf, while below there is coarser-grained material of sandy silt and clay next to one peat layer at ~160 mblf (Wagner et al., 2014).

The "Cerava" site is situated in the southern part of the basin on a lake terrace at a water depth of 125 m (Fig. 4c). The clinoform structures observed by seismic investigations imply lake level fluctuations. Drilling of two holes reached a depth of 90.5 mblf and a composite recovery of 97 %. On-site investigations encountered fine-grained silty clays and clayey silts in the upper 80 mblf, and lithified sediments and shell fragments in the lowermost part (Wagner et al., 2014).
Geophysical borehole logging was conducted by LIAG at all three sites discussed in this thesis. Firstly, the natural GR (with the spectral components U, Th, K), was measured in one run through the drill pipes. The drill pipes were then pulled out successively and the geophysical parameters were measured in open hole conditions at intervals of approximately 40 m. These include MS, R, Vp, Temp/Sal, caliper and dip of the borehole. In addition, vertical seismic profiling was carried out at the DEEP site (Ulfers et al., 2022; Wagner et al., 2014).

The acquired geophysical borehole data are used for paleoenvironmental investigations within the scope of this thesis, e.g. to build an age-depth model and to determine sediment properties (Ulfers et al., 2022).

1.5.3 Sediment description from the DEEP site

Detailed core descriptions of the Pestani and Cerava sites have not yet been published. The existing publications focus primarily on the DEEP site (e.g., Francke et al., 2016; Leicher et al., 2019; Wagner et al., 2019; Wilke et al., 2020). The detailed lithological characterization of the upper ~240 mblf by Francke et al. (2016) describes the clay types of the hemipelagic facies and classifies them into three categories. (1) Calcareous silty clay, which was deposited during interglacial periods, and (2) silty clay during glacial periods. (3) Slightly calcareous silty clay represent a transitional phase between the first two clay types (Fig. 5). The alternation of cold- and warm-climate sediments is reflected in the natural GR, as well as in many other properties (Ulfers et al., 2022; Wagner et al., 2019). An age-depth model for the entire lacustrine sequence of the DEEP site is presented in Wagner et al. (2019). It is based on tephrostratigraphic

correlation of 16 tephra layers, orbital tuning of total organic carbon from sediment core measurements, and two paleomagnetic age reversals.

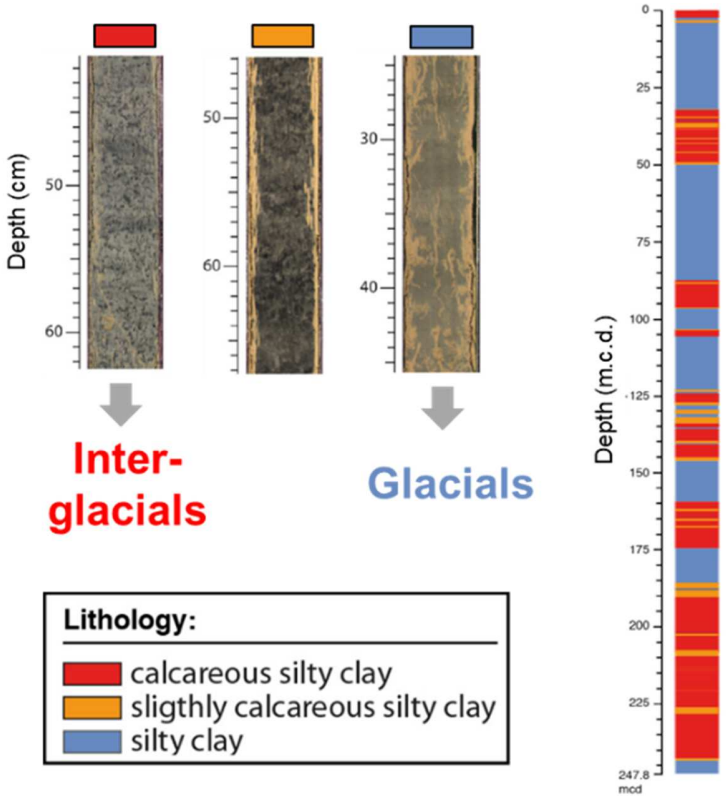

Fig. 5: Sediment characteristics of the main clay types in the hemipelagic facies of Lake Ohrid's DEEP site. The alternation of different clay types reflects cold and warm climate conditions (modified after Francke et al., 2016).

2. Publications

2.1 Peer-reviewed publication (Lake Towuti)

Cyclostratigraphy and paleoenvironmental inference from downhole logging of sediments in tropical Lake Towuti, Indonesia

Ulfers, A., Hesse, K., Zeeden, C., Russell, J.M., Vogel, H., Bijaksana, S., Wonik. T

J Paleolimnol
https://doi.org/10.1007/s10933-020-00171-9

ORIGINAL PAPER

Cyclostratigraphy and paleoenvironmental inference from downhole logging of sediments in tropical Lake Towuti, Indonesia

A. Ulfers · K. Hesse · C. Zeeden · J. M. Russell · H. Vogel · S. Bijaksana · T. Wonik

Received: 19 March 2020 / Accepted: 28 December 2020

Abstract Lake Towuti is located on central Sulawesi/Indonesia, within the Indo Pacific Warm Pool, a globally important region for atmospheric heat and moisture budgets. In 2015 the Towuti Drilling Project recovered more than 1000 m of drill core from the lake, along with downhole geophysical logging data from two drilling sites. The cores constitute the longest continuous lacustrine sediment succession from the Indo Pacific Warm Pool. We combined lithological descriptions with borehole logging data and used multivariate statistics to better understand the cyclic sequence, paleoenvironments, and geochronology of these sediments. Accurate chronologies are crucial to analyze and interpret paleoclimate records. Astronomical tuning can help build age-depth models and fill gaps between age control points. Cyclostratigraphic investigations were conducted on a downhole magnetic susceptibility log from the lacustrine facies (10–98 m below lake floor) from a continuous record of sediments in Lake Towuti. This study provides insights into the sedimentary history of the basin between radiometric ages derived from dating a tephra layer ($\sim$ 797 ka) and C^{14}-ages ($\sim$ 45 ka) in the cores. We derived an age model that spans from late marine isotope stage (MIS) 23 to late MIS 6

Supplementary Information The online version of this article (https://doi.org/10.1007/s10933-020-00171-9) contains supplementary material, which is available to authorized users.

A. Ulfers (✉) · K. Hesse · C. Zeeden · T. Wonik
Leibniz Institute for Applied Geophysics, Stilleweg 2, 30655 Hannover, Germany
e-mail: Arne.Ulfers@leibniz-liag.de

K. Hesse
e-mail: Katja.Hesse@leibniz-liag.de

C. Zeeden
e-mail: Christian.Zeeden@leibniz-liag.de

T. Wonik
e-mail: Thomas.Wonik@leibniz-liag.de

J. M. Russell
Department of Earth, Environmental, and Planetary Sciences, Brown University, Box 1846, Providence, RI 02912, USA
e-mail: James_Russell@brown.edu

H. Vogel
Oeschger Centre for Climate Change Research, Institute of Geological Sciences, University of Bern, Baltzerstrasse 1 + 3, 3012 Bern, Switzerland
e-mail: hendrik.vogel@geo.unibe.ch

S. Bijaksana
Faculty of Mining and Petroleum Engineering, Institut Teknologi Bandung, Bandung 40132, Indonesia
e-mail: satria@fi.itb.ac.id

Published online: 12 February 2021

(903 ± 11 to 131 ± 67 ka). Although uncertainties caused by the relatively short record and the small differences in the physical properties of sediments limited the efficacy of our approach, we suggest that eccentricity cycles and/or global glacial-interglacial climate variability were the main drivers of local variations in hydroclimate in central Indonesia. We generated the first nearly complete age-depth model for the lacustrine facies of Lake Towuti and examined the potential of geophysical downhole logging for time estimation and lithological description. Future lake drilling projects will benefit from this approach, since logging data are available just after the drilling campaign, whereas core descriptions, though more resolved, only become available months to years later.

Keywords Paleoclimate · Geophysical downhole logging · Cyclostratigraphy · Lake Towuti · Indo Pacific Warm Pool

Introduction

Lake Towuti is part of the Malili Lake System in central Sulawesi, Indonesia. It is located within the Indo Pacific Warm Pool (IPWP), one of the most relevant regions for global climate variability on Earth. With sea surface temperatures of ~ 28 °C throughout the year, the IPWP introduces large amounts of heat and moisture into the atmosphere, such that it dominates not only Southeast Asia, but also affects climate on a global scale. The climate (temperature and precipitation) on Sulawesi is the result of interactions between the Australasian monsoons, the El Niño-Southern Oscillation, the Intertropical Convergence Zone (ITCZ), and warm sea surface temperatures (An 2000; De Deckker 2016; Konecky et al. 2016; Wang et al. 2008; Yan et al. 1992). Equatorial regions and the western Pacific had not yet been a focus of "International Continental Scientific Drilling Program" (ICDP) campaigns. One of the main objectives of the "Towuti Drilling Project" (TDP) was to provide a high-resolution record of the tropical western Pacific during the Pleistocene and to understand climate/hydrological and environmental changes in this globally important region. Lake Towuti meets the criteria to address those questions since it is the largest tectonic lake in Southeast Asia and is thought to contain a continuous, undisturbed sediment succession spanning the last ~ 1 Ma (Russell and Bijaksana 2012; Russell et al. 2016).

The TDP is an international research program conducted under the ICDP to understand: (1) long-term climate and environmental change in the tropical western Pacific, (2) impacts of geological and environmental changes on the biological evolution of aquatic taxa, and (3) geomicrobiology and biogeochemistry of metal-rich, ultramafic-hosted lake sediments (Russell et al. 2016). After pre-site surveys between 2007 and 2013, three drill sites were selected using results from seismic surveys and short piston cores (Russell and Bijaksana 2012). To achieve the main objectives, the ICDP drilling campaign was conducted in May–July 2015, using the ICDP Deep Lakes Drilling System (DLDS), operated by DOSECC Exploration Services. A total of ~ 1018 m of sediment core was recovered from three sites, and downhole geophysical logging measurements were obtained from two sites. The longest, undisturbed, lacustrine sediment succession appears in the upper ~ 98 m of Site 1. It consists mainly of two different, well-stratified clay types, and only minor layers of turbidite-like mass movement deposits (MMD) or thin tephra layers. Below 98 m, sediments consist of silts, with layers of peat and sand/gravel, indicating a pre-lacustrine facies. At Site 2, the upper 73 m are characterized by MMD, but below 73 m, the sediments are similar to those in the upper 98 m at Site 1 (Russell et al. 2016).

A robust age-depth model of the sediment succession in Lake Towuti is critical to determine the timing of paleoclimate changes, the rates of biological evolution and biogeochemical cycling in the lake and its sediments. Site 1 meets essential criteria to estimate such models for the complete succession: (1) Radiocarbon dates on 23 samples of organic carbon from short piston cores taken close to Site 1 reveal a maximum age of ~ 45 ka at 9 m below lake floor (mblf) (Russell et al. 2014), (2) one $^{40}Ar/^{39}Ar$-dated volcanic ash layer at ~ 72 mblf (tephra 18, T18) has an age of 797.3 ± 1.6 ka (Russell et al. 2020), and (3) quasi-rhythmic alternation of two clay types probably reflects environmental changes that resulted from orbital-scale changes in insolation and continental ice volume (Russell et al. 2020). Other factors, however, including hydrological changes and the active tectonic setting, are capable of influencing sedimentology in

Lake Towuti and should be considered during interpretations.

For sediment age estimates, we focused on the magnetic susceptibility (MS) record of Site 1, where, in contrast to Site 2, occurrence of MMD is minor. To minimize overestimation of sedimentation rates, segments containing MMD were excluded from the record before cyclostratigraphic analysis. The two clay types that represent most of the lacustrine facies at Site 1 are distinguishable by MS, and in short piston cores MS reflects environmental changes in the sedimentary system linked to glacial/interglacial variability (Russell et al. 2020; Tamuntuan et al. 2014).

This study aimed to: (1) infer sedimentary processes in Lake Towuti from downhole geophysical logging data, (2) establish a chronology for the sediment record at Site 1 by supplementing the radiometric dates between 797 and ∼ 45 ka, and (3) investigate the potential influence of long-term insolation cycles on the undisturbed sediment successions in Lake Towuti.

Background

The geology of central Sulawesi is characterized by ultramafic rocks and lateritic soils. The Malili Lakes catchments are generally underlain by heavy-metal-rich, trace-metal-poor ultramafic rock. Notable exceptions include limestones that partially underlie southwestern Lake Matano, and a metasedimentary complex southeast of Lake Towuti (Costa et al. 2015; Fig. 1a, b). Today the lake is weakly, though permanently stratified, and ultra-oligotrophic, with anoxic conditions below ∼ 120 m water depth (Vuillemin et al. 2016). Two distinctive facies were identified in seismic profiles prior to drilling (Fig. 1d): a lower Unit 2, interpreted as fluviolacustrine sediment, and an upper Unit 1, composed of better-stratified lacustrine sediment (Russell et al. 2016).

During the last glacial maximum (LGM), the region around the Malili Lake System was drier and the decreased precipitation caused lower water level than today (Russell et al. 2014; Vogel et al. 2015; Wicaksono et al. 2015). The water level and the oxic/anoxic boundary decreased simultaneously. Combined with stronger circulation of the water column, this resulted in increased oxygenation at the sediment water interface, which induced changes in the sediment geochemistry and initiated authigenic formation of magnetite and siderite (Tamuntuan et al. 2014). In contrast, enhanced precipitation during wet climate conditions, e.g. during MIS 1 and parts of MIS 3 (Russell et al. 2014) did not only induce higher water levels, resulting in more pronounced stratification of the water body (oxic in surface waters/anoxic in bottom waters), but also enhanced input of organic material, causing an anoxic environment that led to dissolution of magnetite in the sediments. Hence, the magnetic properties of sediments are regulated by a combination of changes in detrital influx, iron oxide dissolution under reducing conditions and the precipitation of magnetite and siderite (Costa et al. 2015; Tamuntuan et al. 2014; Russell et al. 2014). The result was an alternation of deposition of two main clay types in Lake Towuti: (1) Reddish "sideritic clay" was characteristic of oxic conditions, contains magnetite, and shows enhanced siderite and MS, compared to (2) green clay, referred to simply as "clay," which is characteristic of anoxic conditions and lower MS. In addition to the main clay types, 3–5-m-thick layers of diatomaceous ooze occur at all sites. A lack of siderite and low MS is characteristic of these layers, which consist primarily of planktonic diatoms. Multiple thin layers of MMD, consisting of normally graded silts (< 0.5 m) and tephra (usually < 20 cm), are distributed throughout the sediment successions and can cause distinct peaks in MS (Russell et al. 2016, 2020). Rock magnetic properties of lacustrine sediments have been used in previous studies to detect paleoenvironmental changes in lakes (Gebhardt et al. 2013; Stockhausen and Zolitschka 1999; Melles et al. 2012). In Lake Towuti, magnetic susceptibility measurements were carried out on sediments from an ∼ 11-m piston core, obtained as part of a pre-site survey in 2013. MIS 3 and 1 represent wet climate conditions and are marked by low magnetic susceptibility, whereas the drier MIS 2 is characterized by high susceptibility values (Tamuntuan et al. 2014). Assuming this relation continues with depth, together with the observation that initial data from the long ICDP core and borehole logging show clear indications of orbital-scale climate variability during the middle to late Pleistocene (Russell et al. 2016), it is likely that magnetic susceptibility values from downhole measurements are a promising variable that can be used to investigate long-term climate change around Lake Towuti.

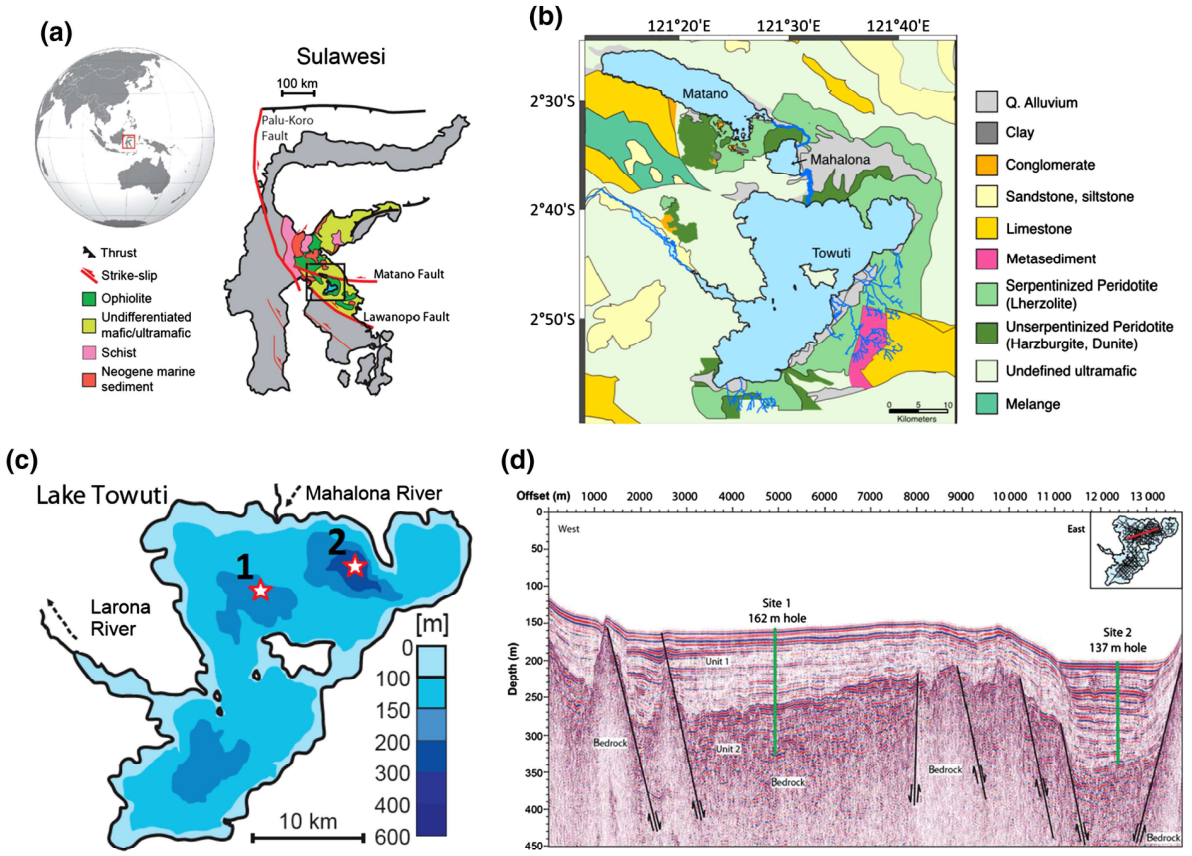

Fig. 1 **a** Geological map of Central Sulawesi, **b** detailed geological map of the Malili Lake System, **c** bathymetric map of Lake Towuti and **d** seismic reflection data from pre-site surveys, showing profile through both sites. Logging locations indicated by red stars (modified from Russell et al. 2016 and Costa et al. 2015)

Materials and methods

Coring sites and core descriptions

Fieldwork was conducted in May–July 2015. Boreholes were drilled using a PQ-type drill string (ø 122.6 mm hole, ø 66 mm sediment core; Russell et al. 2016). The coring sites were selected using seismic data and piston cores that span the last glacial/interglacial cycles (MIS 3–1; Russell et al. 2014). Objectives at Site 1, in the central northern basin, were to retrieve a continuous, turbidite-poor, lacustrine record of Unit 1. For Site 2, the goal was to investigate changes in deltaic sedimentation processes, forced by lake-level fluctuations and possible changes in the river system in the deepest part of the lake, close to the Mahalona River (Fig. 1c). A third site was planned in the southern basin, but, due to organizational problems, finally drilled ~ 1.5 km west of Site 1 (Russell et al. 2016; Vogel et al. 2015). Site 3 is not part of this study, since no geophysical downhole logging was conducted there.

At Site 1, five cores (1A–1F) were drilled, with a maximum depth of ~ 162 mblf achieved at Site 1B where 0.4 m of lithified conglomerate, representing the bedrock, was retrieved. Seismic surveys, together with initial core descriptions, enabled division of the succession into two main units (Figs. 1d, 3). Unit 2 (from 161 to 98 mblf; Fig. 1d) is characterized by silty and/or sandy sediment, interbedded with peat (1.5 m thick maximum), or minor gravel layers (< 0.7 m thick). The upper ~ 98 m represent the lacustrine facies (Unit 1) and are characterized by alternating clay and sideritic clay (Russell et al. 2016, 2020). Unit 1 also includes two thick layers of diatomaceous ooze, intercalated between the clays (3 and 5 m thick each)

and multiple thin tephra layers (< 20 cm) and MMD (< 50 cm). Core recovery differed among the five drill holes (79–99%), with loss occurring almost exclusively in lower Unit 2 (Russell et al. 2016).

At Site 2, three cores (2A–2C) were drilled, to a maximum depth of 138 mblf at Site 2A (Fig. 1d; Electronic Supplementary Material [ESM] Fig. S2). The drilling target was reached at 133 mblf, where the transition from Unit 2 to Unit 1 is located. The lower part of Unit 1 (from 133 to 70 mblf) consists of lacustrine material comparable to the clay/sideritic clay alternation seen at Site 1, Unit 1 (Russell et al. 2016). The upper 70 m are dominated by normally graded silts (MMD with 0.8 m thickness maximum) and contain up to 3-m-thick tephras. These tephras are much thicker than those observed at Site 1, possibly because they contain reworked material associated with MMD. Core recovery differed among the three drill holes (83–99%; Russell et al. 2016).

Physical properties of sediments

Downhole geophysical logging was conducted at Sites 1B, 1F, and 2C, using a set of downhole logging equipment provided by the Leibniz Institute for Applied Geophysics (Fig. 2; Table 1). These included

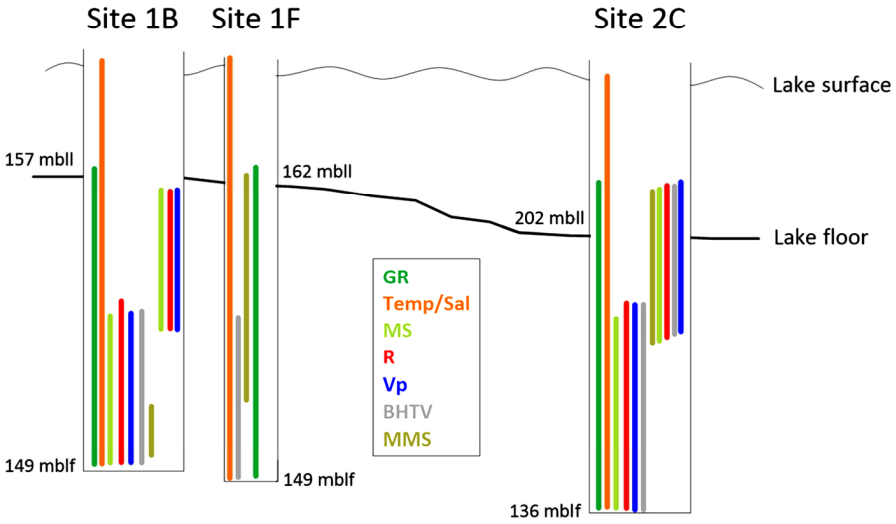

Fig. 2 Logging scheme at Sites 1B/F and 2C. First, specific variables were measured through the drill pipe (spectral gamma ray, temperature and salinity). Then, drill pipes were pulled out partly to sustain hole stability in the upper part, but open-hole conditions for the measurements in the lower section. For the second run, drill pipes were pulled almost completely from the hole. mbll = meters below lake level; mblf = meters below lake floor. Abbreviations of logged variables are shown in Table 1

Table 1 Downhole logging tools used at Lake Towuti

Downhole logging tool	Measured parameter	Abbreviation
Spectral Gamma Ray Sonde SGR 70, type 1419, Antares	Natural gamma radiation, U-, Th-, K-concentration	GR
Susceptibility Sonde, type 1108, Antares	Magnetic susceptibility	MS
Dual Laterolog Sonde, Antares	Resistivity (Rdeep & Rshallow)	R
Sonic Sonde, Antares	Acoustic velocity	Vp
BHTV—FAC40 Televiewer, ALT	Acoustic imaging of borehole-wall	BHTV
Dipmeter ADIP A21, Antares	Caliper, orientation of borehole, dip of strata	Dip
Micro-susceptibility instrument, type 1121, Antares	Magnetic susceptibility	MMS
Salinity/temperature Sonde, Antares	Salinity and temperature of borehole fluid	Temp/sal

spectral gamma ray (GR; including U, K and Th concentrations), magnetic susceptibility (MS), resistivity (R), sonic velocity (Vp), dipmeter (Dip) and ultrasonic imaging of the borehole walls. Since all measurements, except spectral gamma ray, need an open hole, drill pipes were pulled successively after each run (Fig. 2). Geophysical datasets were recorded and partly pre-processed on site, using the software Geobase® (Antares, Germany).

Further processing was conducted using Wellcad© (Advanced Logic Technology, Luxembourg). The whole-core logging datasets for cores from each of the three holes were adjusted to match the depths from borehole logging data and spliced to generate complete downhole logs (Fig. 3). Matching magnetic susceptibility data from multi-sensor core logging (MSCL) and downhole logging measurements enabled correlation of the sediment core to true depth measured from downhole logging, referred to as "meters below lake floor" (mblf). This also enabled matching core descriptions and logging data. Instantaneously deposited layers like tephras and MMD, referred to as "event layers," can confound signals used for cyclostratigraphic analysis (described below) if they are thick enough, and therefore have to be "removed" from the record. Overall, more than 20 tephra layers with thicknesses between 0.7 and 19.3 cm, and about 20 MMDs, from 1.5 to 46.5 cm thick, were described in the sediments from the lacustrine facies (Unit 1) at Site 1B. Exclusion of event layers leads to artificial shortening of the cored succession and thus to a synthetic depth ("depth*"). In the case of data from the lacustrine facies at Site 1B, the total depth shrinking represents 3.65 m of the total 98 m.

To limit the influence on calculations caused by diagenetic processes or post-drilling effects, downhole logs were linearly detrended. The consequence is that absolute measured values were converted to values relative to the median. The mentioned effects can cause trends in downhole logs with depth, which in turn may be problematic for statistical analyses. Such effects include compaction (generally increases with depth) or interaction of drilling fluids with the borehole wall (increases with time of sediment exposure to fluids). For example, the R-log at site 1B shows an increasing linear upward trend toward the lake bottom (Fig. 3). Higher values at the top of the log can be explained by lake water intrusion into the borehole. Vuillemin et al. (2016) and Lehmusluoto et al. (1995) reported the conductivity of Lake Towuti's water varies between 175 and 400 µS/cm (57 Ωm and 25 Ωm, respectively). Migration of these waters into the drill hole and partly into the sediments, can result in higher measured R-values.

Fig. 3 Downhole logging variables, core description (*Lithology description is simplified here, for more information see Russell et al. 2016) and water content of NMR laboratory measurements from Site 1B. All logs are raw data. A change in physical variables at ~ 98 mblf indicates the transition from pre-lacustrine to lacustrine facies. Depth in meters below lake floor (mblf). *GR* total gamma radiation with concentrations of U, Th and K; *MS* magnetic susceptibility; *R* resistivity; *Vp* acoustic velocity; *Sal* salinity; *Temp* temperature; *Wc total* total water content ▶

Cluster analysis was performed to construct continuous, artificial logs, based on their physical properties derived from detrended downhole logging data (GR, Th/K-ratio, MS, R, Vp). The software utilized was the WinSTAT® software for Microsoft® Excel and the cluster distance measure used was Ward's method (Ward Jr 1963). Based on the resulting dendrogram, a specific number of classes was defined and average values for logging variables were calculated for each class. Analyses were conducted for complete-depth logs or shorter sections of special relevance (i.e. 10–98 mblf at Site 1B, representing the lacustrine facies). Since not all variables were available for all sites and depths (Fig. 2), several configurations of variables and methods were tested to achieve a useful classification of sediments.

Cyclostratigraphy

Results were generated using the 'astrochron' package for the R programming language (Meyers 2014; R Core Team 2020). Amplitude spectra were created for intervals of interest. Tracking high-amplitude peaks and relating these to the 110-ka eccentricity (the combination of the 95-ka and 125-ka cycles), the 41-ka obliquity and the 21-ka precession cycles can be used to determine fluctuations in sedimentation rates over depth, assuming these cycles control sedimentation (Eq. 1). Sedimentation rates (*SR* in cm/ka) for each depth can be calculated using the period (*P* in ka) of the assumed orbital cycle and the frequency (*f* in 1/m) tracked in the amplitude spectra.

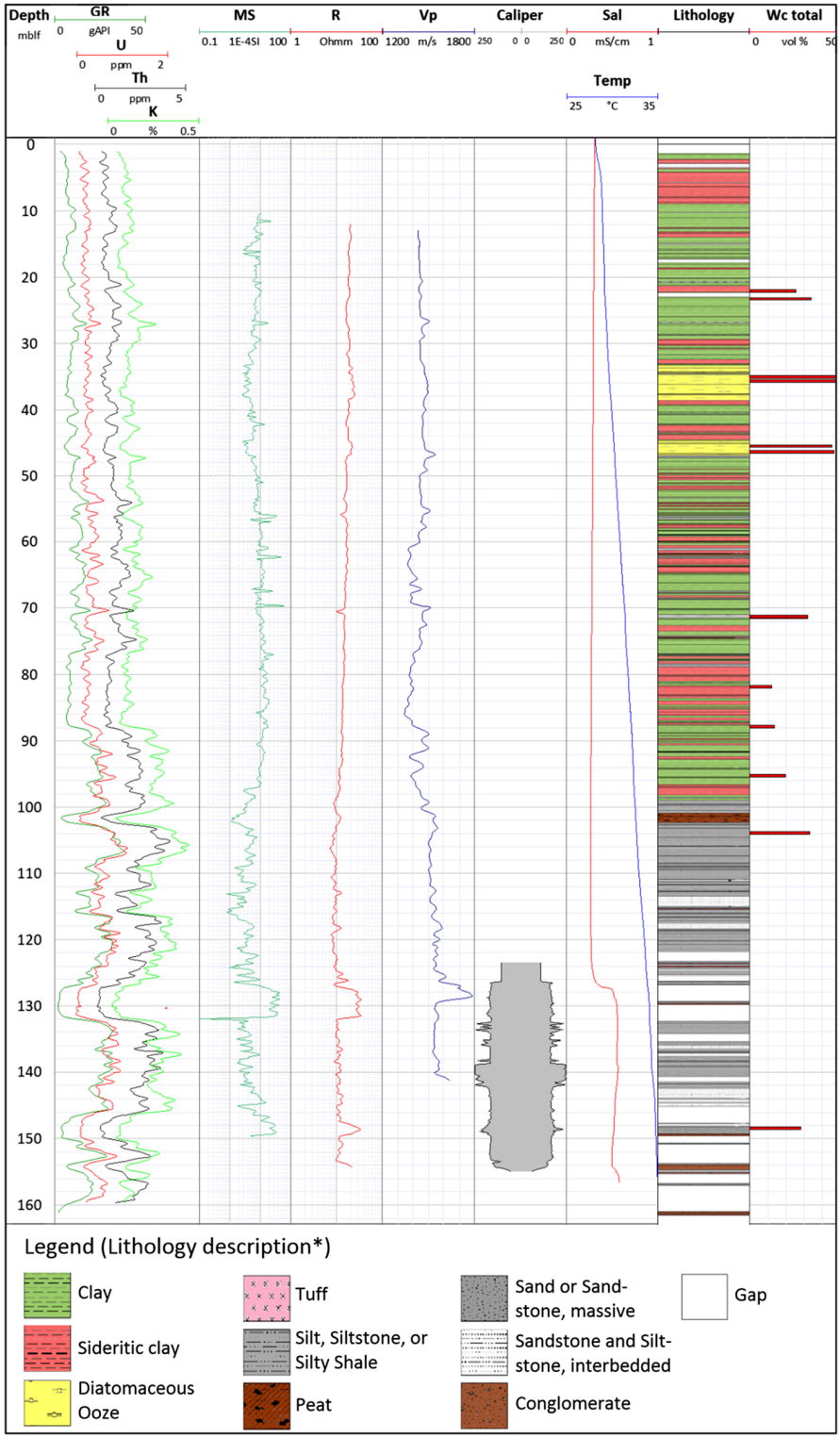
Depth
mblf
GR
0 gAPI 50
U
0 ppm 2
Th
0 ppm 5
K
0 % 0.5
MS
0.1 1E-4SI 100
R
1 Ohmm 100
Vp
1200 m/s 1800
Caliper
250 0 0 250
Sal
0 mS/cm 1
Temp
25 °C 35
Lithology
Wc total
0 vol % 50
0
10
20
30
40
50
60
70
80
90
100
110
120
130
140
150
160
Legend (Lithology description*)
Clay
Sideritic clay
Diatomaceous Ooze
Tuff
Silt, Siltstone, or Silty Shale
Peat
Sand or Sand-stone, massive
Sandstone and Silt-stone, interbedded
Conglomerate
Gap

$$SR = \frac{100}{P} * f \quad (1)$$

Together with radiometric age control points, the SR calculations lead to an age-depth model for the Lake Towuti record. After examining the logging variables, astrochronological analyses were conducted using the MS from downhole logging measurements because it appears to reflect orbital cycles most clearly and distinguishes between the major sediment types, i.e. clay and sideritic clay. The relative age-depth estimations from cyclostratigraphic analysis are anchored to absolute ages derived from radiometric dating. In Lake Towuti, this reference value is a tephra (T18) at a depth* of 72.05 with an age of 797.3 ± 1.6 ka (Russell et al. 2020). Additionally, 23 ^{14}C measurements from a piston core close to Site 1 indicate more rapid sedimentation rates in the upper 9 m of the sediments. The oldest ^{14}C age in this core is ∼ 45 ka at ∼ 9 mblf (Russell et al. 2014).

Event layers (MMD and tephra) are instantaneous deposits and contain a negligible amount of time with respect to cyclostratigraphic determination. Event layers, if not removed from the record, would lead to an overestimation of sedimentation rates (see "Physical properties of sediments"). Even after removing the event layers, the data still contain artefacts of these events caused by the slopes of the peaks originating from these layers. Those border effects were smoothed using polynomic regression (ESM Fig. S1). The importance of careful data pre-processing becomes clear when the corresponding amplitude spectra after each cyclostratigraphic processing step are compared. Smoothing of border effects has a particularly high impact on the quality of the spectra (ESM Fig. S1). The amplitude spectra were created using the sliding-window method (Molinie and Ogg 1990; Weedon 2003). Multiple window lengths were tested to cover the widest range in the downhole logging record, with a focus on different orbital cycles.

Results

Logging features

The lower 98 mblf (Unit 2) of Site 1B are characterized by high-amplitude variations in the logged variables (Fig. 3). Changes in the sediment properties are evident at 98 mblf, at the Unit 2/Unit 1 boundary. GR, and especially MS, indicate this change by showing less distinct alternations in the upper Unit 1. Vp also decreases to values lower than 1500 m/s instantaneously.

However, above 98 mblf (Unit 1) greatest variability is visible in GR and MS. The latter shows distinct peaks, some of which can be correlated to tephra layers and MMD in the core. Typical examples of two peaks caused by MMD occur at ∼ 62 mblf. Those peaks can be related to MMD of 40 cm and 28 cm thickness. An example of a typical peak in MS and GR caused by tephra can be observed at ∼ 27 mblf (Fig. 3). Low MS and high R are correlated to the beds of diatomaceous ooze. Values for Vp are below the velocity of sound in water (∼ 1500 m/s) and show an increasing trend towards the top. Sideritic clay has the lowest Vp, which contradicts the lowest porosity, measured by nuclear magnetic resonance (NMR). A similar contradiction is evident in diatomaceous ooze. There, the slightly greater Vp values are accompanied by high water content, i.e. high porosity.

Two vertically confined horizons in Unit 2 (132–127 and 103–101 mblf) do not follow the pattern in logging data observed elsewhere in the Site 1 stratigraphy. The deeper interval, from 132 to 127 mblf, is characterized by low GR, but considerably higher values of MS, R and Vp, whereas the more recent, from 103 to 101 mblf, is characterized by low GR and MS. The rise in salinity of the borehole fluid at 127 mblf is noteworthy. Caliper measurements show an increase in borehole diameter at 142–139 mblf.

Site 2C shows patterns of logged variables (ESM Fig. S2) similar to Site 1, but a different lithology (Russell et al. 2016), composed of clays with two diatom layers in the lower ∼ 70 mblf, and coarser-grain MMD in the upper part. The clayey layers in the lower part show slightly higher GR than the upper 70 mblf. MS has the largest variance in the record and decreases throughout the lower part, but increases in the upper 70 mblf. The same holds for R, although the changes are not as pronounced. In general, values for most variables in clays and MMD are rather constant, with minor trends. The first exceptions are two layers of diatomaceous ooze, which show clearly lower MS and slightly higher R, similar to Site 1B. The second exceptions are tephra layers. Within the MMD, they are clearly connected to peaks in GR. This is different from tephra layers in clayey material from Site 1 or 2,

where the most suitable variable for this purpose is peaks in MS. Vp and R are also distinctly linked to tephra layers, but associated peaks are less evident.

Cluster analysis

Site 1B

Evaluation of the first cluster analyses from 141 to 13 mblf indicates a major change in lithology at ~ 100 mblf (ESM Table S1). This agrees with core data from Russell et al. (2016), who described a shift from a fluviolacustrine sediment (gravels, sands, peats and silts) to lacustrine and clay-rich facies around this depth.

Subsequently, cluster analyses were conducted for each unit individually (above and below ~ 100 mblf) to improve characterization of sediment types. Analysis was conducted using detrended GR, MS, R, Vp and the Th/K-ratio. Clusters were divided, based on their physical properties, into four (A–D) or three classes (E–G), each representing a lithology type (Fig. 4).

Cluster analysis I (Site 1B, 98–13 mblf, lacustrine facies)

The log created from cluster analysis is dominated by classes A and B, which together make up more than 90% of the upper lacustrine facies (Fig. 4, left). Class B has slightly higher GR and lower MS than class A, but in general they differ only slightly from one another. This makes it difficult to link them to core description data. Class C stands out by virtue of its high R, and represents diatomaceous ooze layers. Many thin layers of class D are distributed in the log. Although representing only 2.2% of the total log, they show clearly higher values of MS and Th/K-ratio than other classes. Compared to the lithologic description from core analysis, those layers match to some of the thicker silty layers interpreted as MMD by Russell et al. (2016). Attempts to identify tephra layers by defining more classes failed, mainly as a consequence of the low thickness of tephra layers (mean thickness of ~ 4.2 cm) relative to the resolution of downhole logging measurements.

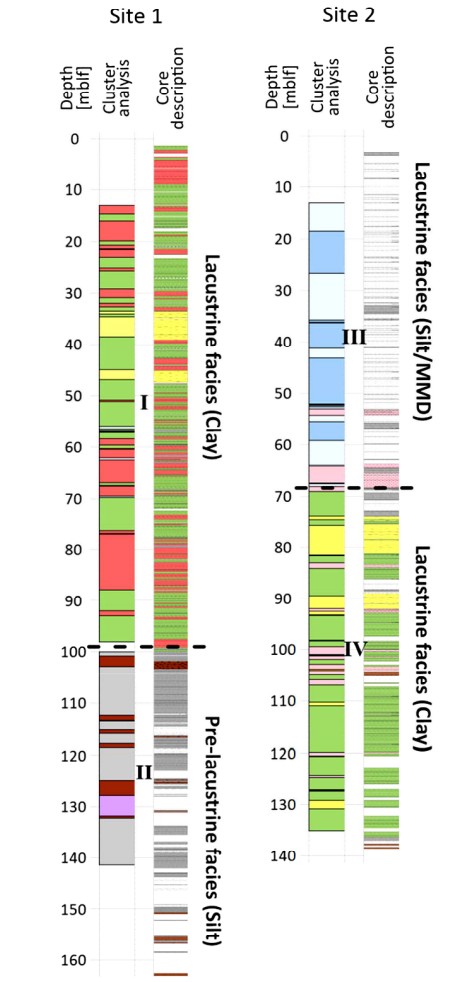

	Class	GR	MS	R	Vp	Th/K	% of section
I	A	8.7	10.2	16.6	1416	7.6	38.0
	B	12.3	7.2	16.1	1467	7.8	52.1
	C	7.6	4.4	20.9	1486	6.8	7.4
	D	9.0	31.4	16.3	1446	8.9	2.2

	Class	GR	MS	R	Vp	Th/K	% of section
II	E	28.1	0.9	7.4	1526	9.8	71.9
	F	14.4	2.6	10.6	1579	8.1	18.4
	G	4.5	26.9	25.7	1595	6.2	9.6

	Class	GR	MS	R	Vp	Th/K	% of section
III	A	7.8	9.5	12.1	1474	6.7	43.1
	B	3.3	20.2	13.2	1496	5.9	48.6
	C	21.8	12.4	18.5	1522	3.4	8.2

	Class	GR	MS	R	Vp	Th/K	% of section
IV	D	9.2	13.1	11.9	1451	7.4	67.8
	E	6.0	9.9	14.2	1473	6.9	18.4
	F	16.4	9.6	10.8	1536	7.5	13.3
	G	34.2	108.4	10.6	1890	2.5	0.4

Fig. 4 Created cluster logs from Site 1B (left) and Site 2C (right) compared to core description data. Physical properties of the cluster log are given in tables below. Roman numerals stand for one cluster analysis each. The dashed line indicates the border of the two clustered sections at each site

Cluster analysis II (Site 1B, 141–100 mblf, fluviolacustrine facies)

The classes as derived from cluster analysis differ mainly with respect to their GR. Class E is characterized by high GR and dominates the section (~ 72%). Class F is characterized by medium GR, but low MS. It can be connected to peat layers. Major core loss in the fluviolacustrine facies made it difficult to make definitive conclusions. Class G is characterized by low GR and higher MS, R and Vp. Missing core material in the interval 132.5–126 mblf prohibits verification with a specific sediment layer.

Site 2C

As at Site 1B, two separate cluster analyses were conducted using detrended data for the upper and lower lithologic units. Since neither cluster analysis over the full log (135–13 mblf), nor major shifts in logged parameters (ESM Fig. S2) indicated changes in lithology, the decision about the coverage of the sections for cluster analyses was based on the core description from Russell et al. (2016). Division into classes was based on physical properties. The upper part, 68–13 mblf was divided into three classes (A–C), whereas the lower part of the section was divided into four classes (D–G, Fig. 4, right).

Cluster analysis III (Site 2C, 68–13 mblf, mass movement deposits MMD)

The upper 68 m of sediments at Site 2 consist mainly of MMD. Compared to class A, class B has lower GR and higher MS. Comparison of cluster classes with core data highlights the limit of cluster analysis in this section. A clear correlation of class A or B to lithologic units is not possible here. In contrast, class C can clearly be connected to thick tephra layers in the core. It is characterized by high GR and R.

Cluster analysis IV (Site 2C, 135–68 mblf, lacustrine facies)

The log of this depth interval is dominated by class D (~ 68%), with intermediate GR and higher MS. It corresponds to clay from the core description. Class E has the lowest GR and the highest R and is correlated to diatomaceous ooze in most parts. Class F is characterized by high GR and low MS. Many tephra layers correlate to this class. In general, tephra layers in the core are thin, but some of the thicker ones are identifiable in the cluster log. Class G appears as a single 30-cm-thick layer at 104 mblf. Compared to other classes, it has extraordinarily high GR, MS and Vp values. The latter indicate a dense material, which is consistent with core analysis that described an interbedded sandstone/shale layer at this depth.

Cyclostratigraphy

The MS and GR records of the lacustrine facies at Site 1B were used for cyclostratigraphic analysis. The MS record that was used has a length of 84 m, from the base of the lacustrine facies at 98 mblf to 10.4 mblf (Fig. 3), minus 3.65 m of excluded event layers. The analyzed GR record spans from 94.4 to 2 mblf and thus covers a broader depth range. We found a window size of 17 m for the sliding-window method (Molinie and Ogg 1990) useful, therefore the depth range of amplitude spectra was 85.9–18.9 mblf for MS and 85.9–10.5 mblf for GR, with half of the window size removed from each end of the record (ESM Fig. S3). The step size of the sliding window was set at 0.5 m, resulting in an estimated sedimentation rate every 0.5 m.

Assuming an average sedimentation rate of 9.0 cm/ka for the investigated interval, suggested by the date on tephra T18 of 797 ka at 72.05 mblf (Russell et al. 2020), the frequencies at which orbital cycles should be expressed in the amplitude spectra are 0.10 cycles/m for a ~ 110-ka eccentricity component (combination of 95/125 ka cycles), and 0.27 cycles/m for the 41-ka obliquity cycle. Precession-related cycles do not appear in the spectra and therefore, the high-frequency area is not illustrated (Fig. 5, ESM Fig. S3).

The amplitude spectra of the MS and GR datasets do not allow unambiguous interpretation of astrochronological cycles over the full depth. Therefore, multiple correlation options were explored (ESM Fig. S3). In the case of MS, the tracked amplitude peak splits three times, resulting in major shifts of more than 20 cm/ka in SR estimations in those intervals (Fig. 5, ESM Fig. S3 left).

In the case of GR, two distinct peaks at approximately 0.09 cycles/m and 0.24 cycles/m, appear in the amplitude spectrum (ESM Fig. S3 right). SR for both were calculated assuming that the corresponding lines

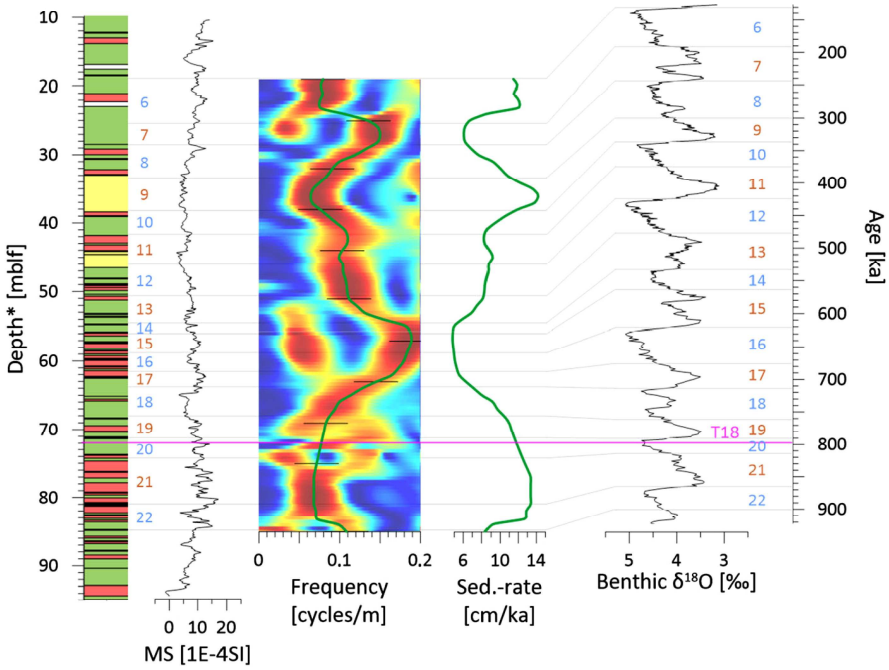

Fig. 5 Comparison (from left to right) of lithology, the magnetic susceptibility without event layers (MS), the amplitude spectrum, estimated sedimentation rates, the LR04 benthic stack (Lisiecki and Raymo 2005) and age, including marine isotope stages. Tephra T18 in pink is the age-control point (Russell et al. 2020). Marine isotope stages (MIS) are colored in blue for glacials and brown for interglacials. (Color figure online)

in the amplitude spectrum are related to the 110-ka eccentricity cycle (dark red and red line), whereas the orange line is interpreted as a 41-ka obliquity cycle. Major differences are expressed in the interval from 75 to 45 mblf, where sedimentation rates for the dark red line drop to < 5 cm/ka (Fig. 5, ESM Fig. S3 right).

The calculated SR enabled construction of age-depth models for the investigated intervals (ESM Fig. S4). Tied to one data point (tephra T18 with a date of 797 ka at 72.05 mblf depth*, from Russell et al. 2020), the constructed age-depth graphs vary. Three of the age-depth models form a cluster, with ages of approximately 370 ka at a depth* of 20 mblf. Assuming this date is accurate, SR in the upper 20 mblf would have to slow considerably. One age-depth model calculated from GR intersects the depth axis at 20 mblf and can thus be excluded from further discussion. One model, calculated from MS, reached an age of approximately 131 ka at a depth of 19 mblf (Fig. 6, ESM Fig. S4). The maximum calculated age of 903 ka at a depth* of 85.9 mblf resulted in a total span of 772 ka and represents the time from late MIS 23 to late MIS 6.

Discussion

It is difficult to interpret paleoenvironmental conditions from the downhole logging data. Differences in the main lithologies of the lacustrine facies are reflected in relatively weak changes in sediment physical properties. Hence, distinction between the main sediment types “clay” and “sideritic clay” is impractical from single downhole logging measurements alone. Particular sediment types, like diatomaceous ooze and MMD, show strong geophysical characteristics that make them interpretable. High-amplitude variations in downhole logging data from the fluviolacustrine facies may be caused by rapid environmental changes and/or tectonically driven variability in the depositional sedimentary system (Russell et al. 2016).

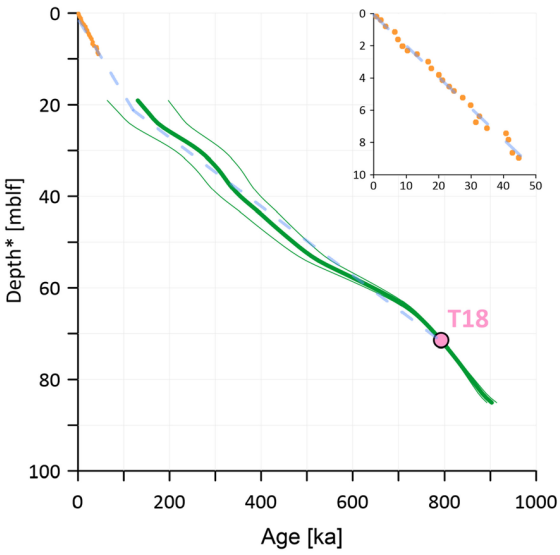

Fig. 6 Age-depth model from interpreting cyclicity of the magnetic susceptibility data, as related to ~ 110-ka eccentricity. Effects of ± 10% uncertainty in amplitude tracking is indicated as thin lines. Orange data are ^{14}C ages from Russell et al. (2014). The dated tephra (T18) is displayed in pink. Note the increase of uncertainty with increasing distance to T18. Inset: detailed view of ^{14}C ages in the upper 10 m (50 ka) of the record from a piston core collected close to Site 1. (Color figure online)

The strongest peak in Vp coincides with distinctive peaks in R and MS, but a drop in GR in Unit 2 at Site 1B (~ 130–126.5 mblf). This leads to a clear separation from other classes in the cluster analysis (Figs. 3, 4). The mentioned variables indicate the presence of an exceptional layer consisting of dense material with high R and high MS, e.g. a lateritic paleosol. The abrupt increase in conductivity, from ~ 0.27 to 0.55 mS/cm may have been caused by humic acids leaking from a peat layer into the borehole. Major core loss in this part of the profile, however, prohibits a clear determination. A second layer with similar values occurs at ~ 150–148 mblf. As the sonic tool was operated only at depths above 141.5 mblf, this was not part of the cluster analysis.

Cluster analysis

Cluster analysis is a useful tool for identification and classification of lithologic units. One constraint, however, is that sediment cores are necessary to verify initial results. Nevertheless, if successful, the results of the cluster analysis can be transferred to other holes and logging sites, and fill coring gaps. Careful preprocessing to eliminate external factors, e.g. interaction of drilling fluids with the borehole wall, are indispensable for robust results.

The characteristics of lithologic units are given in Fig. 4. The logs were detrended before analysis, but the relative values of variables still provide information about sediment characteristics. Values of class A and B in cluster analysis I (Fig. 4, Site 1B, 13–98 mblf) illustrate the difficulties of differentiation. The two classes are similar in their physical properties, whereas classes C and D each have at least one physical variable that distinguishes them from the other classes. In the lower part of Site 1, lithologies and thus physical properties of the sediments vary substantially. This results in stronger differentiation of lithologic units. Several layers of class F can be assigned to peat in the core. The exceptional layer discussed earlier appears as a single ~ 3.5-m-thick layer (class G) around ~ 130 mblf. Cluster analysis from downhole logging data is the only option to investigate depths with major core loss, for instance cluster analysis II from 141 to 100 mblf at Site 1B (Fig. 4).

Heterogeneity of the MMD at Site 2C illustrates the limits of cluster analyses. Although different physical properties (especially MS) result in classification into class A and B, similarities to core description are not apparent. Only class C can be linked clearly to tephra in the core. After applying the same cluster analysis properties to the lacustrine facies at Site 2 (cluster analysis IV, Fig. 4, Site 2C, 135–68 mblf), the comparison of cluster analysis and core lithology is similar to the lacustrine facies at Site 1 (cluster analysis I, Fig. 4, Site 1, 98–13 mblf), except for the identification of tephra layers, which tend to be thicker at Site 2 and thus better recorded by downhole logging tools.

Data from core scanning (X-ray Fluorescence or MSCL) would improve results, but problems like core loss or small depth shifts caused by sediments slipping in the core liners during recovery/transport preclude the creation of continuous data sets. The use of more downhole variables (e.g. element concentrations, neutron porosity) is recommended, but not implementable in international drilling campaigns because of the difficulty of exporting/importing radioactive sources.

Cyclostratigraphy and an age-depth model

The sedimentary succession in Lake Towuti is the result of interactions among the geologic, hydrologic and sedimentary systems in the lake catchment. Factors including tectonic activity and lake connectivity might influence the signal in Lake Towuti, given their potential to change the geologic and hydrologic environment around the lake. Another factor that can modify the MS signal is the formation of magnetic minerals during diagenesis. Such changes are, however, at least partly climate-driven and thus contain information about local climate evolution and astronomical insolation forcing. Here we discuss the extent of the orbital imprint and factors that may affect the orbital signal in the sediments.

A reasonable age-depth model was derived from the MS record, by tracking amplitude peaks with frequencies between 0.06 and 0.19 cycles/m, and interpreting them as a ~ 110-ka cycle (Fig. 5), related to eccentricity or glacial/interglacial climate variability. Anchored to the dated tephra from Russell et al. (2020), and combined with ^{14}C data from Russell et al. (2014), the age-depth model shown in Fig. 6 covers more than 77% of the history of the lacustrine facies at Site 1B, clearly improving our understanding of the age and extent of the sediment record in Lake Towuti. Other configurations of orbital cycles, and interpretations of age-depth models from MS or GR were tested, but failed to describe the sedimentological history of Lake Towuti in the published stratigraphic context (ESM Figs. S3 and S4).

Our results, referring to the dominance of a 110-ka cycle, agree with the eccentricity-related, glacial-interglacial cycles that were the predominant driver of global climate over the last ~ 1 Ma. Also, several other regional records from the Solomon Sea in the southwestern Pacific were driven mainly by an eccentricity component during the last ~ 1 Ma and support our understanding of the regional changes in the Indo Pacific Warm Pool (Chuang et al. 2018). Records of IPWP sea surface temperature, derived from foraminifera Mg/Ca ratios and/or alkenone paleotemperature determinations, show a dominant 100-ka cycle similar to the benthic LR04 $\delta^{18}O$ stack (de Garidel-Thoron et al. 2005; Herbert et al. 2010; Lisiecki and Raymo 2005). Speleothem records from northern Borneo, which span the last 160 ka, show patterns of precession in their records (Carolin et al. 2016), but like the Towuti record, these cycles play a subordinate role to glacial-interglacial variability (ESM, "Testing for particular cyclicities").

It should be possible to resolve individual precession cycles in lake sediments from tropical environments. This, however, was not the case here, possibly because of generally weak expression of precession in sediments from Lake Towuti. In our opinion, complex sedimentology, including different geochemical signatures and tephra layers, prevent precession signals from being identified clearly in downhole geophysical logs. The signal of a 110-ka eccentricity cycle in our interpretation shifts or vanishes at some stages in the amplitude spectrum, which complicates robust, unambiguous interpretation. Two of those shifts appear in the MS data at ~ 56 and ~ 26 mblf, where sedimentation rates clearly differ between the paths in amplitude tracking (Fig. 5).

Uncertainties of the cyclostratigraphy

The main uncertainty is caused by the complex regional setting, where multiple factors can distort orbital signals in the sediment. Enhanced biological activity (diatomaceous ooze) and event layers (MMD/tephras) cause major changes in the absolute amount of deposited material. This can result in an apparent rise of sedimentation rates, making frequency-tracking difficult.

The age model was constructed using only the single dated tephra layer T18, with an age of 797 ka at 72.05 mblf depth* (Russell et al. 2020). The estimated uncertainty is displayed in Fig. 6, where the effect of a ± 10% shift in the tracked frequency results in an age range of 131 ± 67 ka at ~ 19 mblf. In general, sedimentation rate estimates are based on tracking individual peaks in the amplitude spectra. Peaks, however, are characterized by a wider frequency range because the window size here was 17 m, enabling multiple options for tracking maxima. Also, the size of the sliding window has an effect on uncertainty. The peaks displayed at every step in the amplitude spectra represent values averaged over the 17-m window size. These uncertainties have to be considered when developing and interpreting this age-depth model.

To interpret peaks in the amplitude spectrum as eccentricity or obliquity cycles, we used the average sedimentation rate of ~ 9 cm/ka, calculated between T18, with an age of 797 ka at 72.05 mblf, and the

water–sediment interface. This results in frequencies of 0.10 cycles/m for the 110-ka eccentricity cycle, and 0.27 cycles/m for the 41-ka obliquity cycle. Commonly, SR changes over time, allowing a wider range for interpretation of orbital cycles (e.g. a range of 0.18–0.06 cycles/m for the 110 ka eccentricity cycle, with SR from 16 to 5 cm/ka).

Paleoenvironmental indications

The records of MS and benthic $\delta^{18}O$ seem to follow a similar trend from MIS 17 to 12, but in other parts this relation is not evident (MIS 19–17 and 10–6) or even opposite (MIS 20 and 11; Fig. 5). According to Tamuntuan et al. (2014), MS reflects the response of the system to lake level fluctuation and thus, wetter or dryer periods. This relationship seems to continue in the younger part (MIS 9–6), though not as clearly. Sideritic clay is restricted to glacials, despite the main portion of the glacials consisting of clay (Fig. 5). Enhanced bioproductivity during MIS 9 might have resulted in diatom blooms leading to increased SR. This can be seen in a peak in the SR at 36 mblf related to a diatomite layer. Yet the two diatomaceous ooze layers are a factor of uncertainty, since the exact amount of time contributed to the normal background sedimentation of clays is unknown. In the part of the record older than MIS 10, the relationship between clay type and glacial/interglacial variability is not very clear. Although there is clear cyclicity, the patterns can only tentatively be matched to LR04. This leads to the conclusion that factors other than the glacial/interglacial cyclicity played an important role in the deposition of certain clay types, and thus the oxidation state, in the older section of Lake Towuti. These factors include tectonically induced changes of the basin structure, changes in the hydrological environment and/or diagenetic processes. Quantifying these factors is beyond this study, but should be evaluated to establish the full context of sedimentary processes in Lake Towuti. Despite several uncertainties in this highly complex, non-linear sedimentary system, we see distinct cycles related to eccentricity and/or glacial/interglacial climate variability (a combination of 125-ka and 95 ka cycles) in our record. Even if the complete record of Lake Towuti's history was not covered by our investigations, we obtained a useful estimate of the range in SR, between 5 and 14 cm/ka.

Conclusions

Downhole logging data from Lake Towuti are valuable, but challenging in several aspects. First, low variability of physical properties of the sediments makes it difficult to distinguish between different classes in the cluster analysis. Cluster analysis, however, is an appropriate tool to distinguish major lithologic units, and is the only way to characterize the sediment physical properties and make determinations about lost core material (Fig. 4).

A second challenge is identification and interpretation of sedimentation cycles, a difficulty caused by the shortness of the record. The investigated magnetic susceptibility record has a length of 84 m and a maximum age of 903 ± 11 ka. This rather short record, with its limited number of sedimentary cycles, complicates astrochronological interpretation. Nevertheless, a link between different sedimentary environments and marine isotope stages is recognizable, albeit not very clear. The time interval spanning the logging datasets is dependent on the selection of the tracked amplitude in the spectra. For the magnetic susceptibility record, the time span covered by the tracked data is 772 ± 67 ka and likely represents Lake Towuti's sedimentological history most accurately (Fig. 6).

The third challenge is the determination of the calculated sedimentation rate, and the age-depth model, using only a single fixed data point (tephra T18). Despite accurate measurement of the date on this layer, errors of just a few 1000 years may result in shifts of the whole record. Thus, additional age-control points are required to construct a more detailed age-depth model from the logging data.

Acknowledgements This research project was funded by the German Research Foundation (DFG, Grant No. WO672/15-1. The Towuti Drilling Project was funded, in part, by grants from the International Continental Scientific Scientific Drilling Program (ICDP), the US National Science Foundation (NSF), the German Research Foundation (DFG, Grant No. ME 1169/2Rag6), the Swiss National Science Foundation (SNSF; 20FI21_153054/1 and 200021_153053/1), Brown University, Genome British Columbia, and the Ministry of Research, Technology and Higher Education (RISTEK). We thank the Towuti Drilling Project team for helpful discussions of results during and after post-drilling workshops. Our special thanks go to our technical staff, Thomas Grelle and Jan-Thorsten Blanke, for acquisition of geophysical downhole logging data on site, and Henrike Baumgarten and Cornelia Müller, for sample handling and laboratory work in the Leibniz Institute for

Applied Geophysics. We also appreciate the work of anonymous reviewers and editors.

Funding Open Access funding enabled and organized by Projekt DEAL.

References

An Z (2000) The history and variability of the East Asian paleomonsoon climate. Quart Sci Rev 19(1–5):171–187

Carolin SA, Cobb KM, Lynch-Stieglitz J, Moerman JW, Partin JW, Lejau S, Malang J, Clark B, Tuen AA, Adkins JF (2016) Northern Borneo stalagmite records reveal West Pacific hydroclimate across MIS 5 and 6. Earth Planet Sci Lett 439:182–193

Chuang C-K, Lo L, Zeeden C, Chou Y-M, Wei K-Y, Shen C-C, Mii HS, Chang YP, Tung Y-H (2018) Integrated stratigraphy of ODP Site 1115 (Solomon Sea, southwestern equatorial Pacific) over the past 3.2 Ma. Mar Micropaleontol 144:25–37

Costa KM, Russell JM, Vogel H, Bijaksana S (2015) Hydrological connectivity and mixing of Lake Towuti, Indonesia in response to paleoclimatic changes over the last 60,000 years. Palaeogeogr Palaeoclimatol Palaeoecol 417:467–475

De Deckker P (2016) The Indo-Pacific Warm Pool: critical to world oceanography and world climate. Geosci Lett 3(1):20

de Garidel-Thoron T, Rosenthal Y, Bassinot F, Beaufort L (2005) Stable sea surface temperatures in the western Pacific warm pool over the past 1.75 million years. Nature 433(7023):294

Gebhardt AC, Francke A, Kück J, Sauerbrey MA, Niessen F, Wennrich V, Melles M (2013) Petrophysical characterization of the lacustrine sediment succession drilled in Lake El'gygytgyn, far East Russian Arctic. Clim Past 9:1933–1947

Herbert TD, Peterson LC, Lawrence KT, Liu Z (2010) Tropical ocean temperatures over the past 3.5 million years. Science 328(5985):1530–1534

Konecky BL, Russell JM, Bijaksana S (2016) Glacial aridity in central Indonesia coeval with intensified monsoon circulation. Earth Planet Sc Lett 437:15–24

Lehmusluoto P, Machbub B, Terangna N, Rusmiputro S, Achmad F, Boer L, Brahmana SS, Priadi B, Setiadji B, Sayuman O, Margana A (1995) National inventory of the major lakes and reservoirs in Indonesia. Expedition Indodanau Technical Report, Edita Oy

Lisiecki LE, Raymo ME (2005) A Pliocene-Pleistocene stack of 57 globally distributed benthic $\delta^{18}O$ records. Paleoceanography 20(1):PA1003

Melles M, Bringham-Grette J, Minyuk P, Nowaczyk N, Wennrich V, DeConto R, Anderson PM, Andreev AA, Coletti A, Cook TL, Haltia-Hovi E, Wagner B (2012) 2.8 Million years of arctic climate change from Lake El'gygytgyn. NE Russia. Science 337(6092):315–320

Meyers SR (2014) Astrochron: an R package for astrochronology. https://cran.r-project.org/package=astrochron

Molinie AJ, Ogg JG (1990) Sedimentation rate curves and discontinuities from sliding-window spectral analysis of logs. Log Anal 31(06):370–374

Russell JM, Bijaksana S (2012) The Towuti drilling project: paleoenvironments, biological evolution, and geomicrobiology of a tropical Pacific lake. Sci Drill 14:68–71

Russell JM, Vogel H, Konecky BL, Huang Y, Melles M, Wattrus N, Costa K, King JW (2014) Glacial forcing of central Indonesian hydroclimate since 60,000 y BP. Proc Natl Acad Sci 111(14):5100–5105

Russell JM, Bijaksana S, Vogel H, Melles M, Kallmeyer J, Ariztegui D, Crowe S, Fajar S, Hafidz A, Haffner D, Hasberg A, Ivory S, Kelly C, King J, Kirana K, Morlock M, Noren A, O'Grady R, Ordonez L, Stevenson J, von Rintelen T, Vuillemin A, Watkinson I, Wattrus N, Wicaksono S, Wonik T, Bauer K, Deino A, Friese A, Henny C, Imran, Marwoto R, Ngkoimani LO, Nomosatryo S, Safiuddin LO, Simister R, Tamuntuan G (2016) The Towuti Drilling Project: paleoenvironments, biological evolution, and geomicrobiology of a tropical Pacific lake. Sci Dril 21:29–40

Russell JM, Vogel H, Bijaksana S, Melles M, Deino A, Hafidz A, Haffner D, Hasberg AKM, Morlock M, von Rintelen T, Sheppard R, Stelbrink B, Stevenson J (2020) The late quaternary tectonic, biogeochemical, and environmental evolution of ferruginous Lake Towuti, Indonesia. Palaeogeogr Palaeoclimatol Palaeoecol 556:109905

Stockhausen H, Zolitschka B (1999) Environmental changes since 13,000 cal. BP reflected in magnetic and sedimentological properties of sediments from Lake Holzmaar (Germany). Quat Sci Rev 18(7):913–925. https://doi.org/10.1016/s0277-3791(99)00005-0

Tamuntuan G, Bijaksana S, King J, Russell JM, Fauzi U, Maryunani K, Aufa N (2014) Variation of magnetic properties in sediments from Lake Towuti, Indonesia, and its paleoclimatic significance. Palaeogeogr Palaeoclimatol Palaeoecol 420:163–172

Team R C (2020) R: a language and environment for statistical computing. R Foundation for Statistical Computing, Vienna, Austria. https://www.R-project.org/

Vogel H, Russell JM, Cahyarini SY, Bijaksana S, Wattrus N, Rethemeyer J, Melles M (2015) Depositional modes and

lake-level variability at Lake Towuti, Indonesia, during the past ~ 29 kyr BP. J Paleolimnol 54(4):359–377
Vuillemin A, Friese A, Alawi M, Henny C, Nomosatryo S, Wagner D, Crowe SA, Kallmeyer J (2016) Geomicrobiological features of ferruginous sediments from Lake Towuti, Indonesia. Front Microbiol 7:1007
Wang Y, Cheng H, Edwards RL, Kong X, Shao X, Chen S, Wu J, Jiang X, Wang X, An Z (2008) Millennial- and orbital-scale changes in the East Asian monsoon over the past 224,000 years. Nature 451(7182):1090–1093
Ward JH Jr (1963) Hierarchical grouping to optimize an objective function. J Am Stat Assoc 58:236–244
Weedon GP (2003) Time-series analysis and cyclostratigraphy; examining stratigraphic records of environmental cycles. Cambridge University Press, Cambridge
Wicaksono SA, Russell JM, Bijaksana S (2015) Compound-specific carbon isotope records of vegetation and hydrologic change in central Sulawesi, Indonesia, since 53,000 yr BP. Palaeogeogr Palaeoclimatol Palaeoecol 430:47–56
Yan XH, Ho CR, Zheng Q, Klemas V (1992) Temperature and size variabilities of the Western Pacific Warm Pool. Science 5088:1643–1645

2.2 Peer-reviewed publication (Lake Ohrid)

Borehole logging and seismic data from Lake Ohrid (North Macedonia/Albania) as a basis for age-depth modelling over the last one million years

Ulfers, A., Zeeden, C., Wagner, B., Krastel, S., Buness, H., Wonik. T

Quaternary Science Reviews 276 (2022) 107295

Contents lists available at ScienceDirect

Quaternary Science Reviews

journal homepage: www.elsevier.com/locate/quascirev

Borehole logging and seismic data from Lake Ohrid (North Macedonia/Albania) as a basis for age-depth modelling over the last one million years

A. Ulfers [a, *], C. Zeeden [a], B. Wagner [b], S. Krastel [c], H. Buness [a], T. Wonik [a]

[a] Leibniz Institute for Applied Geophysics, Stilleweg 2, 30655, Hannover, Germany
[b] Institute of Geology and Mineralogy, University of Cologne, Zuelpicher Str. 49a, 50674, Cologne, Germany
[c] Institute of Geosciences, Christian-Albrechts-Universitaet zu Kiel, Otto-Hahn-Platz 1, 24118, Kiel, Germany

ARTICLE INFO

Article history:
Received 29 May 2021
Received in revised form
13 November 2021
Accepted 22 November 2021
Available online xxx

Handling Editor: A. Voelker

Keywords:
Downhole methods
Time-series analysis
Cyclostratigraphy
Seismic interpretation
Sediment properties

ABSTRACT

Robust age-depth models are essential for developing sophisticated interpretations of the sedimentological history in lake basins. In most cases, such models are created using an integrated geoscientific approach, including biostratigraphy, magnetostratigraphy and radiometric dating. In this study, we present an approach to construct age-depth models based on integrating downhole logging and seismic survey data when there are no samples available for dating. An example of this method is shown using data from Lake Ohrid (North Macedonia/Albania).

First, we interpret seismic data and correlate downhole logging data from three sites - DEEP, Pestani and Cerava - to the LR04 benthic stack. We cross-check the resulting age-depth models using cyclostratigraphic methods, which deliver sedimentation rates that are on the same order of magnitude. The maximum age of the investigated sediments is based on lacustrine seismic marker horizons and is approximately 1 million years at DEEP/Pestani and 0.6 million years at Cerava.

In the second step, we construct an artificial lithological log based on cluster analysis using the physical properties of the sediments and integrate it with the age-depth model. This allows an initial interpretation of the sedimentological history at Cerava and Pestani.

Our methodological approach cannot substitute classical sediment core investigations, but we suggest that this two-step approach be applied to future projects of the International Continental Scientific Drilling Program. It can rapidly provide preliminary results on age and sediment type and is particularly useful when datable material is not available.

1. Introduction

1.1. Aim of the study and state of the art

Many studies have been carried out on sediment cores from marine and terrestrial environments to gain insight into climate dynamics and its forcing factors during various geological periods. For the Quaternary, lakes have proven to be valuable climate archives since sedimentation rates are usually high, which yields good temporal resolution of the proxy data. The uniqueness of lake systems is challenging for individual studies and drilling projects, but the results offer the possibility to precisely determine the influence of local climate variability (Litt and Anselmetti, 2014; Melles et al., 2011; Russell et al., 2016; Stein, 2012; Verschuren et al., 2013; Zolitschka et al., 2013).

A crucial step towards interpreting lacustrine sediment records is the development of robust age-depth models. Currently, age estimates in lake drilling projects are often generated using core-based investigations (e.g., Goldstein et al., 2020; Nowaczyk et al., 2013; Shanahan et al., 2013; Stockhecke et al., 2014). This approach is time consuming and can be successful only if suitable core material is available. In some cases, tuning of geophysical downhole logging data has also been applied (e.g., Baumgarten et al., 2015; Baumgarten and Wonik, 2015). Further development

* Corresponding author.
E-mail addresses: Arne.Ulfers@leibniz-liag.de (A. Ulfers), Christian.Zeeden@leibniz-liag.de (C. Zeeden), wagnerb@uni-koeln.de (B. Wagner), sebastian.krastel@ifg.uni-kiel.de (S. Krastel), Hermann.Buness@leibniz-liag.de (H. Buness), Thomas.Wonik@leibniz-liag.de (T. Wonik).

https://doi.org/10.1016/j.quascirev.2021.107295

of an approach to gain chronological information independent of core material can be advantageous for future drilling projects, especially early in a drilling project, when detailed age models based on core material are not available.

One aim of this study is to evaluate the potential, challenges and limits of age-depth models created by using only geophysical downhole logging and seismic data. An example of this is shown for three drill sites (DEEP, Pestani, Cerava) in Lake Ohrid (North Macedonia/Albania). Age-depth models are created through correlation to a reference record. The reliability of the correlation is supported by seismic horizons; the quality of the age-depth models is evaluated using cyclostratigraphic methods on downhole logging data. A second goal is to integrate an artificial lithological log derived from cluster analysis with the time series. This link between the sediment characteristics and the age-depth models provides the first insights into the sedimentological history at the Pestani and Cerava drill sites, as there are no published records for those two sites. A flowchart summarizing the individual steps of all analyses is in the supplement (Fig. S1).

1.2. Site description and sedimentological characterization

Lake Ohrid is located on the Balkan Peninsula between Albania and North Macedonia. From north to south, it extends ~30 km, and from east to west ~15 km, with a maximum water depth of 293 m in the central basin (Fig. 1, Lindhorst et al., 2015). The highest proportion of water input comes from karst aquifers (~50%); direct precipitation and riverine inflow each account for ~25% (Matzinger et al., 2007; Wagner et al., 2010). The surface water has an electrical conductivity of ~200 µS cm^{-1} (corresponding to a resistivity of ~50 Ωm; Matter et al., 2010). Lake Ohrid is considered Europe's oldest lake, and thus, it is a valuable archive for studies that focus on changes in local (hydro)climate during the last 1.36 Myr (e.g., Francke et al., 2016; Wagner et al., 2014, 2019).

Sedimentation processes vary between the investigated drill sites DEEP, Pestani and Cerava (Fig. 1). Francke et al. (2016) presented a detailed sedimentological description of the upper ~250 m from the DEEP site. The sedimentary record consists of mainly undisturbed, continuous, hemipelagic sediments: These include calcareous silty clays deposited during interglacials, with higher primary production and reduced mixing of bottom waters, and clastic, silty clays deposited during glacials, when low primary production and enhanced mixing persisted. Thin (<5 cm), coarse silt/fine sand mass-movement deposits (MMDs) are interspersed sporadically, and several layers of volcanic ash allow tephrostratigraphic analysis (Francke et al., 2016; Leicher et al., 2016, submitted; Wagner et al., 2019).

A high-resolution, core-based age-depth model for the last 1.36 Myr is available for the DEEP site (Francke et al., 2016; Wagner et al., 2019). This age-depth model is based on the correlation of tephra with radiometrically dated proximal ash layers, tuning of the total organic carbon content to orbital parameters and cross-evaluation

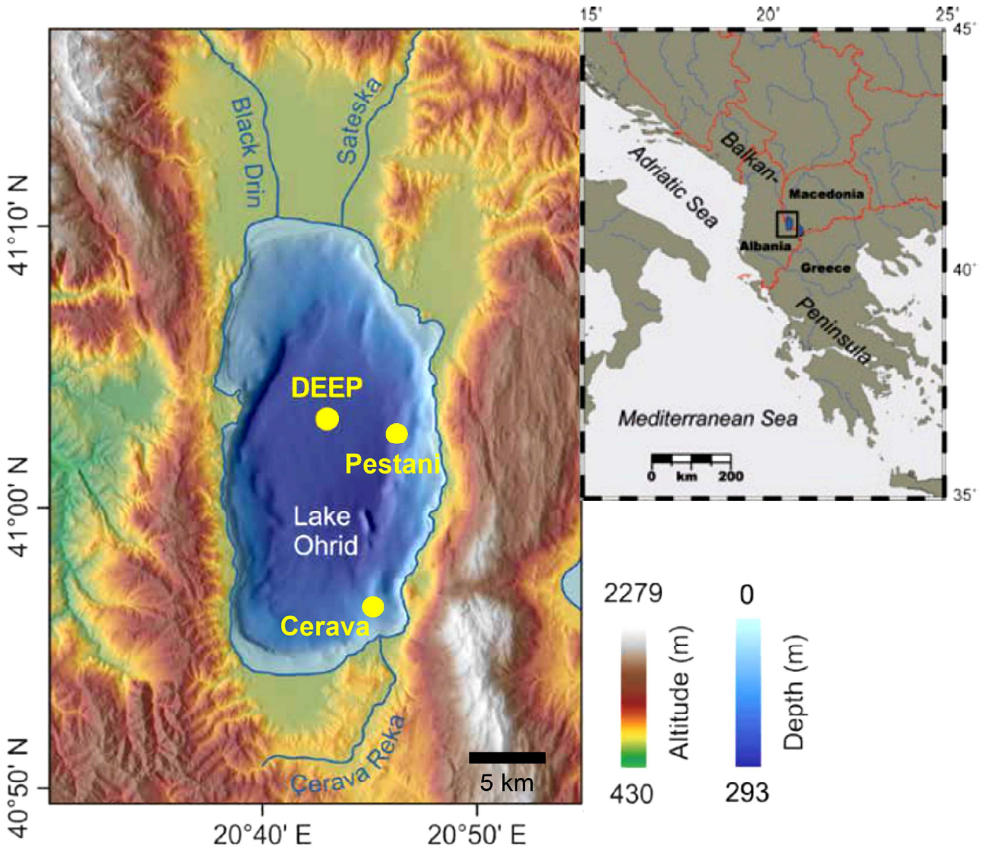

Fig. 1. Digital elevation map and bathymetric overview of Lake Ohrid. Drill sites investigated in this study are marked by yellow circles. Note the position of Cerava in relatively shallow water on the paleodelta close to the southern shore. In comparison, DEEP and Pestani are in the central basin and on its flank, respectively. Modified after Wilke et al. (2020); inset after Lindhorst et al. (2012). (For interpretation of the references to colour in this figure legend, the reader is referred to the Web version of this article.)

of two paleomagnetic age reversals. To date, cyclostratigraphic analysis of downhole logging data has been carried out only on the upper part of the record from the DEEP site, where an age-depth model for the last 630 ka was developed using sliding-window analysis of gamma ray data (Baumgarten et al., 2015).

Age-depth estimates or lithological descriptions of the sediment records from the Pestani and Cerava sites have not yet been published. Seismic interpretations of the Ohrid basin data have focused on the sedimentary and tectonic evolution of the lake (Lindhorst et al. 2010, 2015; Reicherter et al., 2011) and specialized topics such as MMDs (Lindhorst et al., 2012; Wagner et al., 2012b).

2. Material and methods

2.1. Fieldwork

An International Continental Scientific Drilling Program (ICDP) campaign in 2013 was based on several pre-site studies from the early 2000s onwards, which included investigations of short cores (e.g., Matzinger et al., 2007; Vogel et al., 2010a; Wagner et al., 2008) and hydroacoustic surveys (e.g., Lindhorst et al., 2012, 2015; Wagner et al., 2008). During the 2013 drilling campaign, several sites were drilled, some with parallel holes, and composite sediment cores were established. The DEEP site in the central basin (243 m water depth) was selected to obtain an undisturbed and continuous stratigraphic record. The maximum drilling depth was 569 m below the sediment surface, with a core recovery of 95%. The aim at the Pestani site (262 m water depth) was to reach sediments deposited directly above the bedrock at approximately 200 m below the sediment surface. The maximum drilling depth reached 194.5 m with a sediment core recovery of 91%. The Cerava site is located on a lake terrace (125 m water depth) close to the southern shore and was selected to investigate lake level fluctuations that have been indicated by clinoform structures in the subsurface. The maximum drilling depth was 90.5 m below the sediment surface, with a core recovery of 97%. All holes were drilled with a diameter of 149 mm and water-based mud (Baumgarten et al., 2015). Further information about the drilling operations is given in Wagner et al. (2014).

Geophysical downhole logging by the Leibniz Institute for Applied Geophysics acquired continuous datasets of physical properties at the DEEP, Pestani and Cerava sites. The measured parameters were natural gamma radiation (GR), including its components (uranium (U in ppm), potassium (K in %) and thorium (Th in ppm) concentrations), magnetic susceptibility (MS), deep resistivity (R), seismic velocity (Vp), borehole diameter (Cal) and borehole inclination (Dip) (Fig. 2, S2, S3 and S4). As common in unconsolidated (lacustrine) sediments, the GR probe was run inside the drill pipe, while all other probes were run in the open hole after successive lifting of the drill string. We consider the attenuation of the GR signal through the drill pipe as negligible, because it is a systematic error and does not affect the relative change of GR between the different sediment types. The uppermost 30 mblf could not be logged by tools which require open-hole conditions, since drill pipes were kept in the hole to allow downhole probes to enter. This procedure minimizes the risk of a borehole collapse and associated issues such as the inaccessibility of deeper sections or even probe loss. After geophysical downhole logging was completed, all drill pipes were pulled out and the well is abandoned. The vertical resolution of the geophysical downhole logging tools that were used is in the range of ~10–20 cm. A detailed description of logging procedures (e.g., logging speed, diameter of probes, etc.) is given in Baumgarten et al. (2015). General principles of measurements are described by Rider and Kennedy (2011). Data acquisition and (pre)processing were carried out using GeoBase® (Antares, Germany) and WellCAD® (Advanced Logic Technology, Luxembourg).

Multichannel seismic survey data used in our study were recorded with different air gun specifications in 2007 and 2008. In 2007, acquisition gave deeper penetration, whereas in 2008, a higher resolution was preferred (for details see Lindhorst et al., 2015). A total of 47 seismic lines were collected of which we used six in this study (Fig. S5). We used OpendTect© software for seismic interpretation in this study.

2.2. Data processing

The time-depth conversion of seismic profiles was executed with SeisSpace® ProMAX® Seismic Processing Software. The sound velocity of sediments is from average-filtered Vp logs at each site (Figs. S2, S3 and S4), and one average Vp value was calculated every 10 m (Table S1). We used 1480 m/s as the sound velocity of the water body. The time section was shifted until the lake floor reflection coincided with the bathymetric depth after conversion to account for errors in trigger times and/or deviating sound velocities in the water column. The conversion is not valid for complete profiles but restricted to the proximal areas of the drill sites because the complex geologic setting (especially in the lateral parts of the basin) suggests lateral velocity variations. Thus, the correlations between borehole seismic profiles were conducted in the time domain (Figs. S6 and S7).

We traced lacustrine sediment layers from the DEEP to Pestani and Cerava sites. Suitable horizons have to meet two main criteria: They must be continuous between the respective sites, i.e. neither interrupted by faults nor by sedimentary structures like slide deposits. They must be clearly distinguishable from adjacent layers. Tracing was conducted semi-manually using automated tracing (including visual verification) in the central basin and manual picking of sediment horizons in complex settings. In automated tracing, only some points (=seeds) of a horizon are picked and the OpendTect© software follows the horizons to a certain threshold. This technique enables fast tracking, provided that the two criteria described above are fulfilled.

Cyclostratigraphic analyses and sedimentation rate estimates of the upper part (0–240 mblf) of the DEEP site are discussed in Baumgarten et al. (2015). Our cyclostratigraphic investigations were carried out using the 'astrochron' package for the R programming language (Meyers, 2014; R Core Team, 2020). The R code is available in the supplementary material. To evaluate amplitude variations, we used spectral analysis (evolutive harmonic analysis) of (un)tuned records (Thomson, 1982) and wavelet analysis (Gouhier et al., 2019). The latter was conducted using a morlet mother wavelet. Tuned GR data was sampled evenly spaced at 0.5 ka resolution. Other more specific methods include 'testPrecession', an astrochronological testing method, which compares observed precession-scale amplitude modulation to that expected from the theoretical eccentricity solutions. To reduce artificial eccentricity modulations during tuning and data processing, this method implements a series of filters and evaluates the statistical significance of the results using Monte Carlo simulations (Zeeden et al., 2015). The astronomical solution we used is from Laskar et al. (2004). We applied the 'timeOpt', and the 'timeOptTemplate' methods to investigate amplitude modulation and frequency ratios in stratigraphic data and to further determine an optimal time scale for the investigated record. In this study, we utilized linearly decreasing sedimentation rate models with different means and slopes; each of these represents a linearly decreasing sedimentation rate with increasing depth (Meyers et al., 2019).

Cluster analysis was performed using WinSTAT® software for Microsoft Excel®. We created continuous lithological logs for the

physical properties (GR, Th/K, MS, R and Vp). The GR depends on the overall detrital clastics content, while the Th/K ratio is a more specific indicator for different types of clay minerals such as potassium rich feldspar or heavy thorium-bearing minerals (Rider and Kennedy, 2011). MS is determined by the magnetic response (diamagnetic, paramagnetic and ferromagnetic) of the sediment and is mostly used as an indicator for specific mineral compositions. R and Vp are sensitive to porosity and texture of the sediments and give indications on e.g. sorting and grain size (Buecker et al., 2000; Rider and Kennedy, 2011). We used Ward's method as a cluster distance measure (Ward, 1963) and estimated the physical properties for each class in the resulting dendrogram. Subsequently, the classes were colour-coded, imported into Well-CAD® software and compared with core description data (if available).

3. Results

3.1. Logging data

The interval of interest for this study is 0–335 m below lake floor (mblf) at the DEEP site. This interval represents the major part of the lacustrine facies. The lower boundary is given by the interconnection of seismic horizons (Figs. S6 and S7). Although lacustrine sediments occur below this boundary, we refrain from characterizing these parts because the correlation of horizons based on hydro-acoustic data is not unambiguous (see chapter 3.2 Seismic correlation'). The logging data at this site show prominent quasi-cyclicity (Fig. 2), which is particularly visible in the GR and its components (U, K and Th concentrations, as published by Baumgarten et al. (2015) for the upper 240 mblf). The period of the cycles in the GR log decreases below ~260 mblf. MS and R show similar cyclic patterns but are less distinctive above ~170 mblf than below. The upper sections of the MS and R records are characterized by overall increases towards the top. Vp decreases from 38 mblf (top of log) to ~ 110 mblf, where it reaches a minimum of 1330 m/s. Below ~110 mblf, Vp values increase with depth. On average, Vp is 1515 ± 73 m/s in the investigated part of the record. The caliper measurements are relatively constant with some minor peaks and indicate widening of the borehole in the upper part, which is characteristic of boreholes in unconsolidated material. The inclination of <2.5° shows that the drill hole is relatively vertical.

For similar reasons as for DEEP (see above), the interval of interest at Pestani is 0–121.5 mblf, while we investigate the complete record (0–90 mblf) from Cerava. The GR and the U, K and Th concentrations at both sites feature similar cyclic patterns as those at the DEEP site (Figs. S3 and S4). Compared with that of the GR logs, MS and R show similar but less pronounced cyclicity. As at DEEP, increasing values of MS and R occur towards the top in the upper ~70 mblf at Pestani. At Cerava, a sudden increase in R below ~76 mblf coincides with an amplitude change in MS. The sonic velocities at Pestani and Cerava are relatively constant and increase slightly with depth. At both sites, the sonic velocities are low, and Vp averages 1430 ± 20 m/s (min = 1275 m/s; max = 1590 m/s) in the interval of interest at Pestani and 1465 ± 41 m/s (min = 1200 m/s; max = 1730 m/s) at Cerava. The caliper measurements at Pestani indicate that higher GR values correlate with smaller borehole diameters, particularly in the upper ~100 mblf. At Cerava, this correlation is much weaker and present in only the upper 60 mblf. In general, the borehole diameter decreases with depth at both sites. The inclination of both boreholes is commonly less than 5°, defining almost vertical drilling paths.

At all sites, the GR log features the most distinct cyclic patterns compared with other logged parameters. This is why we focus on GR for cyclostratigraphic analysis and time estimates (Chapters 3.3 'Correlation of GR and the LR04 benthic stack' and 3.4 'Cyclostratigraphy'). For the construction of artificial lithological logs, we combine various parameters to make inferences about sediment characteristics (Chapter 3.5 'Cluster analysis'). The integration of age information and sediment characteristics allows an initial description of the sedimentological history at the investigated sites.

3.2. Seismic correlation

Fig. 3 shows depth-converted seismic profiles crossing the investigated sites. While the sediment layers at DEEP are relatively horizontal and well stratified, the geologic situation in the lateral part of the basin is more complex. Disturbed sediments west of Pestani impede tracing of some layers between Pestani and DEEP (Fig. S6). However, certain horizons in the upper and lower parts of the Pestani record can be correlated to DEEP, and age information can be transferred. The dark blue horizon represents the lowermost reliable reflector that connects DEEP and Pestani sites and thus defines the limit of the intervals of interest for this study. Sediments below this horizon are not marked by strong reflectors and interfere with seismic multiples, making a reliable tracing of primary reflectors impossible (Fig. S6).

The correlation of horizons between DEEP and Cerava is hampered by various MMDs in the southern basin (southern part of profile 0820 in Fig. S7). A fault system on the slope of the Cerava plateau adds to the complexity of the setting, and unambiguous tracing of horizons through this zone is impeded (profile 0826 in Fig. S7). Nevertheless, the seismic correlation provides a rough framework for the GR correlation in the lower half of the Cerava record.

Despite not directly affecting the tracing of horizons, several clinoform structures and/or MMDs close to Cerava add complexity to the geology (southern part of profile 0804 in Fig. S7). The main bodies of these structures are located several hundred metres south of the drill site, but their lateral extensions reach the borehole. This interbedding of a different sediment type has a direct influence on the measured parameters in the downhole logs. Depths of all seismic horizons are given in Table S2.

3.3. Correlation of GR and the LR04 benthic stack

To establish a chronology of the Lake Ohrid sedimentation history, the GR logs from the DEEP, Pestani and Cerava sites were correlated with the LR04 stack of Lisiecki and Raymo (2005; Fig. 4). The correlation for the DEEP site follows Baumgarten et al. (2015) and is now extended to ~1 Ma. Most parts of the records from Pestani can also be correlated with the LR04 benthic stack. For Cerava, an unambiguous correlation of the GR record with the LR04 benthic stack is not possible. The more complex geological setting of the Cerava plateau directly influences the cyclic pattern of the GR record. For example, the lateral extension of a clinoform structure at approximately 70 mblf disrupts lacustrine sedimentation and causes a disturbance of the GR signal. At Cerava, information from the seismic correlation is necessary to give an approximate timeframe for our interpretations.

Based on the GR log correlation, the sedimentation rates (SRs) at all three sites were calculated in "cm/ka" for each marine isotope stage (MIS; Fig. 4) using equation (1).

$$SR = \frac{\Delta Depth\ [mblf] * 100}{\Delta Time\ [ka]} \quad \text{(Eq 1)}$$

The mean SR at DEEP is 34.8 cm/ka. The linear trendline of the SR shows an upward increase (dashed blue line in Fig. 4). Moreover, the SR (blue line) in glacial periods is slightly enhanced

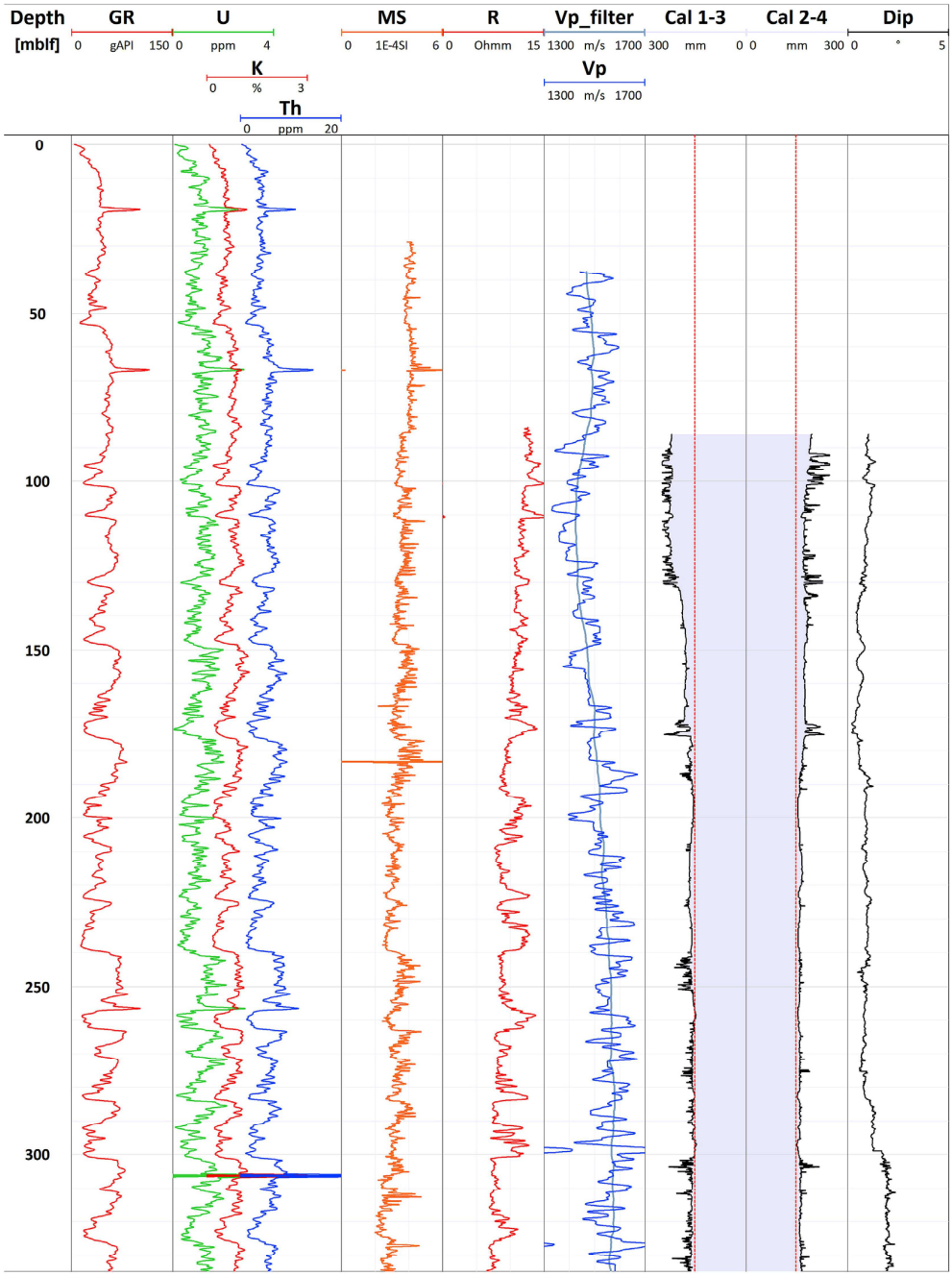

Fig. 2. Section of the downhole logging data from the DEEP site. GR has a distinct cyclic pattern. R increases towards the top in the upper ~170 mblf (probably due to fluid/sediment interaction). Vp increases with depth below ~110 mblf. Abbreviations: mblf = metres below lake floor, GR = natural gamma radiation, U, K and Th concentrations, MS = magnetic susceptibility, R = deep resistivity, Vp = sonic velocity, Vp_filter = sonic velocity filtered with a moving average over 50 m, Cal 1–3, Cal 2–4 = caliper logs/borehole diameter, Dip = dip of drill path, the size of the drill bit is indicated as red dashed line on caliper logs. (For interpretation of the references to colour in this figure legend, the reader is referred to the Web version of this article.)

(mean = 35.5 cm/ka) compared with that in neighbouring interglacial periods (mean = 31.2 cm/ka; e.g., MIS 20, 18, 14 and 06 in Fig. 4).

The SR at Pestani (mean = 13.7 cm/ka) is lower than that at DEEP. The increase in SR towards the upper part of the record is not as pronounced as at DEEP. The SR is slightly increased in interglacials (mean = 14.5 cm/ka) compared with neighbouring glacials (mean = 12.8 cm/ka). MIS 14 exhibits a particularly low SR of 2.7 cm/ka.

The mean SR at Cerava is 15.3 cm/ka. As at DEEP, the SR is

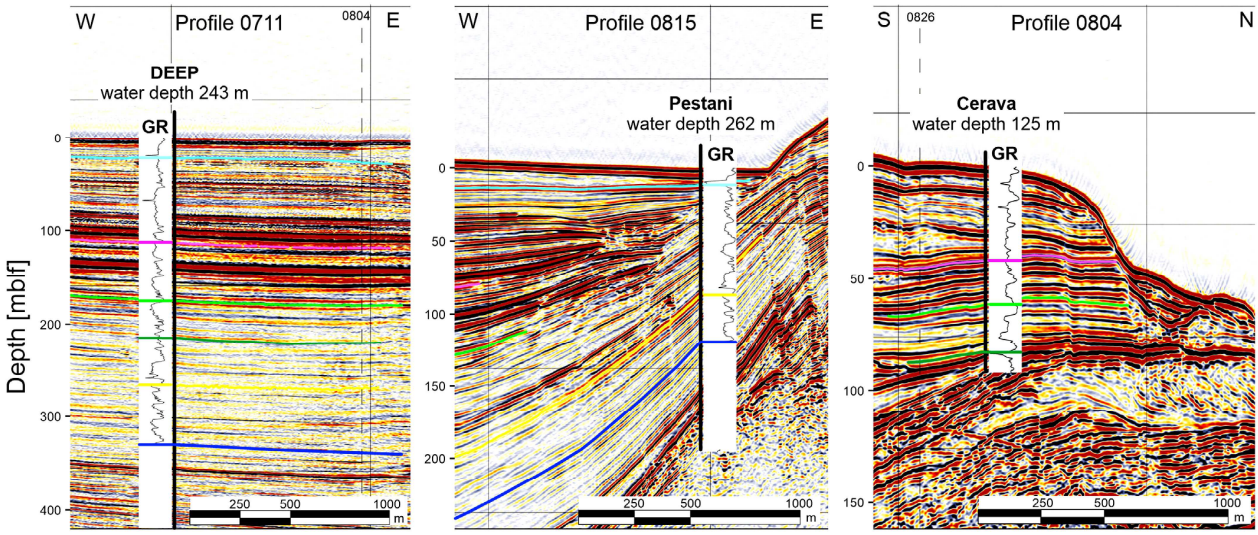

Fig. 3. Seismic profiles at the DEEP, Pestani and Cerava sites after depth conversion. The basis for the correlations between boreholes is shown in Figs. S6 and S7. Schematic natural gamma ray (GR) logs are shown next to each borehole. A detailed plot of GR correlations between all sites, including the coloured seismic horizons, is shown in Fig. 4. Location of seismic lines in an overview map of Lake Ohrid in Fig. S5. Seismic profiles are actually longer, here we show only the vicinity of the respective sites.

enhanced during glacials (mean = 16.0 cm/ka) compared with interglacials (mean = 14.7 cm/ka). Notably, the SR maxima are 32 cm/ka during MIS 6 and 37 cm/ka during MIS 1.

3.4. Cyclostratigraphy

At the DEEP site, the investigated GR record has a length of 335 m (Fig. 5a). As a result of the sliding window approach used for evolutive harmonic analysis, the top and bottom part of a record do not have representative spectra. A similar approach is used in Baumgarten et al. (2015) and the upper 240 mblf are separated into two intervals (45–110 mblf and 110–240 mblf), which are dominated by spectral peaks of 45 m and 30 m wavelengths, respectively. Because cyclostratigraphic features of the upper part are discussed in Baumgarten et al. (2015), we focus on the lower part of the record at DEEP, the corresponding logs obtained at the Pestani and Cerava sites, and additionally apply wavelet analysis.

The dominance of a single frequency in the upper part of the amplitude spectrum at DEEP is replaced by a more complex composition of orbital signals below ~200 mblf (Fig. 5b). Although a strong influence of the 30 m cycle is still present, prominent signals with wavelengths of 75 m and 20 m appear in the record. At depth intervals in which these frequencies attenuate (260-230 mblf and below 280 mblf), high-frequency signals with wavelengths of 13–10 m and 8 m emerge in the record. Wavelet analysis shows a similar shift towards higher frequencies at ~550 ka, where shorter period signals begin to superimpose the long-period signals (Fig. 5c).

The evolutive spectrum for Pestani indicates a similar complexity of dominant cycles with depth (Figs. S8 and S10). A difference from the DEEP site is most evident in a short interval of the upper part (30-20 mblf); various short cycles appear at Pestani, whereas no such configuration of cycles in observable in the upper ~200-45 mblf at DEEP. The limits of the sliding window approach prevent the comparison of the uppermost parts (45-0 mblf at DEEP and 20-0 mblf at Pestani). The main cyclicity throughout the Pestani record has a wavelength between 20 m and 13 m. Other intervals show different spectral properties; especially in the upper (<30 mblf) and the lower depth sections (>90 mblf), where wavelengths of 10 m and 6.5 m occur, respectively.

At Cerava, the clear dominance of any particular spectral peak in the amplitude spectrum is challenging to determine (Figs. S9 and S10). The upper part (55-20 mblf) shows a dominant cyclicity of 12.5 m wavelength, but this peak splits between 30 mblf and 45 mblf. In the lower part (>55 mblf), this dominant signal shifts towards longer periods (17 m), and other cyclicities (9 m and 7 m) appear in the record. As at DEEP, the complexity of cycle components increases with depth, and a single dominant wavelength is not present.

Overall, the GR record at DEEP exhibits a high potential for high-quality cyclostratigraphic investigations, while the patterns from Pestani and especially Cerava are more challenging. At all three sites, the complexity of the orbital signal increases with depth, thus making interpretation more difficult.

We use the timeOptTemplate method (Meyers 2015, 2019) on GR logs from DEEP and Pestani to estimate average SR, utilizing a model with linearly increasing SR (Figs. S11 and S12). Both the average SR and the linearly increasing trendlines of SR towards the top are used to test the depth-age estimates from direct correlation to the LR04 benthic stack (see the mean SR and the quasi-linear trend in Fig. 4, dashed blue lines). The results of both methods and calculated SRs are shown in Table 1.

Using the timeOptTemplate method at DEEP, the best fit for average SR is 35.8 cm/ka (min = 28.7 cm/ka; max = 44.0 cm/ka; Fig. S11), whereas the mean SR derived from direct correlation is 34.8 cm/ka. Comparing the linear trendlines of SR from both methods, the similarity of slopes suggests an almost perfect match of the timeOptTemplate with the LR04 to GR correlation (Fig. S13). The age of sediments at 335 mblf derived through the timeOptTemplate method is estimated to be 935 ka. From Fig. 4, the estimated age at this depth using the direct GR to LR04 correlation is approximately the base of MIS 27 (≙ 982 ka).

At Pestani, the average SR estimates of both methods differ by 2.5 cm/ka: The average SR derived by timeOptTemplate is 16.2 cm/ka (min = 14.4 cm/ka; max = 18.0 cm/ka; Fig. S12), whereas the SR from direct correlation is 13.7 cm/ka. As a result, the age estimate

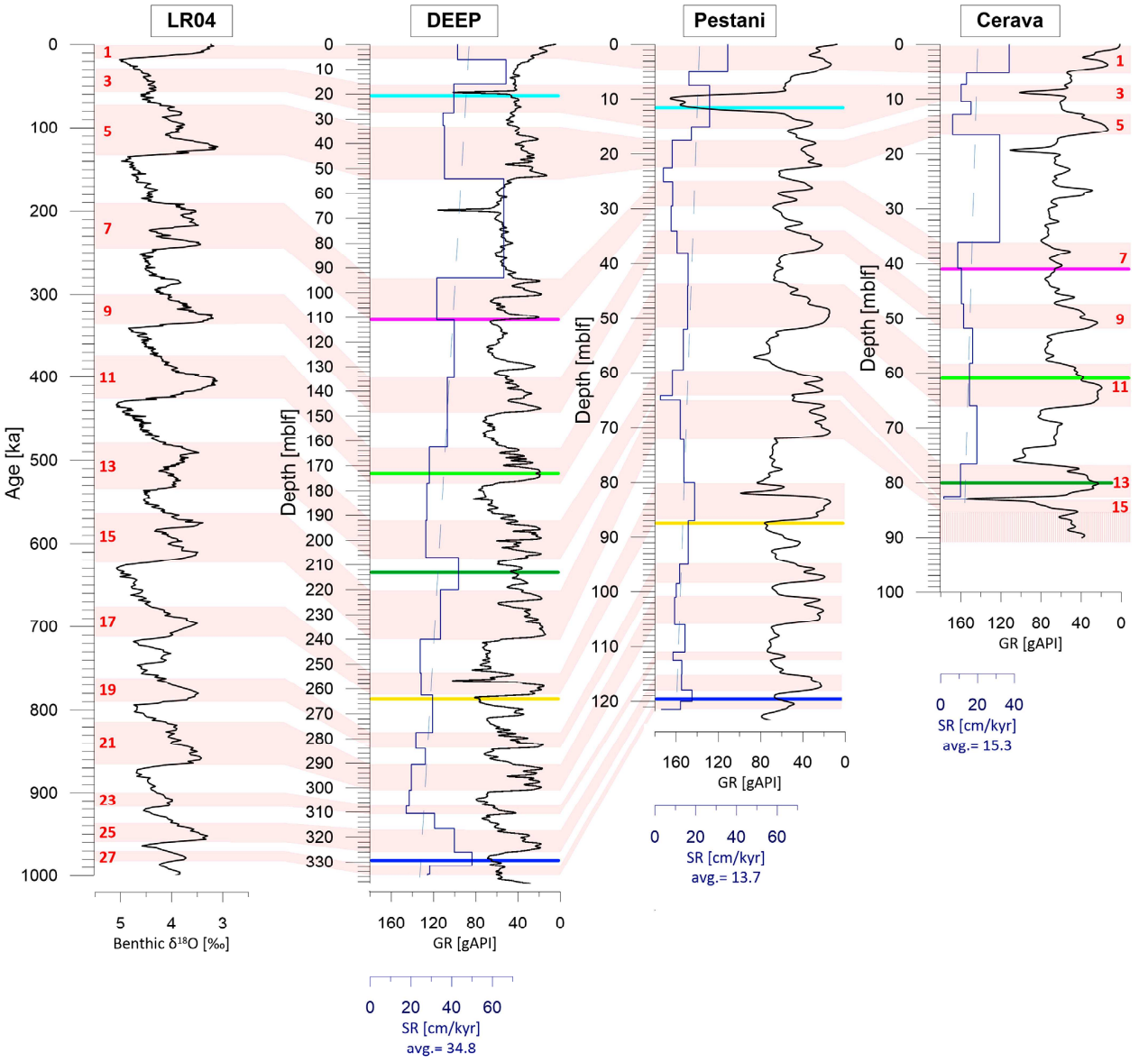

Fig. 4. Correlation of the LR04 benthic stack (Lisiecki and Raymo, 2005) with GR logs from Lake Ohrid. Tiepoints equal the MIS borders. Sedimentation rates (SRs) are plotted in blue. Dashed blue lines are linear trendlines of SRs. Interglacials are indicated in red numbers. Coloured lines are from seismic interpretations (Fig. 3, Table S2). Note that horizons of seismic investigations provide only a rough framework for log-based interpretations. Due to the inaccuracy of time-depth conversion in seismic processing and the different depth scales, they can deviate by several metres from the interpretation of the GR correlation. The interpretation of the upper ~240 mblf at DEEP is similar to the one in Baumgarten et al. (2015). Note the enhanced thickness of marine isotope stage (MIS) 6 at the DEEP and Cerava sites. It is likely that this effect is caused by mass-movement deposits and does not reflect only detrital SRs. Scales for benthic $\delta^{18}O$ and GR are inverted. (For interpretation of the references to colour in this figure legend, the reader is referred to the Web version of this article.)

for a depth of 121.5 mblf is 751 ka for timeOptTemplate but approximately the base of MIS 27 (≙ 982 ka) for direct GR to LR04 correlation. The age is therefore underestimated using the timeOptTemplate approach at the Pestani site. This demonstrates the limitations of this method, as orbital cycles may not be as well preserved at Pestani as they are at DEEP. The generally lower sedimentation rate (with strong minima in e.g. MIS 6 and 14, Fig. 4), and the proximal location of Pestani in the lake basin are two important factors leading to a less accurate recording and preservation of orbital cycles. Since this also applies to Cerava and due to the even shorter record, we do not apply the TimeOptTemplate to Cerava.

3.5. Cluster analysis

Cluster analysis for DEEP was performed using GR, Th/K, MS, R and Vp data over full depth range (Fig. S14), however, we here refer only to the interval of interest (0–335 mblf; Fig. 6). The division into cluster classes is based on dendrograms (Fig. S15) and resulted in well-distinguishable sediment types. The two classes in the interval

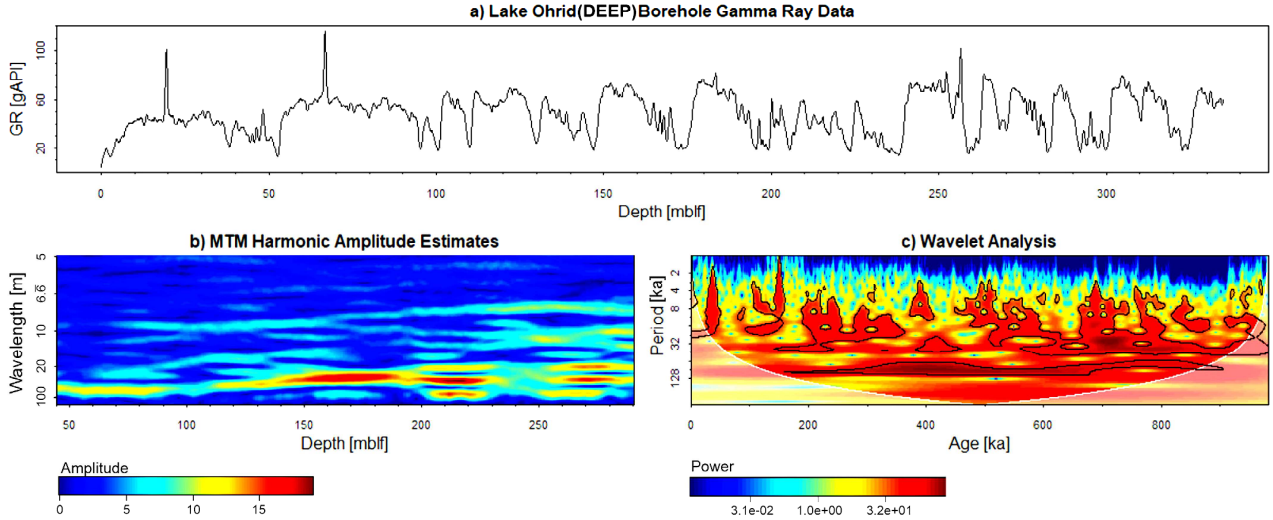

Fig. 5. GR log from the DEEP site (a) and resulting evolutive harmonic analysis (b). Due to window size of 90 m the upper and lower 45 m are missing. Wavelet analysis (c) was performed on the age scale using tie points as shown in Fig. 4.

Table 1
Comparison of two different methods to estimate average sedimentation rates (SRs) and ages at the base of the interval of interest. Values are in cm/ka and ka, respectively.

	DEEP		Pestani	
	SR [cm/ka]	Age at 335 mblf [ka]	SR [cm/ka]	Age at 121.5 mblf [ka]
TimeOptTemplate method	35.8 (28.7–44.0)	935	16.2 (14.4–18.0)	751
Direct GR to LR04 correlation (Fig. 4)	34.8 (17.6–66.7)	982	13.7 (2.7–35.7)	982
Difference in % between both methods	2.8	4.9	16.7	26.7

of interest differ mainly in their GR and R (Fig. 6 and S14). The mismatch between "metres composite depth" (mcd), used in the core descriptions, and "metres below lake floor" (mblf), used in downhole logging, is indicated by grey connections for the interval of interest in Fig. 6. Depth matching for the upper ~250 mblf was performed by Franke et al. (2016) using K counts from XRF core scanning and K concentrations from spectral gamma radiation downhole measurements. We followed the same procedure for the part below 250 mblf. The largest offset of 8.9 m is located in the deeper section (~324 mblf) while almost no shift occurs in the interval of 215–220 mblf (Table S3). These shifts are often caused by expansion effects in the sediment cores, e.g. due to gas release (e.g. Friese et al., 2017; Wagner et al., 2009).

The artificial lithological log and the core description are highly similar. Despite the lower resolution of the artificial log, the correspondence with the core descriptions of Franke et al. (2016) is evident. Strong contrasts in sediment properties are beneficial for grouping sediment types into different classes in a cluster analysis. The "slightly calcareous silty clay" class from the core description depicts a transitional component from calcareous to non-calcareous material and cannot be differentiated in the cluster analysis.

We applied cluster analysis with the same set of parameters and cluster distance measurement methods for Pestani and Cerava (Fig. S14). In both cases, comparison with core material is not possible since the core lithologies are not published.

4. Discussion

4.1. Logging data

Quasi-cyclicity is expressed in all sediment parameters presented in this study and in various proxy data from direct core measurements at the DEEP site (e.g., detrital input, pollen, total inorganic carbon, δ^{18}O-calcite and δ^{13}C-calcite; Wagner et al., 2019). Post-drilling factors, such as fluid intruding the pore space, can bias the downhole logging properties and may weaken or disturb the amplitude of sedimentary proxies related to paleolimnology and paleoclimatology. At DEEP this effect is visible in R above 170 mblf where lake water substitutes/dilutes pore water in the sediment. As the lake water has a relatively higher R of 50–67 Ωm (Wagner et al., 2017) compared to R of the sediment, the average R in the sediment increases. The process of lake water superimposing in situ sediment characteristics is stronger in the upper part, where the longest exposure time to lake water occurred. Similar effects are indicated in the R log at Pestani (Fig. S3). These are challenges to consider in e.g. the interpretation of the cluster analysis.

Another quasi-linear feature at DEEP is the downward increase in Vp below ~110 mblf, which is likely caused by increasing compaction with depth. However, compared with the velocity of typical shale (Erickson and Jarrard, 1998; Rider and Kennedy, 2011), the mean velocity at DEEP is relatively slow (1515 ± 73 m/s), indi-

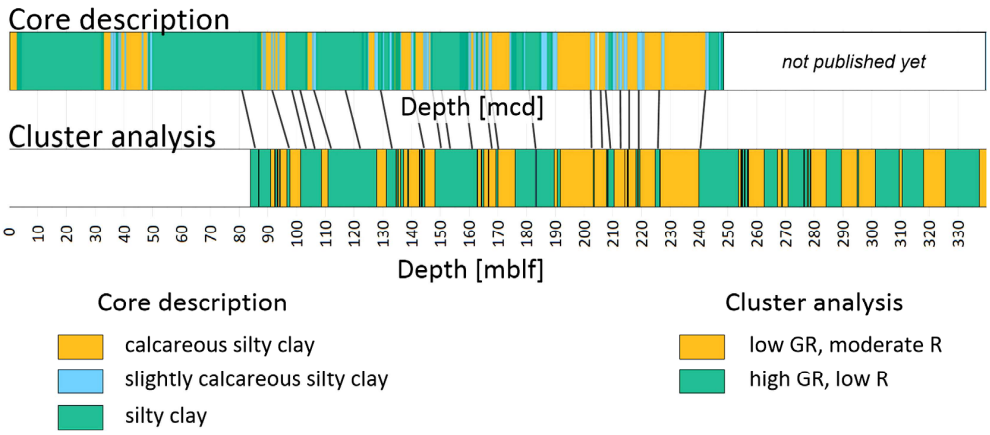

Fig. 6. Comparison of the core description and artificial lithological logs derived from cluster analysis at the DEEP site, showing a high similarity for most parts. Cluster analysis from downhole measurements (in metres below lake floor, mblf) and core descriptions (in metres composite depth, mcd) after Francke et al. (2016) are connected by grey lines indicating depth shifts as listed in Table S3. The legend for cluster analysis is based on values in Fig. S14 and only valid for DEEP down to 335 mblf. Abbreviations: GR = natural gamma radiation, R = deep resistivity. "Slightly calcareous silty clay" is not differentiated in the cluster analysis.

cating highly unconsolidated material. The Vp logs at Pestani and Cerava exhibit similar features (Figs. S3 and S4).

A possible explanation for the minimum of 1330 m/s around 110 mblf at DEEP is a combination of two interrelated factors. Firstly, formation of gas in the pore space. Wagner et al. (2009) describe notable CH_4 release and gas expansion of sediments from piston cores in Lake Ohrid. Secondly, an increase in the caliper of the borehole in this part. The minimum in Vp cannot be accounted to a drastic change in lithology, as the sediments in this area resemble the overall pattern in Lake Ohrid (calcareous silty clay and silty clay; Fig. 6). Low values in Vp are common in (lake) environments with highly unconsolidated material. E.g. in a significant part of the sediments in the upper ~100 m of Lake Towuti (Indonesia), the Vp is below 1400 m/s (Ulfers et al., 2021) and Warrick et al. (1974) describe P-wave velocities of 1360 m/s of unconsolidated mud in the San Francisco Bay.

At the sites other than at DEEP, the caliper logs exhibit a correlation to GR. It implies that sediments with a low GR value can be washed out more easily than sediments with higher GR values. This effect is most important for the low-GR material representing calcareous silty clay deposited during interglacials (Francke et al., 2016). Through the process of outwash, the GR measured in the borehole decreases even further. This "amplification" of the low-GR signature results in a better differentiation of the two main lithologies. This feature intensifies in the upper part of the boreholes.

4.2. Correlative age-depth models

To support the age-depth relationships, we use prominent seismic reflectors deposited during different MISs. Depth shifts between the interpreted seismic horizons and the MIS horizons derived from the GR to LR04 correlation vary by up to several metres (Fig. 4). This is mainly due to the inaccuracy of time-depth conversion in seismic processing and the different depth scales used in seismic investigation and downhole logging. However, the correlation of prominent seismic reflectors at the investigated sites provides a reliable framework for age estimation. Not all identified horizons at the DEEP site are traceable throughout the Ohrid basin. Thinning of sedimentary units beneath the seismic resolution towards the lateral parts of the basin may result in apparent terminations of reflectors. This is relevant for the Pestani site; tectonic features west of the Pestani site further hamper tracing of horizons between Pestani and DEEP (Fig. 3 and S6). The correlation of seismic reflectors from DEEP to Cerava is hindered by tectonically induced slides in the southern central basin (Lindhorst et al., 2012) and by tectonic structures between the southern central basin and the Cerava plateau (Fig. 3 and S7). Despite this being a factor of uncertainty, we suggest using the horizons in Fig. 3 as a framework for the more detailed GR to LR04 correlation (Fig. 4).

In general, the correlation of GR logs from DEEP and Pestani to the LR04 benthic stack is possible, with a few difficulties in the upper part (MIS 1–6). The GR logs from all sites are displayed on a common age scale in Fig. 7. The LR04 benthic stack is very similar to the GR log from DEEP and somewhat less similar to that from Pestani.

Correlating the record from Cerava to both the LR04 benthic stack and the GR logs from the other sites is difficult. In particular, the lower part of the record (older than MIS 11) is complex, and the resulting age-depth model should be considered preliminary.

A comparison of our age-depth model based on geophysical data at DEEP with an independent core-based model from Wagner et al. (2019) shows high similarity between the age models (Fig. 8). We estimate the first age-depth models for the Pestani and Cerava sites using only geophysical downhole logging and seismic data (no sediment core data available). At Pestani, the maximum age of investigation is the base of MIS 27 (≙ 982 ka) at 121.5 mblf. At Cerava, the oldest part of the record is marked by the MIS 14/15 boundary (≙ 563 ka) at 83 mblf. The accurate age of the lowermost part (83–90 mblf) of the record remains unclear at Cerava; thus, the exact position of the MIS 15/16 boundary, if it was recorded as such, is also unclear.

Note that the "metres below lake floor" (mblf) used in this study deviates from the "metres composite depth" (mcd) used in studies using core material (Francke et al., 2016; Wagner et al. 2014, 2019) because the core splicing and sediment expansion after core recovery will naturally result in different composite depths than the borehole logging data (Figs. 6 and 8 and Table S3).

Our data indicate that there are no hiatuses at the DEEP site, which is confirmed by sediment core data (Francke et al., 2016; Wagner et al., 2019). Geophysical downhole logging data are continuous, but detecting small sedimentological hiatuses in the logs may not be possible. Specifically, at Pestani and Cerava site,

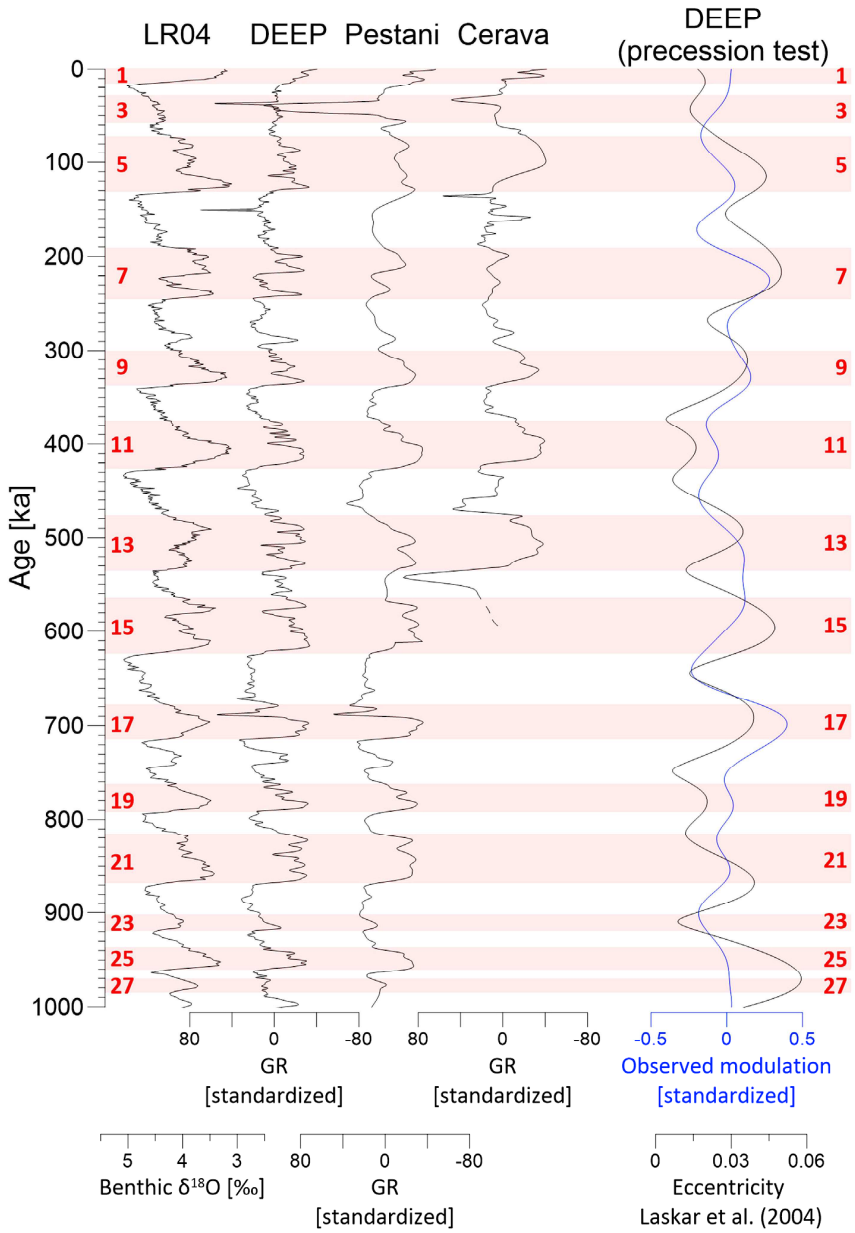

Fig. 7. LR04 benthic stack (Lisiecki and Raymo, 2005) compared to tuned, normalized to mean, GR logs from investigated sites. MIS interglacials are numbered in red. GR is without scale since data were linearly detrended. Whereas the LR04 benthic stack, DEEP GR and Pestani GR correlate relatively well, the sedimentological setting at Cerava complicates the correlation. The dashed line at Cerava during MIS 15 indicates that the record is continuing further down, but we do not assign a definite age to those lowermost ~7 m of Cerava. The precession test for the DEEP site is relevant for the confidence of cyclostratigraphic methods. Blue: observed precession-scale amplitude modulations. Black: theoretical eccentricity from Laskar et al. (2004). See Chapter 4.3 for interpretation. (For interpretation of the references to colour in this figure legend, the reader is referred to the Web version of this article.)

there are stages with lower-than-average SRs (Fig. 4 and Fig. 8), which may include times of no deposition or sediment removal by mass wasting or lake internal currents (Vogel et al., 2010b; Wagner et al., 2012a).

As described by Francke et al. (2016) and Vogel et al. (2010a), SR during glacials is enhanced due to increased hinterland erosion, which is caused by less dense vegetation in the catchment area. We find such trends at DEEP and Cerava, but at Pestani, SR is (on average) higher by 1.7 cm/ka during interglacials. This shows the different sedimentological evolution of the three investigated sites and depicts the local variability of sedimentation history in Lake Ohrid.

4.3. Cyclostratigraphy and time series analysis

The orbital signals in the investigated GR records from Lake Ohrid vary in their characteristics and suitability for statistical cyclostratigraphic analysis. Ideal (lacustrine) records for such studies do not contain hiatuses, have a high depth/temporal resolution, and show the imprint of several orbital cycles. In this study,

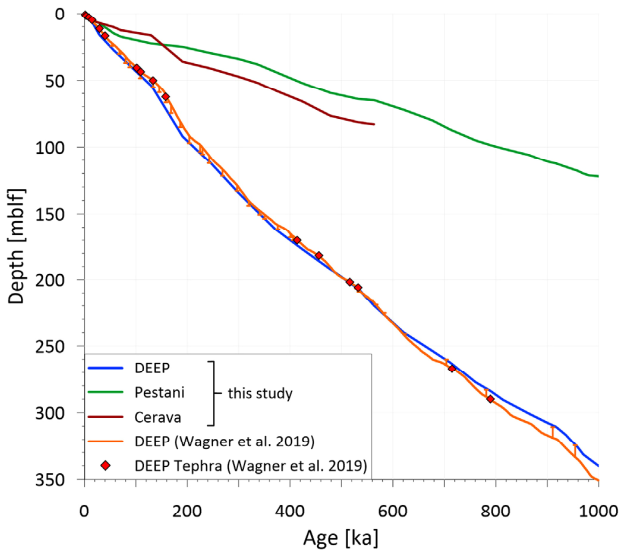

Fig. 8. Age-depth models of investigated sites DEEP, Pestani and Cerava in meters below lake floor (mblf) from geophysical downhole logging. The model from DEEP is compared to data from Wagner et al. (2019). The results from Wagner et al. (2019) are based on the tephrostratigraphic correlation of 16 tephra layers (red diamonds) and tuning of sediment proxy data to orbital parameters. Note that data from Wagner et al. (2019) are in meters composite depth (mcd) based on sediment core measurements. Depth shifts between different depths ("mcd" and "mblf") are indicated as vertical orange bars on data from Wagner et al. (2019) and are based on data in Table S3. We do not show age errors of tephras because error bars are too short to be viewed accurately in this figure (maximum error is ±5.62 ka). Less inclined sections indicate periods of low sedimentation rates and may include hiatuses and/or sediment removal by mass wasting. Steeply inclined sections characterize periods with high sedimentation rates and may include the deposition of mass waste deposits and/or sediments from clinoform structures (Cerava). (For interpretation of the references to colour in this figure legend, the reader is referred to the Web version of this article.)

these criteria hold best for the DEEP site with its setting in the central and deepest part of the lake. At the other sites, which are closer to the shore, tectonic movements and/or mass wasting may bias the orbital signal in the sediments more severely.

Based on the sliding-window approach used by Baumgarten et al. (2015) for the DEEP site, they identify orbital eccentricity and discuss a sharp increase in SR from 30 to 45 cm/ka at 110 mblf. In addition, they use a correlative method involving the LR04 and tephra layers, which is highly similar to our methodological approach. We observe the same change in the amplitude spectrum at 110 mblf (Fig. 5b), but suggest a smooth increase of SR towards the top with a quasi-linear trend (Fig. 4 and S13).

Although SR increases with time towards the recent (Figs. 4 and 8), we initially assume an average SR of ~30 cm/ka for the lower part of the record (200–335 mblf), as this is a precondition for cycle interpretation from the evolutive harmonic analysis (EHA) amplitude spectrum (Fig. 5b and S10). Applying this assumption to interpret the described low-frequency cycles (75 m, 30 m and 20 m wavelengths; see Chapter 3.4 'Cyclostratigraphy') shows that the 30 m period signal represents a combination of the 125 ka- and 95 ka-eccentricity cycle components (Fig. 5b and S10). Following this idea, the prominent signals at 13-10 m and 8 m wavelengths can be identified as obliquity and precession cycles, respectively. A similar shift towards signals with shorter wavelengths is observed in the wavelet analysis (Fig. 5c). This might be related to the decrease in SR and/or indicate a shift to shorter climate cycles towards the deeper part of the record. Our results from the DEEP site are consistent with core-based proxy data (total inorganic carbon and deciduous oak pollen data) from Wagner et al. (2019), which suggest a ~100 ka orbital frequency during the last 700 ka and a pronounced 41 ka orbital frequency before 700 ka. Weak, ~21 ka orbital frequencies occur most prominently in the pollen record (Wagner et al., 2019). This conforms to patterns shown in amplitude spectra (Fig. S10), where prominent eccentricity cycles prevail in the younger part but a more noticeable obliquity component occurs in the older part (>600 ka). We propose that this change is evidence of the Mid-Pleistocene Transition, when a shift from an obliquity-to an eccentricity-dominated world occurs (Pisias and Moore, 1981).

Assuming a constant SR (~14 cm/ka) for the Pestani GR log, the main amplitude (wavelength of 20–13 m; Figs. S8 and S10) represents the 125 ka- and 95 ka-eccentricity cycle. Other prominent cyclicity signals represent obliquity, but precession signals are not detectable in the EHA amplitude spectrum. The wavelet analysis shows a quasi-continuous ~110 ka signal (Fig. S8c), but the obliquity signal vanishes in certain parts, and precession signals cannot be detected. Despite the absence of strong precession cycles, we apply the timeOptTemplate method to estimate SR (Table 1).

The record at Cerava is complex in terms of orbital signal identification. This is probably due to sudden changes in the SR. The EHA data contain a component related to eccentricity and/or glacial/interglacial changes. Obliquity and precession cycles are not obvious, and we therefore refrain from interpreting obliquity and precession cycles at Cerava (Fig. S9).

The reliability of the timeOptTemplate method for estimating SR is based on the quality of precession signals in the investigated records. Testing for precession in the tuned DEEP record was carried out using the method of Zeeden et al. (2015) and is plotted in Fig. 7. The observed match of precession-scale amplitude modulations and the theoretical eccentricity solutions from Laskar et al. (2004) indicate the presence of precession signals for most parts of the GR record. Discrepancies occur in parts at ~520 ka and older than 950 ka, where the precession signal is weak, and the dataset (as in several other late Quaternary datasets; Zeeden et al., 2015) is of limited use for investigating precession amplitude. In the rest of the record, the match of precession amplitude and eccentricity is good for both ~100 ka- and ~400 ka-eccentricity components. It is essential to know that the GR record from the DEEP site has well-resolved precession cycles to use the timeOptTemplate method. In contrast, the SR estimates from timeOptTemplate at Pestani site vary by several cm/ka from the direct GR to LR04 correlation (Table 1). The quality of the precession signal in the GR log from Pestani is also not as obvious as that from DEEP.

The similarity between precession amplitude and eccentricity provides confidence in our age model, especially when considering that the GR record was not tuned to precession but correlated to the LR04 benthic stack only. It is not expected that this leads to artificial similarity. Additionally, the algorithm accounts for correlation-induced signal properties (Zeeden et al. 2015, 2019).

4.4. Integration of cluster lithology in age-depth models

As a final step, we merge information about the timing and sediment characteristics as derived by cluster analysis (Fig. 9). At the DEEP site, sharp contrasts in physical sediment properties allow direct linkage of cluster classes (see Chapter 3.5 'Cluster analysis') to MISs. Difficulties arise when glacial/interglacial changes are not distinctive (e.g., the relatively "warm" glacials MIS 14 and 18 in Fig. 7). and the sedimentation does not completely switch from predominant calcareous silty clay deposition to predominant silty clay deposition or vice versa (e.g., ~215 mblf in Fig. 6 or ~550 ka, which is estimated to be MIS 14, in Fig. 9). This shows that the sedimentation is sensitive to short, suborbital climate change and that sedimentation changes do not strictly occur at MIS boundaries.

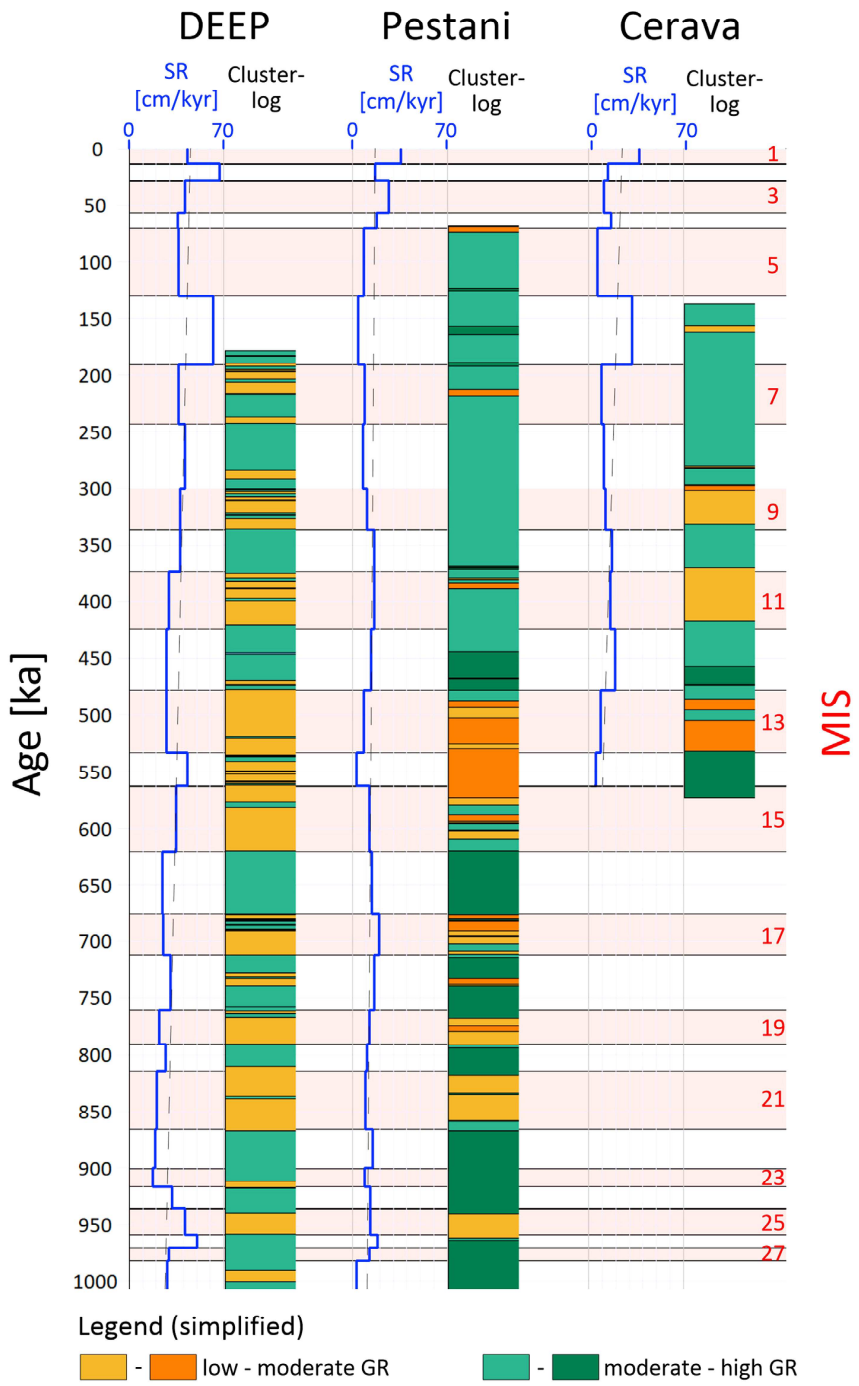

Fig. 9. Artificial lithological log derived by cluster analysis on a time scale. MIS interglacials are indicated in red. Sedimentation rates are in blue as in Fig. 4. Linear sedimentation trends are marked as dashed grey lines. Legend is simplified. Details about the properties of cluster classes are shown in Fig. S14. (For interpretation of the references to colour in this figure legend, the reader is referred to the Web version of this article.)

Despite these effects, physical properties at the DEEP site reflect most MISs for the last ~1 Ma.

Additional information about the characteristics of past environmental changes is provided by the patterns of cluster classes. Sharp contrasts at the bases of interglacials reflect quick changes in the sedimentary system from cold to warm conditions, while changes in cluster classes during the transition from interglacials to glacials document smoother environmental changes (e.g., MIS 19, 17 and 11 of the DEEP record in Fig. 9), as they are known from global climate and ice volume records, including the LR04 benthic stack (e.g., Lisiecki and Raymo, 2005; Imbrie and Imbrie, 1980).

The linkage of cluster lithology to MIS at Pestani is more

challenging. Especially in sediments younger than 450 ka, no clear differentiation of cluster classes exists. In the central part of the Pestani record (960–450 ka), linkage of sediment properties to MISs is possible, although the MIS linkage at Pestani is not as distinct as that at DEEP. At Cerava, the upper part (MIS 6–8) is not differentiated by cluster analysis, but in the older part of the record (>300 ka), the cluster classes are in good agreement with the boundaries of most MISs. In both cases, fluid-sediment interactions may have led to changes in sediment conditions, which superimpose the in situ sediment properties (see increasing R towards the top; Fig. S3). These post-drilling effects could be responsible for the disordered classification of certain segments during the cluster analysis.

4.5. Data quality and uncertainties

Geophysical datasets have to meet certain requirements to provide robust age estimates:

1. Complete/continuous records (MMD or hiatuses are factors adding uncertainty to stratigraphic records).
2. High sedimentation rates (in relation to the vertical resolution of borehole logging tools and seismic data).
3. Distinct changes in climate-sensitive sediment proxies (e.g., high organic matter or $CaCO_3$ accumulation during interglacials and low organic matter and $CaCO_3$ during glacial periods).
4. Preservation of certain orbital parameters in the sediment succession for cyclostratigraphic analysis (e.g., precession signals are essential for the use of the timeOptTemplate method).

The geophysical datasets used in this study meet the listed criteria in different ways. Data from DEEP offer the best quality dataset for the purpose of age estimation. This is demonstrated by the good similarity of the age-depth models from the DEEP site derived in this study by geophysical data and the age-depth model derived for the drilled core by means of a combination of dating methods (Wagner et al., 2019). The criteria are less well met at the Pestani and Cerava sites. Uncertainties emerge at Pestani between MIS 1 and MIS 6, where correlation of the GR log to the LR04 benthic stack is difficult, and at Cerava, where cyclostratigraphic investigations are impeded due to missing precession signals and possible MMDs and/or clinoforms. Nevertheless, distinct changes in climate-relevant sediment proxies and information from seismic reflectors can be traced throughout large parts of the Ohrid basin. This allows for the transfer of age information between individual sites and enables the first reliable age estimations based on geophysical data alone at these sites. Generally, we suggest that our age-depth models are reliable at resolutions greater than glacial/interglacial variability, possibly ~40 ka.

5. Conclusions

This study examines an integrated approach to derive age-depth estimates and lithological descriptions based on geophysical data alone. We use seismic data to trace prominent marker horizons to identify time-equivalent horizons at different drill sites. An age-depth model is established through the correlation of downhole logging data to the LR04 benthic stack (Lisiecki and Raymo, 2005) and by implementation of cyclostratigraphic analysis. We perform cluster analyses on geophysical downhole logging data to generate artificial lithological logs and integrate them into age-depth models.

Sedimentation rates at the three sites, DEEP, Pestani and Cerava, increase towards the tops of the records. During specific glacials or interglacials, opposite patterns of SR at the different sites show that the sedimentation in Lake Ohrid is diverse. This is underlined by seismic data, which show undisturbed sedimentation at DEEP and more disturbed sedimentation at Pestani and Cerava. While sediment properties are able to reflect most of the glacial/interglacial cycles at DEEP, a direct link of sediment properties to MISs is more challenging at Pestani and Cerava sites.

The data for such an investigation have to meet several criteria regarding quality and quantity. An important aspect for cyclostratigraphic analysis is the continuity of the records. Only the DEEP record features no hiatuses or larger MMDs, while sedimentation at Pestani and Cerava is more discontinuous or disturbed. Our study also shows the importance of detailed (seismic) pre-site surveys and a careful selection of drill sites to meet the necessary criteria for robust (cyclostratigraphic) analysis. Various measurements (e.g., geophysical downhole logging and seismic surveys) are required, and multiple statistical methods (e.g., cyclostratigraphy and cluster analysis) must be applied to obtain the first reliable age-depth models and lithological interpretations based on geophysical data alone. This approach has the potential to improve future drilling projects by delivering age-depth models and descriptions of sediment properties before core opening or in cases where no (suitable) core material is available.

Author contributions

Arne Ulfers - Interpretation of the geological/geophysical datasets, performing analyses (cluster analysis/cyclostratigraphy) and writing the major part of the manuscript. Christian Zeeden, - Scientific support and discussion, especially for cyclostratigraphic investigations. Bernd Wagner - Scientific support and discussion, especially for regional geology and sedimentology in Lake Ohrid. Sebastian Krastel - Provision and pre-processing of seismic data. Discussion and support interpreting seismic survey. Hermann Buness - Time-depth conversion of seismic data. Support for chapter 2.2 Data processing. Thomas Wonik - Scientific support and discussion, especially in downhole logging data acquisition and interpretation.

Data availability

The data underlying this article will be shared on reasonable request to the corresponding author.

Declaration of competing interest

The authors declare that they have no known competing financial interests or personal relationships that could have appeared to influence the work reported in this paper.

Acknowledgements

This research project was possible due to funding from the German Research Foundation (grants WO672/10-1 and WO672/15-1/2). The “Scientific Collaboration on Past Speciation Conditions in Lake Ohrid” (SCOPSCO) drilling project was partly funded by grants from the International Continental Scientific Drilling Program (ICDP), the German Ministry of Higher Education and Research, the German Research Foundation, the University of Cologne, the British Geological Survey, the Italian National Institute of Geophysics and Volcanology and the Italian National Research Council and the governments of the republics of North Macedonia (or FYROM) and Albania. We would like to thank the whole SCOPSCO team for helpful discussions about the results. The boreholes were drilled by Drilling, Observation and Sampling of the Earth's Continental Crust, Inc. Our special thanks go to Thomas Grelle, Jan-Thorsten Blanke

and Dr. Henrike Baumgarten of the Leibniz Institute for Applied Geophysics for the acquisition of the geophysical downhole logging data. We also appreciate the work of anonymous reviewers and editors.

Appendix A. Supplementary data

Supplementary data to this article can be found online at https://doi.org/10.1016/j.quascirev.2021.107295.

References

Baumgarten, H., Wonik, T., 2015. Cyclostratigraphic studies of sediments from Lake Van (Turkey) based on their uranium contents obtained from downhole logging and paleoclimatic implications. Int. J. Earth Sci. 104 (6), 1639–1654.

Baumgarten, H., Wonik, T., Tanner, D.C., Francke, A., Wagner, B., Zanchetta, G., Sulpizio, R., Giaccio, B., Nomade, S., 2015. Age-depth model of the past 630 kyr for Lake Ohrid (FYROM/Albania) based on cyclostratigraphic analysis of downhole gamma ray data. Biogeosciences 12, 7453–7465.

Buecker, C.J., Jarrard, R.D., Wonik, T., Brink, J.D., 2000. Analysis of downhole logging data from CRP-2/2A, Victoria Land Basin, Antarctica; a multivariate statistical approach. Terra Antartica 7, 299–310.

Erickson, S.N., Jarrard, R.D., 1998. Velocity-porosity relationships for water-saturated siliciclastic sediments. J. Geophys. Res. Solid Earth 103 (B12), 30385–30406.

Francke, A., Wagner, B., Just, J., Leicher, N., Gromig, R., Baumgarten, H., Vogel, H., Lacey, J.H., Sadori, L., Wonik, T., Leng, M.J., 2016. Sedimentological processes and environmental variability at Lake Ohrid (Macedonia, Albania) between 637 ka and the present. Biogeosciences 13, 1179–1196.

Friese, A., Kallmeyer, J., Axel Kitte, J., Montaño Martínez, I., Bijaksana, S., Wagner, D., 2017. A simple and inexpensive technique for assessing contamination during drilling operations. the ICDP Lake Chalco Drilling Science Team and the ICDP Towuti Drilling Science Team Limnol Oceanogr. Methods 15, 200–211.

Goldstein, S.L., Kiro, Y., Torfstein, A., Kitagawa, H., Tierney, J., Stein, M., 2020. Revised chronology of the ICDP Dead Sea deep drill core relates drier-wetter-drier climate cycles to insolation over the past 220 kyr. Quat. Sci. Rev. 244, 106460.

Gouhier, T.C., Grinsted, A., Simko, V., 2019. R Package Biwavelet: Conduct Univariate and Bivariate Wavelet Analyses, Version 0.20.19.

Imbrie, J., Imbrie, J.Z., 1980. Modeling the climatic response to orbital variations. Science 207 (4434), 943–953.

Laskar, J., Robutel, P., Joutel, F., Gastineau, M., Correia, A.C.M., Levrard, B., 2004. A long-term numerical solution for the insolation quantities of the Earth. Astron. Astrophys. 428 (1), 261–285.

Leicher, N., Zanchetta, G., Sulpizio, R., Giaccio, B., Wagner, B., Nomade, S., Francke, A., Del Carlo, P., 2016. First tephrostratigraphic results of the DEEP site record from Lake Ohrid (Macedonia and Albania). Biogeosciences 13, 2151–2178.

Leicher, N., Giaccio, B., Zanchetta, G., Sulpizio, R., Albert, P., Tomlinson, E., Lagos, M., Francke, A. & Wagner, B., submitted. Lake Ohrid's Tephrochronological Dataset Reveals 1.36 Ma of Mediterranean Explosive Volcanic Activity, Nature Scientific Data.

Lindhorst, K., Vogel, H., Krastel, S., Wagner, B., Hilgers, A., Zander, A., Schwenk, T., Wessels, M., Daut, G., 2010. Stratigraphic analysis of lake level fluctuations in Lake Ohrid: an integration of high resolution hydro-acoustic data and sediment cores. Biogeosciences 11, 3531–3548.

Lindhorst, K., 2012. *Sedimentary and Neotectonic History of Lake Ohrid (Albania/Macedonia): Acquisition and Interpretation of New Hydro-Acoustic and Seismic Data*, PhD Thesis. Christian-Albrechts Universität, Kiel.

Lindhorst, K., Gruen, M., Krastel, S., Schwenk, T., 2012. Hydroacoustic analysis of mass wasting deposits in Lake Ohrid (FYR Macedonia/Albania). In: Yamada, Y., Kawamura, K., Ikehara, K., Ogawa, Y., Urgeles, R., Mosher, D., Chaytor, J., Strasser, M. (Eds.), Submarine Mass Movements and Their Consequences. Advances in Natural and Technological Hazards Research, vol. 31. Springer, Dordrecht, pp. 245–253.

Lindhorst, K., Krastel, S., Reicherter, K., Stipp, M., Wagner, B., Schwenk, T., 2015. Sedimentary and tectonic evolution of lake Ohrid (Macedonia/Albania). Basin Res. 1. 84–101.

Lisiecki, L.E., Raymo, M.E., 2005. A Pliocene-Pleistocene stack of 57 globally distributed benthic δ18O records. Paleoceanography 20 (1).

Litt, T., Anselmetti, F.S., 2014. Lake Van deep drilling project PALEOVAN. Quat. Sci. Rev. 104, 1–7.

Matter, M., Anselmetti, F.S., Jordanoska, B., Wagner, B., Wessels, M., Wuest, A., 2010. Carbonate sedimentation and effects of eutrophication observed at the Kališta subaquatic springs in Lake Ohrid (Macedonia). Biogeosciences 7 (11), 3755–3767.

Matzinger, A., Schmid, M., Veljanoska-Sarafiloska, E., Patceva, S., Guseska, D., Wagner, B., Müller, B., Sturm, M., Wuest, A., 2007. Eutrophication of ancient Lake Ohrid: global warming amplifies detrimental effects of increased nutrient inputs. Limnol. Oceanogr. 52 (1), 338–353.

Melles, M., Brigham-Grette, J., Minyuk, P., Koeberl, C., Andreev, A., Cook, T., Fedorov, G., Gebhardt, C., Haltia-Hovi, E., Kukkonen, M., Nowaczyk, N., Schwamborn, G., Wennrich, V., the Elgygytgyn Scientific Party, 2011. the Lake Elgygytgyn scientific drilling project – conquering Arctic challenges through continental drilling. Sci. Drill. 11, 29–40.

Meyers, S.R., 2014. Astrochron: an R Package for Astrochronology. https://cran.r-project.org/package=astrochron.

Meyers, S.R., 2015. The evaluation of eccentricity-related amplitude modulation and bundling in paleoclimate data: an inverse approach for astrochronologic testing and time scale optimization. Paleoceanography 30 (12), 1625–1640.

Meyers, S.R., 2019. Cyclostratigraphy and the problem of astrochronologic testing. Earth Sci. Rev. 190, 190–223.

Nowaczyk, N.R., Haltia, E.M., Ulbricht, D., Wennrich, V., Sauerbrey, M.A., Rosén, P., Vogel, H., Francke, A., Meyer-Jacob, C., Andreev, A.A., Lozhkin, A.V., 2013. Chronology of Lake El'gygytgyn sediments – a combined magnetostratigraphic, palaeoclimatic and orbital tuning study based on multi-parameter analyses. Clim. Past 9, 2413–2432.

Pisias, N.G., Moore, T.C., 1981. The evolution of Pleistocene climate: a time series approach. Earth Planet Sci. Lett. 52, 450–458.

R Core Team, 2020. R: A Language and Environment for Statistical Computing. R Foundation for Statistical Computing. Vienna, Austria. URL. https://www.R-project.org/.

Reicherter, K., Hoffmann, N., Lindhorst, K., Krastel, S., Fernández-Steeger, T., Grützner, C., Wiatr, T., 2011. Active basins and neotectonics: morphotectonics of the Lake Ohrid Basin (FYROM and Albania) [Aktive Becken und Neotektonik: die Morphotektonik des Ohridbeckens (FYROM und Albanien).]. Zeitschrift der Dtsch. Gesellschaft fuer Geowissenschaften 162 (2), 217–234.

Rider, M., Kennedy, M., 2011. The Geological Interpretation of Well Logs, third ed. Rider-French Consulting Ltd.

Russell, J.M., Bijaksana, S., Vogel, H., Melles, M., Kallmeyer, J., Ariztegui, D., Crowe, S., Fajar, S., Hafidz, A., Haffner, D., Hasberg, A., Ivory, S., Kelly, C., King, J., Kirana, K., Morlock, M., Noren, A., O'Grady, R., Ordonez, L., Stevenson, J., von Rintelen, T., Vuillemin, A., Watkinson, I., Wattrus, N., Wicaksono, S., Wonik, T., Bauer, K., Deino, A., Friese, A., Henny, C., Imran Marwoto, R., Ngkoimani, L.O., Nomosatryo, S., Safiuddin, L.O., Simister, R., Tamuntuan, G., 2016. The Towuti Drilling Project: paleoenvironments, biological evolution, and geomicrobiology of a tropical Pacific lake. Sci. Drill. 21, 29–40.

Shanahan, T.M., Peck, J.A., McKay, N., Heil Jr., C.W., King, J., Forman, S.L., Hoffmann, D.L., Richards, D.A., Overpeck, J.T., Scholz, C., 2013. Age models for long lacustrine sediment records using multiple dating approaches—an example from Lake Bosumtwi, Ghana. Quat. Geochronol. 15, 47–60.

Stein, M., 2012. The ICDP Dead Sea Deep Drilling Project. GSOI.

Stockhecke, M., Kwiecien, O., Vigliotti, L., Anselmetti, F.S., Beer, J., Namik Çağatay, M., Channell, J.E.T., Kipfer, R., Lachner, J., Litt, T., Pickarski, N., Sturm, M., 2014. Chronostratigraphy of the 600,000 year old continental record of Lake Van (Turkey). Quat. Sci. Rev. 104, 8–17.

Thomson, D.J., 1982. Spectrum analysis and harmonic analysis. Proc. IEEE 70 (9), 1055–1096.

Verschuren, D., Olago, D.O., Rucina, S.M., Odhengo, P.O., ICDP DeepCHALLA Consortium, 2013. DeepCHALLA: two glacial cycles of climate and ecosystem dynamics from equatorial East Africa. Sci. Drill. 15, 72–76.

Vogel, H., Wagner, B., Zanchetta, G., Sulpizio, R., Rosén, P., 2010a. A paleoclimate record with tephrochronological age control for the last glacial-interglacial cycle from Lake Ohrid, Albania and Macedonia. J. Paleolimnol. 44 (1), 295–310.

Vogel, H., Wessels, M., Albrecht, C., Stich, H.B., Wagner, B., 2010b. Spatial variability of recent sedimentation in Lake Ohrid (Albania/Macedonia). Biogeosciences 7 (10), 3333–3342.

Wagner, B., Reicherter, K., Daut, G., Wessels, M., Matzinger, A., Schwalb, A., Spirkovski, Z., Sanxhaku, M., 2008. The potential of Lake Ohrid for long-term palaeoenvironmental reconstructions. Palaeogeogr. Palaeoclimatol. Palaeoecol. 259 (2–3), 341–356.

Wagner, B., Lotter, A.F., Nowaczyk, N., Reed, J.M., Schwalb, A., Sulpizio, R., Valsecchi, V., Wessels, M., Zanchetta, G., 2009. A 40,000-year record of environmental change from ancient Lake Ohrid (Albania and Macedonia). J. Paleolimnol. 41, 407–430.

Wagner, B., Vogel, H., Zanchetta, G., Sulpizio, R., 2010. Environmental change within the Balkan region during the past ca. 50 ka recorded in the sediments from lakes Prespa and Ohrid. Biogeosciences 7 (10), 3187–3198.

Wagner, B., Aufgebauer, A., Vogel, H., Zanchetta, G., Sulpizio, R., Damaschke, M., 2012a. Late Pleistocene and Holocene contourite drift in lake Prespa (Albania/FYR of Macedonia/Greece). Quat. Int. 274, 112–121.

Wagner, B., Francke, A., Sulpizio, R., Zanchetta, G., Lindhorst, K., Krastel, S., Vogel, H., Rethemeyer, J., Daut, G., Grazhdani, A., Lushaj, B., Trajanovski, S., 2012b. Possible earthquake trigger for 6th century mass wasting deposit at Lake Ohrid (Macedonia/Albania). Clim. Past 8, 2069–2078.

Wagner, B., Wilke, T., Krastel, S., Zanchetta, G., Sulpizio, R., Reicherter, K., Leng, M.J., Grazhdani, A., Trajanovski, S., Francke, A., Lindhorst, K., Levkov, Z., Cvetkoska, A., Reed, J.M., Zhang, X., Lacey, J.H., Wonik, T., Baumgarten, H., Vogel, H., 2014. The SCOPSCO drilling project recovers more than 1.2 million years of history from Lake Ohrid. Sci. Drill. 17, 19–29.

Wagner, B., Wilke, T., Francke, A., Albrecht, C., Baumgarten, H., Bertini, A., Combourieu-Nebout, N., Cvetkoska, A., D'Addabbo, M., Donders, T.H., Föller, K., Giaccio, B., Grazhdani, A., Hauffe, T., Holtvoeth, J., Joannin, S., Jovanovska, E., Just, J., Kouli, K., Koutsodendris, A., Krastel, S., Lacey, J.H., Leicher, N., Leng, M.J., Levkov, Z., Lindhorst, K., Masi, A., Mercuri, A.M., Nomade, S., Nowaczyk, N., Panagiotopoulos, K., Peyron, O., Reed, J.M., Regattieri, E., Sadori, L., Sagnotti, L., Stelbrink, B., Sulpizio, R., Tofilovska, S., Torri, P., Vogel, H., Wagner, T., Wagner-Cremer, F., Wolff, G.A., Wonik, T., Zanchetta, G., Zhang, X.S., 2017. The

environmental and evolutionary history of Lake Ohrid (FYROM/Albania): interim results from the SCOPSCO deep drilling project. Biogeosciences 14, 2033–2054.

Wagner, B., Vogel, H., Francke, A., Friedrich, T., Donders, T., Lacey, J.H., Leng, M.J., Regattieri, E., Sadori, L., Wilke, T., Zanchetta, G., Albrecht, C., Bertini, A., Combourieu-Nebout, N., Cvetkoska, A., Giaccio, B., Grazhdani, A., Hauffe, T., Holtvoeth, J., Joannin, S., Jovanovska, E., Just, J., Kouli, K., Kousis, I., Koutsodendris, A., Krastel, S., Lagos, M., Leicher, N., Levkov, Z., Lindhorst, K., Masi, A., Melles, M., Mercuri, A.M., Nomade, S., Nowaczyk, N., Panagiotopoulos, K., Peyron, O., Reed, J.M., Sagnotti, L., Sinopoli, G., Stelbrink, B., Sulpizio, R., Timmermann, A., Tofilovska, S., Torri, P., Wagner-Cremer, F., Wonik, T., Zanchetta, G., 2019. Mediterranean winter rainfall in phase with African monsoons during the past 1.36 million years. Nature 573 (7773), 256–260.

Ward Jr., J.H., 1963. Hierarchical grouping to optimize an objective function. J. Am. Stat. Assoc. 58 (301), 236–244.

Wilke, T., Hauffe, T., Jovanovska, E., Cvetkoska, A., Donders, T., Ekschmitt, K., Francke, A., Lacey, J.H., Levkov, Z., Marshall, C.R., Neubauer, T.A., Silvestro, D., Stelbrink, B., Vogel, H., Albrecht, C., Holtvoeth, J., Krastel, S., Leicher, N., Leng, M.J., Lindhorst, K., Masi, A., Ognjanova-Rumenova, N., Panagiotopoulos, K., Reed, J.M., Sadori, L., Tofilovska, S., Van Bocxlaer, B., Wagner-Cremer, F., Wesselingh, F.P., Wolters, V., Zanchetta, G., Zhang, X., Wagner, B., 2020. Deep drilling reveals massive shifts in evolutionary dynamics after formation of ancient ecosystem. Sci. Adv. 6 (40), eabb2943.

Zeeden, C., Meyers, S.R., Lourens, L.J., Hilgen, F.J., 2015. Testing astronomically tuned age models. Paleoceanography 30 (4), 369–383.

Zeeden, C., Meyers, S.R., Hilgen, F.J., Lourens, L.J., Laskar, J., 2019. Time scale evaluation and the quantification of obliquity forcing. Quat. Sci. Rev. 209, 100–113.

Zolitschka, B., Anselmetti, F., Ariztegui, D., Corbella, H., Francus, P., Lücke, A., Maidanah, N.I., Ohlendorf, C., Schäbitz, F., Wastegård, S., 2013. Environment and climate of the last 51,000 years–new insights from the Potrok Aike maar lake Sediment Archive Drilling prOject (PASADO). Quat. Sci. Rev. 71, 1–12.

2.3 Peer-reviewed publication (Half-precession in Lake Ohrid and Europe)

Half-precession signals in Lake Ohrid (Balkan) and their spatio-temporal relations to climate records from the European realm

Ulfers, A., Zeeden, C., Voigt, S., Sardar Abadi, M., Wonik. T

Quaternary Science Reviews 280 (2022) 107413

Contents lists available at ScienceDirect

Quaternary Science Reviews

journal homepage: www.elsevier.com/locate/quascirev

Half-precession signals in Lake Ohrid (Balkan) and their spatio-temporal relations to climate records from the European realm

Arne Ulfers [a, *], Christian Zeeden [a], Silke Voigt [b], Mehrdad Sardar Abadi [a], Thomas Wonik [a]

[a] Leibniz Institute for Applied Geophysics, Stilleweg 2, 30655, Hannover, Germany
[b] Institute of Geosciences, Goethe University Frankfurt, Altenhöferallee 1, 60438, Frankfurt, Germany

ARTICLE INFO

Article history:
Received 30 June 2021
Received in revised form
14 December 2021
Accepted 31 January 2022
Available online 17 February 2022

Handling Editor: A. Voelker

ABSTRACT

The nature of half-precession (HP) cycles (~9000–12,000 years), although identified in numerous records, is still poorly understood. Here we focus on HP signals in Lake Ohrid and in a variety of different marine and terrestrial proxy records from Europe and the Northern Atlantic region. Our study examines the temporal evolution of the HP signal from the early/middle Pleistocene to the present, discusses the results across the latitudes of the Mediterranean and Europe, and assesses the potential of the HP to reflect the connectivity of climate systems over time.

We apply filters on the datasets that remove the classical orbital cycles (eccentricity, obliquity, precession) and high frequency signals to focus exclusively on the bandwidth of the HP signal. Evolutionary wavelet spectra and correlation techniques are used to study the evolution of frequencies through the different records.

Next to a connection of HP cycles to interglacials, we see a more pronounced HP signal in the younger part of several proxy records. Although the HP signal is present in all of the investigated sites, we observe a more pronounced HP signal in the southeast compared to records from the north. The latter is consistent with the assumption that HP is an equatorial signal and can be transmitted northward via various pathways. The appearance of HP signals in mid- and high-latitude records can thus be an indicator for the intensity of the mechanisms driving these pathways. The African Monsoon probably plays a major role in this context, as its magnitude directly influences the climate systems of the Mediterranean and Southern Europe.

1. Introduction

1.1. Characteristics of half-precession cycles and state of the art

After Milutin Milanković published his theories on orbital cycles in the first half of the 20th century, it took decades until these were accepted as catalysts for warm/cold periods (Milanković, 1920, 1941; Hays et al., 1976). Since then, major progress was made in cyclostratigraphy and the impact of orbital forcing on the climate system (e.g. Weedon, 2003; Hinnov, 2000 and references therein). Most studies focused on the role of the three major cycles (eccentricity, obliquity, precession), while sub-Milanković frequencies (less than 15 ka) usually received only secondary attention. In this study, we specifically address cycles between 12 and 9 ka. This frequency band, referred to as half-precession (HP), is a harmonic of the 23–19 ka precession cycles (Berger et al., 1997). The HP signal is considered to be most intense in the intertropical zone, as it results from the twice-yearly passage of the sun across the equator (Short et al., 1991; Berger et al., 2006). Studies on marine records first proved the occurrence of HP (e.g. Hagelberg et al., 1994; Hinnov et al., 2002). HP cycles were also described as a response to monsoon rainfall in lacustrine records from Africa (Trauth et al., 2003; Verschuren et al., 2009; Scholz et al., 2007). Deposits from the Chinese Loess Plateau suggest that mid-latitude terrestrial records are able to reflect HP signals which originate from the East Asian summer monsoon in the tropical Pacific Ocean (Sun and Huang, 2006). Similar observations about the HP signal were made by Turney et al. (2004) who suggest that climate variations in the tropical Pacific Ocean exert an influence on North Atlantic climate through atmospheric and oceanic teleconnections on

* Corresponding author.
E-mail addresses: Arne.Ulfers@leibniz-liag.de (A. Ulfers), Christian.Zeeden@leibniz-liag.de (C. Zeeden), s.voigt@em.uni-frankfurt.de (S. Voigt), Mehrdad.SardarAbadi@leibniz-liag.de (M. Sardar Abadi), Thomas.Wonik@leibniz-liag.de (T. Wonik).

https://doi.org/10.1016/j.quascirev.2022.107413

orbital timescales. In comparison to marine records, terrestrial records (lacustrine and loess) are usually relatively short. The longest terrestrial record mentioned in the references above has an age of 175 ka (Trauth et al., 2003), while marine records often span longer periods with millions of years (e.g. Hagelberg et al., 1994; Grant et al., 2017). Controversy is still ongoing about how HP affects climate and is transferred into geological records (Hinnov et al., 2002; De Vleeschouwer et al., 2012, and references therein). In this context, it is important to recognize that insolation forcing is only one step in an astronomical theory of paleoclimate (Berger et al., 2006), and that astronomical climate forcing can act nonlinear and complex (e.g. Meyers, 2019; Liebrand and de Bakker, 2019).

1.2. Aim of the study

HP is observable in various marine (e.g. Hagelberg et al., 1994; Grant et al., 2017) as well as terrestrial records (e.g. Antoine et al., 2013; Colcord et al., 2018) but is often not described in detail or further investigated (e.g. Hodell et al., 2013). In some of the just referenced records and Lake Ohrid data (see chapter 1.3 'Setting of Lake Ohrid'), HP cycles are very distinctly developed.

In our study, we use various proxy records in and around Europe to characterize and quantify the HP signal. We (1) investigate HP cycles in Lake Ohrid and (2) set the results in temporal and spatial connection to other records containing clear HP cyclicity. We observe HP over a period of more than 1 Ma in Lake Ohrid and in other long-term records with (in)direct impact of climate systems influencing Europe. Further, we show that HP is also present in high-latitude records, even if not very pronounced and/or superimposed by the main orbital cycles (eccentricity, obliquity, precession). We assess the influence of HP on records from Europe and surrounding regions with the aim to better understand its spatial and temporal occurrence. Assuming that the HP signal originates in tropical regions (Hagelberg et al., 1994; Short et al., 1991), its influence on Europe is largely determined by how the signal is carried northward. As an example, the Nile River transmits information from tropical Africa to the Mediterranean Sea (e.g. Rohling et al., 2015; Rossignol-Strick, 1985). The occurrence of HP in mid-to high-latitudes can thus be used as a measure of connectivity between tropical and subtropical/temperate/subpolar climate zones in the past.

1.3. Setting of Lake Ohrid

Lake Ohrid is located on the Balkan Peninsula between Albania and North Macedonia. It is considered Europe's oldest lake, and therefore it is a valuable archive for studies that focus on changes in local (hydro)climate during the last ~1.36 Ma (e.g. Wagner et al., 2014, 2019). Simplified, the succession consists of two types of hemipelagic sediments: calcareous silty clay deposited during interglacials and clastic, silty clay deposited during glacials (Francke et al., 2016). Several layers of volcanic ash allow tephrostratigraphic analyses, which are the basis for the development of a robust age-depth model besides the borehole logging data (Leicher et al., 2016; Wagner et al., 2019; Ulfers et al., 2022).

The present day climate around Lake Ohrid is mostly a Mediterranean type climate with hot/arid summers and typically rainfall maxima during mild winters (Schemmel et al., 2016). The principal climate systems of the region are highlighted in Fig. 1. There is a pronounced sensitivity to the variability of atmospheric circulation patterns, such as the Siberian High intensity, the North Atlantic Oscillation modes (NAO^+/NAO^-), and the monsoon systems (e.g. Schemmel et al., 2016; Lionello et al., 2012; Wanner et al., 2001). Southward displacement of the westerly track reflects growth of the Fennoscandian ice sheet (Ünal-İmer et al., 2015). Proxy records from Lake Ohrid and climate models suggest that North Atlantic low-pressure systems entering the Mediterranean Sea are strengthened during periods of low continental ice volume. This increases the winter rainfall in the Mediterranean Sea (Wagner et al., 2019; Kutzbach et al., 2014). Wagner et al. (2019) also demonstrate a connection of Lake Ohrid's precipitation proxies with Mediterranean sapropels. The latter are organic rich layers in marine sediments which indicate enhanced African monsoons activity (e.g. Rohling et al., 2015; Rossignol-Strick, 1985).

2. Material and Methods

2.1. Data description and pre-processing

Multi-proxy studies as from Li et al. (2019) are of significant value as they allow to assess the individual suitability of a proxy to reflect astronomical forcing. The records used in this study include a variety of proxies, time intervals, and locations around Europe and the North Atlantic.

The datasets from Lake Ohrid are from an ICDP drilling campaign in 2013. Geophysical downhole logging was conducted by the Leibniz Institute for Applied Geophysics and several continuous data sets of physical properties were obtained. The parameters used in this study are gamma radiation (GR, including concentrations of U, K, Th) and magnetic susceptibility (MS), each with a vertical resolution of 10–20 cm. Principals of logging techniques are described in Rider and Kennedy (2011), details about the logging procedure in Lake Ohrid are given by Baumgarten et al. (2015). Pre-processing of data was performed with the GeoBase® (Antares, Germany) and WellCAD® software (Advanced Logic Technology, Luxembourg). The GR in Lake Ohrid is connected to detrital input of clay minerals, which contain radioactive elements like U, K and Th. The detrital input is higher in glacials due to increased erosion in the hinterland caused by reduced vegetation (Vogel et al., 2010).

Core based analyses of sediments from Lake Ohrid are obtained after the creation of a composite record. The proxies used in this study are listed in Table 1. Total inorganic carbon (TIC) and total organic carbon (TOC) contents were determined at the University of Cologne and relative quartz concentrations (Qz) at the University of Bern using Fourier transform infrared spectroscopy.

The majority of carbonates in the sediments of Lake Ohrid is endogenous calcite, which is formed predominantly by the photosynthetically induced formation of calcite crystals in the epilimnion. The precipitation occurs at warm temperatures, as long as Ca^{2+} and HCO_3^- ions are available (Francke et al., 2016; Vogel et al., 2010). This supply is provided during interglacials by increased karst flow through the mountains consisting of limestone east of Lake Ohrid. The source of the increased hydrological pressure is the elevated Lake Prespa on the eastern side of the mountain range (Wagner et al., 2010).

Palynological investigations were conducted by several investigators across European laboratories. Deciduous oak pollen represent the combined percentages of *Quercus robur* and *Quercus cerris* types (Q.dec), which are commonly used as an indicator for mid-elevation, relatively humid forest across the Mediterranean. Relative abundances of arboreal pollen excluding *Pinus* pollen (AP.Pin) are based on the sum of the total terrestrial pollen excluding *Pinus* owing to overrepresentation and potential long-distance transport of this taxon. In general, pollen abundance decreases in glacials (Sadori et al., 2016; Wagner et al., 2019; Hooghiemstra, 2006).

Additionally, we use datasets with various climate-sensitive proxies in the European and North Atlantic regions for

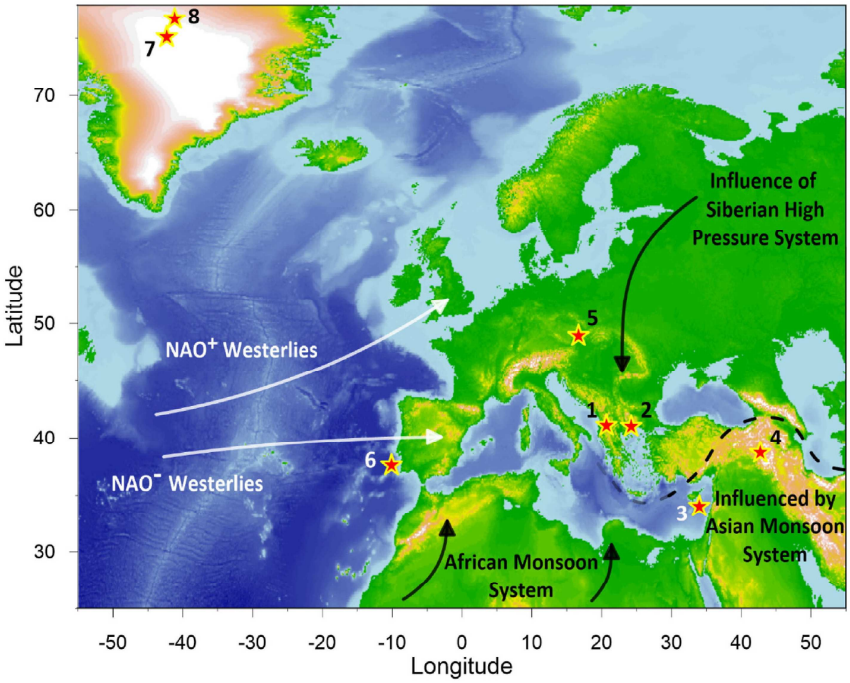

Fig. 1. Overview of data locations used in this study. Schematic atmospheric circulation patterns affecting the Mediterranean are indicated by arrows (after Schemmel et al., 2016). Dashed line represents influence of Asian Monsoon Systems. North Atlantic Oscillation (NAO) in positive and negative mode influencing the Westerlies and thus heat and moisture transport towards the Mediterranean (for details see Wanner et al., 2001). Selected sites have met at least one of the following criteria: Possibly covering long time intervals, sufficient resolution to record half-precession cycles, obvious presence of half-precession cycles and data availability. 1. Lake Ohrid, Albania/North Macedonia; 2. Tenaghi Philippon, Greece; 3. ODP Site 967, Eastern Mediterranean; 4. Lake Van, Turkey; 5. Dolní Věstonice, Czech Republic; 6. IODP Site U1385 "Shackleton site", Iberian Margin; 7. NGRIP, Greenland; 8. Synthetic record, Greenland; there is no position given in the synthetic record, we therefore use the center of Greenland for latitude dependent analysis with this record (see Table 1 for details). Map data are from the US National Oceanic and Atmospheric Administration (NOAA; Amante and Eakins, 2009).

comparison with the Lake Ohrid records (Table 1; Fig. 1). The wet-dry index from ODP expedition 967 in the Eastern Mediterranean is a combination of a sapropel/monsoon run-off proxy yielded by XRF data and a dust record from the same site. This results in a new index for changes in relative humidity and aridity in Northwest Africa (Grant et al., 2017; Larrasoaña et al., 2003). The Ca/Ti ratio measured in cores from the Iberian Margin is a proxy that reflects relative changes of biogenic carbonate and detrital sediment, whereas biogenic carbonate is increased during interglacials (Hodell et al., 2015; Thomson et al., 1999). The Greenland synthetic temperature record (GL_T_syn) is based on the thermal bipolar seesaw model, which proposes opposite temperature responses in the two hemispheres (Broecker, 1998; Stocker and Johnsen, 2003). Temperature changes are estimated using methane-tuned temperature records from Greenland and Antarctica to reconstruct the Greenland records beyond the present limit (Barker et al., 2011). The total organic carbon content in Lake Van (L.Van.TOC) is connected to productivity and lake level fluctuations. Both are associated with glacial-interglacial variability, with increased TOC during warmer/wetter periods as a result of higher lake levels and increased productivity (Stockhecke et al., 2014b). For more details about paleoenvironmental characteristics of the proxies from Table 1, please see references therein.

Most of the analyzed records spans over more than the last 1 Ma (Tab. 1). Each dataset has its own time resolution spanning from 0.05 ka in the synthetic temperature record from Greenland (GL_T_syn) to ~2 ka in the pollen records from Lake Ohrid (Q.dec and AP.Pin). Several utilized methods require equally spaced sampling in time. This is why we interpolate each dataset to its individual mean resolution for further analysis. We utilize the age-models created in the original studies listed in Table 1 (see references therein for details about methods of age-model construction).

2.2. Time series analysis

For data analyses we use the 'astrochron' package for the open-source software 'R' (Meyers et al., 2021; R Core Team, 2021). The R code is provided as Supplement Material 02.

We perform wavelet analyses according to the method of Torrence and Compo (1998) and Liu et al. (2007) using a Morlet mother wavelet. As described above, the datasets are evenly spaced, each at its individual mean resolution. To emphasize the focus on the HP signal, our plots cover only the periodicities between 25 ka to 4 ka.

We apply a Taner bandpass filter (Taner, 1992) to all datasets in the time domain. Taner filters are well established in the field of cyclostratigraphy as they are convenient to apply and filter properties can be adjusted precisely (Zeeden et al., 2018). The roll-off rate of Taner filters can be set steeply (in our case almost vertical at the cutoff frequency, Fig. 2), while the shape of e.g. Gaussian filters allows areas outside the edges of the cutoff frequencies to pass (Kodama and Hinnov, 2014). Given that the HP signal has a narrow bandwidth (12–9 ka), it is important for our study that this is sharply cut from other frequencies. The cutoff frequency of the used filters is set between 1/13 and 1/8.5. Fig. 2 illustrates the filter settings using the amplitude spectrum of GR in Lake Ohrid as an example. This proxy has already proven suitable in previous studies to characterize orbital cycles (Baumgarten et al., 2015; Ulfers et al., 2022). Spectra of Lake Ohrid: GR, K, TIC, Q.dec; Eastern Mediterranean, ODP wet-dry index; Lake Van, TOC; Iberian Margin, Ca/Ti

Table 1
Proxy datasets used in this study. The eight proxies highlighted in bold are discussed and displayed in more detail (e.g. Figs. 3 and 4). All other records are shown in the Supplement Material 01. *This is not a generalization, but valid for the listed site (i.e. in Lake Ohrid GR is a proxy for detrital input). The proxy descriptions are simplified. For details see the corresponding references.

Site	Parameter	Abbreviation	Proxy for*	Age [ka]	Reference
Lake Ohrid	**Gamma radiation**	**GR**	**Detrital input (high GR = high input)**	**0 −1081**	Baumgarten et al. (2015) Ulfers et al. (2022)
Lake Ohrid	Uranium concentration	U	Detrital input (high U = high input. May be biased by organic matter (TOC)	0 −1081	Ulfers et al. (2022)
Lake Ohrid	**Potassium concentration**	**K**	**Detrital input (high K = high input)**	**0 −1081**	Baumgarten et al. (2015) Ulfers et al. (2022)
Lake Ohrid	Thorium concentration	Th	Detrital input (high Th = high input)	0 −1081	Ulfers et al. (2022)
Lake Ohrid	Magnetic susceptibility	MS	Magnetic minerals (may be biased by diagenetic processes	61 −1081	Ulfers et al. (2022)
Lake Ohrid	**Total inorganic carbon**	**TIC**	**Hydrology (high TIC = high temperature and/or karst runoff)**	**1 −1364**	Wagner et al. (2019)
Lake Ohrid	Total organic carbon	TOC	Biologic productivity and organic matter delivery and burial	1 −1364	Wagner et al. (2019)
Lake Ohrid	Relative sedimentary quartz	Qz	Detrital input (high Qz = high detrital input).	2 −1363	Wagner et al. (2019)
Lake Ohrid	**Deciduous oak pollen (Q.dec)**	**Q.dec**	**Vegetation catchment (indicator for mid-elevation, relatively humid forest)**	**0 −1362**	Wagner et al. (2019)
Lake Ohrid	Arboreal pollen without Pinus	AP.Pin	Vegetation catchment	0 −1362	Wagner et al. (2019)
Greece - Tenaghi Philippon	Arboreal pollen	TPhi.AP	Vegetation catchment	0 −1101	Tzedakis et al. (2006)
East. Mediterranean - ODP 967	**ODP wet-dry index**	**wet-dry index**	**Relative humidity and aridity**	**4 −3000**	Grant et al. (2017)
Turkey - Lake Van	**Total organic carbon**	**L.Van.TOC**	Biologic productivity and organic matter delivery and burial	**1−264**	Stockhecke et al. (2014a)
Czech Republic - Dolní Věstonice	Magnetic susceptibility	DolVes.MS	Aeolian sedimentation and loess deposits	22 −126	Antoine et al. (2013)
Atlantic - Iberian Margin	Sea surface temperature	IbM.SST	Temperature	0 −1017	Rodrigues et al. (2017)
Atlantic - Iberian Margin	**Ca/Ti**	**IbM.Ca/Ti**	**Detrital input and bioproductivity**	**0 −1429**	Hodell et al. (2015)
Greenland	$\delta^{18}O$	NGRIP.$\delta^{18}O$	Temperature	0−120	NGRIP members, 2004
Greenland	**Synthetic temperature variability**	**GL_T_syn**	**Temperature**	**5−798**	Barker et al. (2011)

and Greenland, synthetic temperature, are included in Supplementary Material 03. Even if the HP signal in Fig. 2 does not appear obvious at first view, there are several peaks above the AR(1) 99% confidence level in Fig. 2b. Additional information on the detection of the HP signal and its significance is provided in Supplementary Material 04, again using the example of GR in Lake Ohrid.

Subsequently we create an envelope for the filtered signal using the Hilbert transform function. The envelope is then smoothed using a Taner low-pass filter with a cutoff frequency of 0.0125 (≙ 80 ka). This filter will omit high-frequency amplitude components not related to eccentricity, but capture all eccentricity components (here the ~100 ka and ~405 ka) to allow a reasonable comparison with eccentricity as from the calculations of Laskar et al. (2004).

We determine the Pearson correlation coefficients between the original data and the Taner-filtered signal to provide a quantitative evaluation of the HP signal in the stratigraphic series. This is conducted using the 'surrogateCor' function, which is included in the 'R' package 'astrochron' (Meyers, 2014; R Core Team, 2021). The statistical significance of the obtained coefficients is assessed using 1000 Monte Carlo simulations. We use this method for entire records as well as for intervals of special interest (e.g. the time after the Mid-Pleistocene Transition). We employ the same approach to determine the correlation between eccentricity and the filtered signal from the Hilbert envelope.

To illustrate how the correlation between the original data and the Taner-filtered signal (and thus the clarity of the HP cycle) evolve with time, we use the moving window cross-correlation after Sageman and Hollander (1999). In this method, two stratigraphic series are compared using a certain window size. In our study we select a 100-ka-window to display the long-term evolution of the HP signal.

3. Results

3.1. Wavelet analysis

The results of the wavelet analyses of the eight highlighted records in Table 1 are given in Fig. 3. A compilation of all examined records is available in Supplement Material 05. In many records, clear precession signals (period between 19 and 23 ka; e.g., in Fig. 3e and g) or high-frequency signals (period <8 ka; e.g., Fig. 3g and h) are evident. The focus in this study is on the frequency range of HP (9−12 ka), indicated by the white dashed lines in Fig. 3.

Within the last 1 Ma, the HP signal in the different proxy records reveals quite different characteristics. In the borehole data (Fig. 3a and b), we observe that a distinct HP signal is visible more common in interglacials (e.g. MIS 15, 13, 11, 7). This pattern is even more evident in the core data from Lake Ohrid (Fig. 3c and d). In particular in the TIC record, one can observe a direct link of the HP signal to interglacials and its disappearance in glacials.

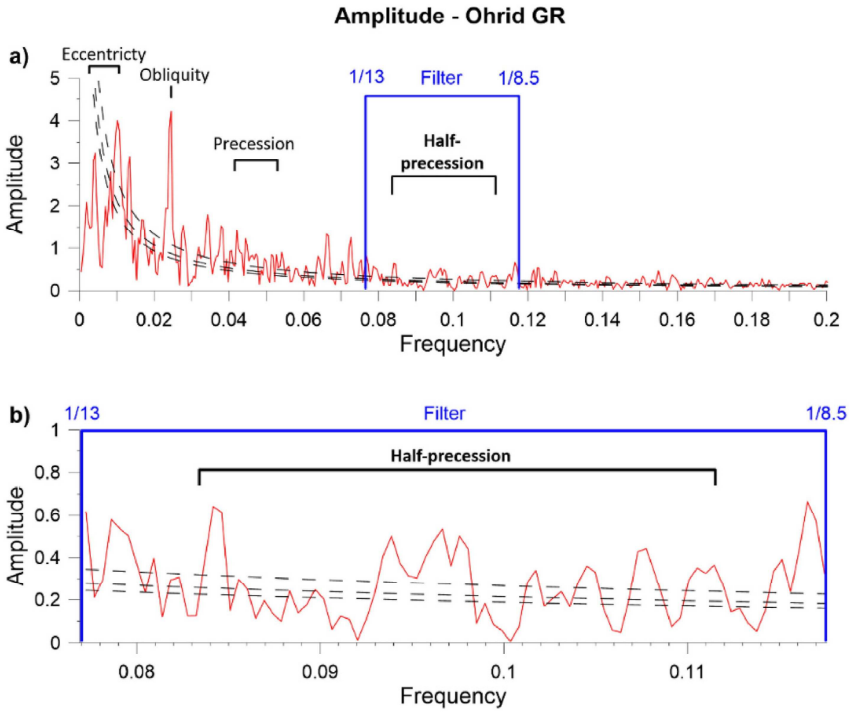

Fig. 2. Amplitude spectrum of gamma radiation record from Lake Ohrid. Filter settings in blue (13–8.5 ka) focusing on half-precession (12–9 ka). The filter is selected wider than HP's actual bandwidth to account for uncertainties. In a) with complete frequency range up to 0.2 (= 5 ka) including Milanković cycles. In b) focusing on the spectra within the filter settings. In both figures dashed lines from top to bottom represent AR(1), 99%, 95% and 90% confidence levels, respectively. The original data and the resulting filtered signal are displayed in Fig. 4a. All datasets examined in this study are filtered in this way, GR only serves as an example here. (For interpretation of the references to color in this figure legend, the reader is referred to the Web version of this article.)

The HP signal is also subject to (quasi-periodic) variations in the ODP wet-dry index (Fig. 3e). Even though the tendency is still towards a connection of HP and interglacials, there are glacials with clear HP signal as well (e.g. MIS 16 and 12). The TOC data from Lake Van is the shortest record presented here (Fig. 3f). The HP signal is most evident in MIS 11, in the transition from MIS 7/6, and MIS 5, i.e. mostly in interglacials. In the Ca/Ti record from the Iberian Margin (Fig. 3g) the HP signal is well recognizable, but a clear assignment to interglacials or glacials is not possible. For example, the two most prominent maxima are at the transition between MIS 13/12 and MIS 9/8. Pronounced minima are located in glacials (e.g., MIS 22, 18, 6), but there are also glacials with a strong HP signal (e.g., 20, 14, 12). In the record from Greenland, a clear connection of HP to glacial/interglacial variability is not visible. It looks as if the HP signal is permanently present in the record. However, this also applies to other periods (outside the range of HP). In particular, the low-frequency signals (<8 ka) are pronounced. The only slightly recognizable pattern is a tendency for the HP signal to be stronger in the interval younger than ~340 ka.

3.2. Correlative estimates

Fig. 4 shows a selection of investigated records from this study. Examining the original data (black lines), it is apparent that the amplitude variation of most proxies is increased in interglacials. For example, Lake Ohrid TIC hardly exhibits any variations during glacials. Although TIC is showing the common feature of "low-variability in glacials" particularly prominent, a similar pattern is present for most parameters, whether downhole-, geochemical-, pollen- or synthetic data.

Comparing the original data (black lines in Fig. 3) with the filtered signal (thin red lines), we can observe a similarity of strong peaks in some time intervals of all proxies. This is especially prominent during interglacials and in transitions from interglacials to glacials. A good example is MIS 13 and its transition into MIS 12, where several cycles with a period of 13–8.5 ka are visible in the GR, the K, the Q.dec and the Ibm.Ca/Ti (Fig. 4a, b and 4d; Supplement Material 01). Similar observations are made for MIS 7. Even though individual cycles in the original record are absent (e.g. in TIC at ~228 ka) or weak (in GR and IbM.Ca/Ti at ~228 ka), this is a good illustration of sub-Milanković cycles in interglacials. In some records, these cyclic patterns proceed into the next glacial as seen for example in MIS 6 (Q.dec, L.Van.TOC, and IbM.Ca/Ti; Fig. 4d, f and 4g).

The relation of eccentricity (Fig. 4i) to the signal of the filtered HP envelopes (Fig. 4, purple) is more complex and the respective proxy records have to be examined individually. In some parts, the amplitudes are in phase or just slightly offset. To give two examples of such a case, we point out to the Lake Ohrid GR between MIS 15–11, or to the younger section (<530 ka) of the IbM.Ca/Ti (Fig. 4a and g). Cases with no apparent correlation between eccentricity and filtered signal can be observed e.g. for Lake Ohrid K between MIS 11–5 or in wet-dry index between MIS 16–8 (Fig. 4b and e).

In Fig. 4, we qualitatively display some relationships between HP and orbital cycles. To quantify these relations, we determine the Pearson correlation coefficients for complete records or for intervals of particular interest (see chapter 2. 'Material and Methods'). The Pearson correlation coefficients between the original data (black lines in Fig. 4) and the Taner filtered signal (thin red lines in Fig. 4) for each entire record are listed in Fig. 5. When

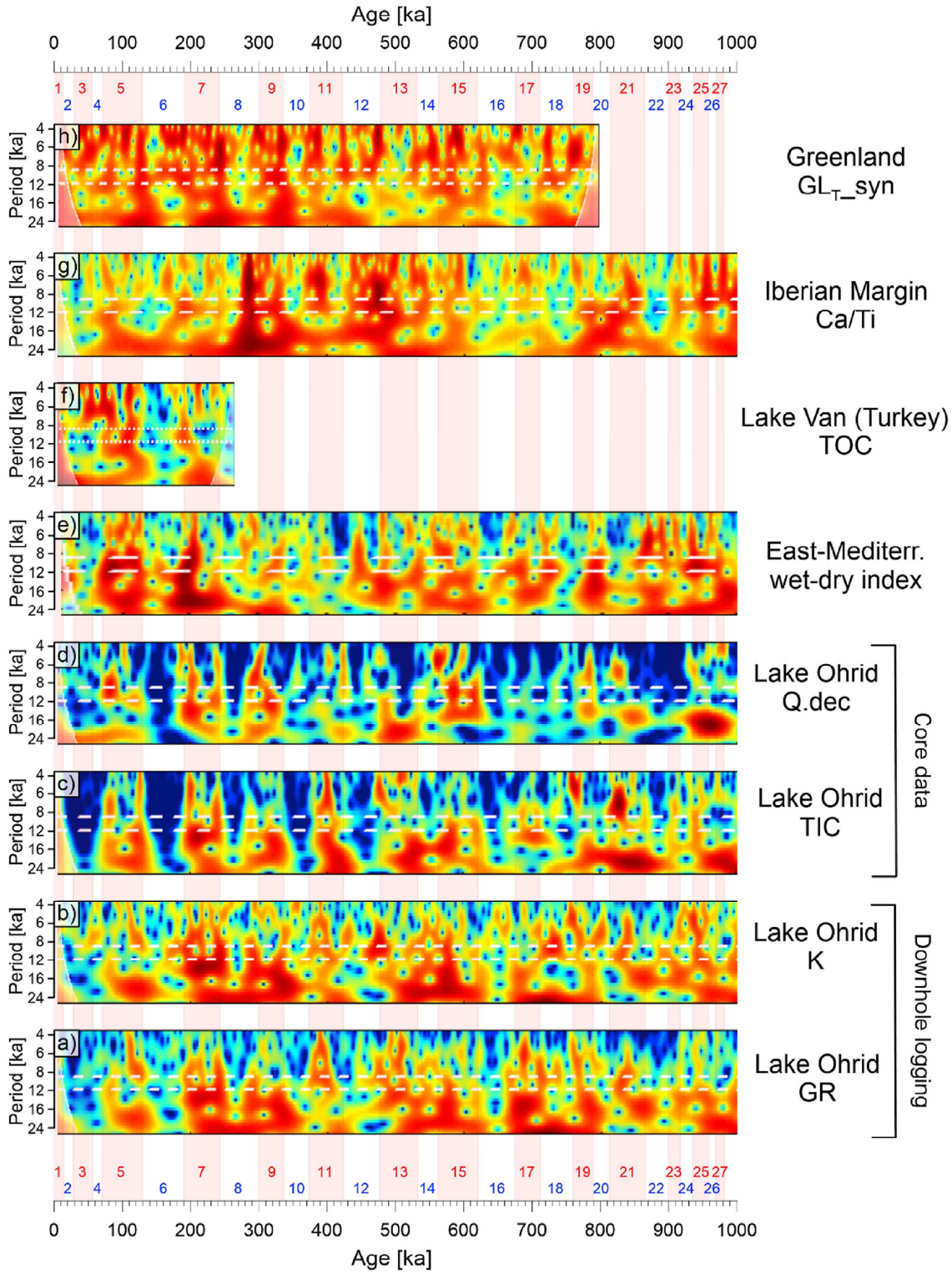

Fig. 3. Wavelet analyses for different proxy signals over the last 1 Ma. Marine isotope stages are indicated in red (interglacials) and blue (glacials) numbered above/below age axes. Reddish background color highlights interglacials. In all spectra high power is indicated by red color, while low power is blue. The period ranges from ~4 to 24 ka, thus even contains the precession signals. The interval of HP (9–12 ka) is located between the dashed white lines. Especially in core data from Lake Ohrid (c and d), the HP signal is stronger in interglacials compared to glacials. In the record from Greenland (h) no connectivity of the HP signal at a certain age is recognizable. All other records exhibit, at least partially, a relationship between HP and interglacials. (For interpretation of the references to color in this figure legend, the reader is referred to the Web version of this article.)

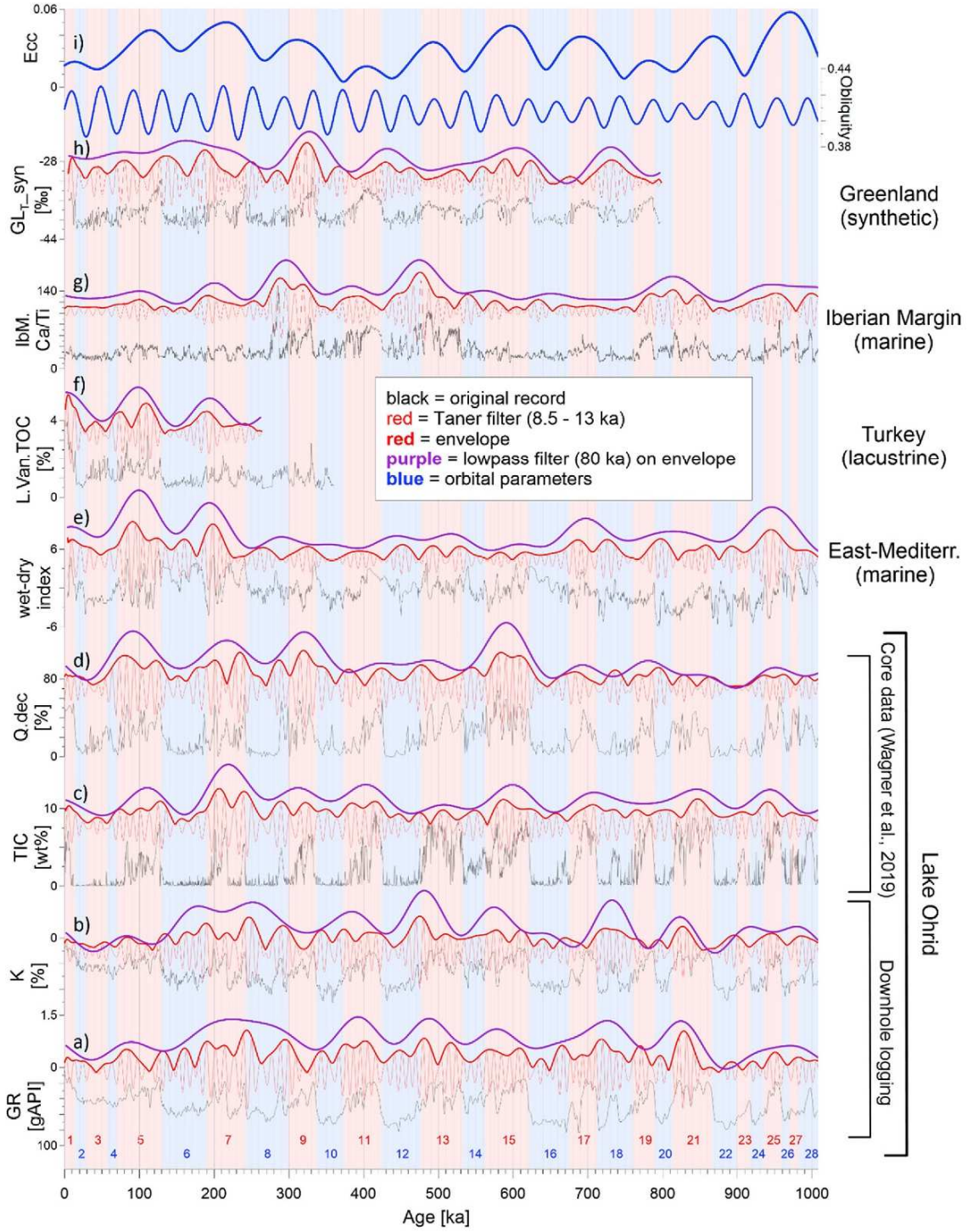

Fig. 4. Eight of the investigated records (GR, K, TIC, Q.dec, wet-dry index, L.Van.TOC, Ibm.Ca/Ti, GL_T syn and obliquity, eccentricity) with original data (black), the signal after applying the bandpass filter (thin red line) and its envelope (thick red line). The purple line represents the lowpass-filtered envelope which omits high-frequency amplitude components not related to eccentricity (detailed information on filter settings in chapter 2. 'Material and Methods'). At the top are obliquity and eccentricity from Laskar et al. (2004). Abbreviations of proxies as in Table 1. Y-axes are for original data only. We do not show axes for the filtered signals to avoid unambiguity. Background color is red for interglacials and blue for glacials. Numbers of MIS stages are indicated above the abscissa at the figure bottom. Tie points for tuning of the downhole logging data are given in the Supplement Material 06. (For interpretation of the references to color in this figure legend, the reader is referred to the Web version of this article.)

examining the correlation coefficients, the fact that low variability is present in glacials needs to be considered. Generally, signals from glacials, where we usually see a lower correlation, drag down the overall correlation values. However, even if these values are generally low, they are of statistical relevance (p-value is constantly <0.01). This is also confirmed for the shorter records: Loess from Dolní Věstonice (126–22 ka), $\delta^{18}O$ from Greenland ice (120–0 ka), and TOC from the Lake Van record (264–1 ka; see Table 1 for details).

The records from the south (TOC from Lake Van, wet-dry index from ODP site 967) tend to have higher correlation values (Fig. 5) than those from the north ($\delta^{18}O$ and synthetic records from Greenland). In between are the records from the Iberian Margin, from the Tenaghi Philippon in Greece and most of the records from Lake Ohrid. The correlation coefficients of the different proxies from Lake Ohrid show a wide spread. The maximum value is 0.26 for one of the pollen records (Q.dec; which is at the same time the highest value of all long term (>1 Ma) records). The lowest correlation coefficient of 0.17 is reached in the TIC record (here we have to consider the effect of "low-variability in glacials" described above). The average value for all records of Lake Ohrid results in a correlation coefficient of 0.20 ± 0.03.

The highest correlation (Lake Van, TOC) occurs in a relatively short and young record. This is (at least partly) due to the effect of older parts of the long records generally showing little relation between the original record (black lines in Fig. 4) and the filtered signal (thin red lines in Fig. 4), which lowers their mean correlation coefficient values. To test this variability over time, we determine the correlation coefficients for the time range from 621 ka until recent and for the range from 243 ka until recent. The trend of low values in the north and higher values in the south persists, but the overall correlation coefficients are higher, the younger the time interval. For details see Supplement Material 07.

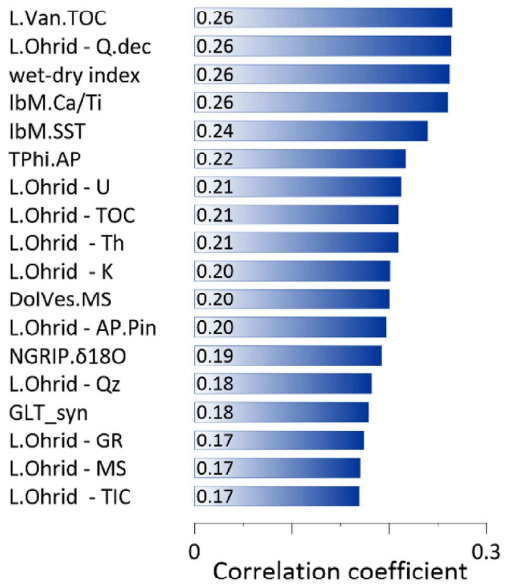

Fig. 5. Correlation coefficients between the original record (black line in Fig. 4) and the bandpassed signal (thin red line in Fig. 4). This table includes all of the investigated data of this study. It has to be taken into account, that three records are significantly shorter (DolVes.MS = 126–22 ka), NGRIP.δ18O = 120–0 ka), and L.Van.TOC = 264–1 ka). All other records cover more than 800 ka. Note that all correlations are significant at >99% confidence. (For interpretation of the references to color in this figure legend, the reader is referred to the Web version of this article.)

3.3. Moving window correlation

Further investigations on the time dependency of the correlation coefficients are possible using the moving window correlation as by Sageman et al. (1999); see chapter 2. 'Material and Methods'. Fig. 6 shows the temporal development of correlation coefficients between original data and the filtered signal (black and thin red line in Fig. 4) of selected proxy records. Overall, the values vary between ~0–0.6 with negligible exceptions of negative correlation (e.g., IbM.Ca/Ti at 232 ka or Q.dec between 885 ka and 845 ka, Fig. 6g and d).

Correlation coefficients are generally higher in the younger part of the records (Fig. 6). Linear fits through the respective running correlation coefficients illustrate this increase. The clarity of the HP signal increases towards the younger parts. The only exception is the record from Lake Van, which is too short for statements about the long-term evolution of the coefficients (Fig. 6f). Despite this divergence of the Lake Van data to the other records, it follows a trend described in the subsequent paragraph.

To some extent, the moving window correlations follow the 405-ka-eccentricity cycle (E_{405}). Although it may be overprinted by effects of the glacial-interglacial variability, we see several similarities between the E_{405} and the pattern of correlation coefficients (Fig. 6) which are high between 600 and 500 ka, and around 200 ka. A good contrary example is MIS 11 where the minimum in E_{405} coincides with minima in correlation coefficients in all shown records. The maximum of E_{405} around MIS 8–6 is reflected in the correlation coefficients of most proxies. Even in glacials, high values in the correlation coefficients are reached (e.g., MIS 8 in the records from Lake Ohrid or MIS 6 in the wet-dry-index from ODP 967 and the Ca/Ti record from the Iberian Margin; Fig. 6a, e and 6g). To some extent this is also true for the older E_{405} maximum (see maximum in MIS 15–13 in GR or Q.dec; Fig. 6a and d), but a clear response is not apparent in this part of the records.

We see a stronger connection of HP to the long-term eccentricity during the last ~621 ka, therefore we focus on this time interval for further investigations on the ~100-ka-eccentricity cycle (E_{100}). We correlate eccentricity to the smoothed envelope derived from the HP signal (purple lines in Fig. 4). The crossplots in Fig. 7 show a wide range of correlation coefficients (r from 0 to 0.74). We notice that the correlation values are highest for the parameters measured on the sediment core of Lake Ohrid (Fig. 7c and d). For most other proxies a clear relationship, and thus the role of E_{100} onto HP, is ambiguous. As described in chapter 2.2 'Time series analysis', we use low-pass filter to assess eccentricity components of the HP amplitude. While a specific eccentricity filter may give clearer results, the applied approach tests if the long term components of the HP amplitude match eccentricity, or if these are influenced by other effects. It should be noted that low correlations do not necessarily mean that there is no relationship between E_{100} and the smoothed HP envelopes. A delayed response of the HP signal to E_{100} is not traceable with this method. For instance, the R-value in the Ca/Ti dataset is 0 (Fig. 7g). Nevertheless, in Fig. 4g we see that the HP envelope (purple line) and the eccentricity (Fig. 4i) are nearly parallel during the last ~500 ka. A systematic offset of ~20 ka is enough to cause this decrease of the correlation value.

We also examined the records for a correlation between obliquity and the envelope of the HP signal (thick red lines and obliquity in Fig. 4. An unambiguous correlation could not be found for any record (see Supplement Material 08).

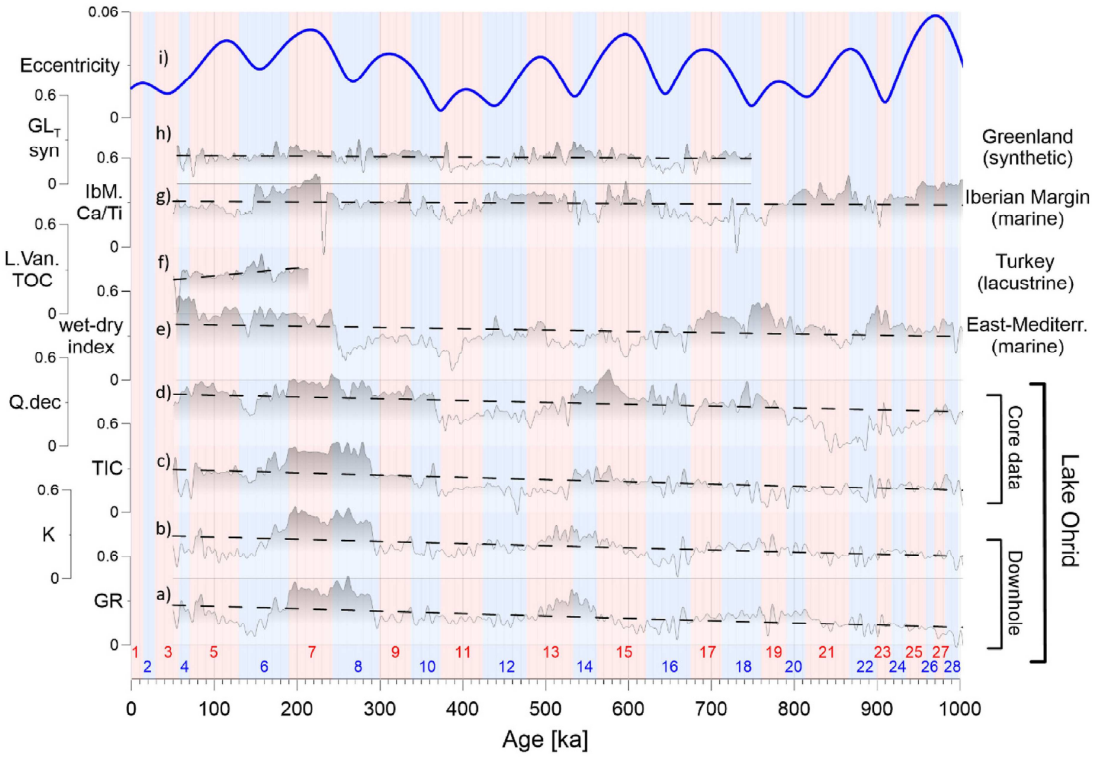

Fig. 6. Relation of correlation coefficients between the original records (black lines in Fig. 4) and the filtered signals (thin red lines in Fig. 4) over time using moving window correlation and trends thereof. Shaded areas indicate periods of high correlation. Details about proxies are listed in Table 1. Dashed lines are linear fits and increase towards the recent (except Lake Van). Marine isotope stages are indicated in red (interglacials) and blue (glacials) numbers. (For interpretation of the references to color in this figure legend, the reader is referred to the Web version of this article.)

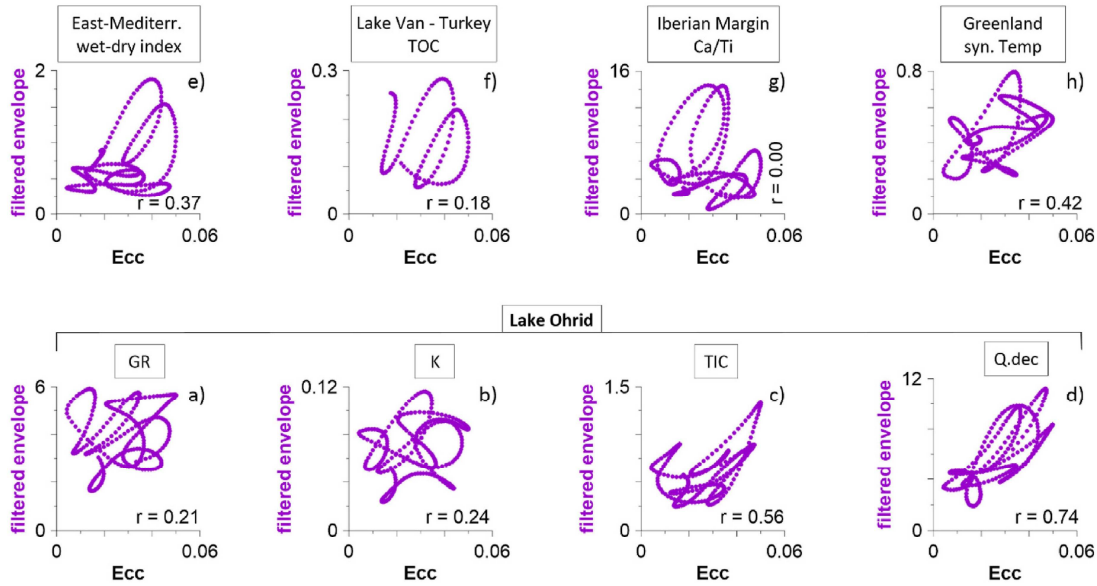

Fig. 7. Crossplots of the filtered envelope (purple line in Fig. 4) to eccentricity (Ecc.). For these plots, only the interval <621 ka (younger than MIS 16) is considered. We observe from Fig. 4 that the relationship of eccentricity to the envelope is ambiguous in parts >621 ka. Coefficients 'r' from Pearson correlation are in the lower right corner. (For interpretation of the references to color in this figure legend, the reader is referred to the Web version of this article.)

4. Discussion

4.1. Detection of the half-precession signal

We use several different methods to characterize the HP signal and its intensity through time. In this regard, all methods have their advantages and challenges, and it is also necessary to consider the different properties of the records.

Power/amplitude spectra are a common tool in cyclostratigraphy. In case orbital cycles are prominently present in a record, they can be recognized rapidly and clearly (Fig. 2; Supplement Material 03). However, amplitude spectra usually represent the complete record and thus also parts where HP is weak and/or superimposed by other frequencies. For this reason, it is possible to get the impression of there being no HP in a record, even though the HP signal is significant in certain time intervals (Supplement Material 04).

Wavelet analysis is an effective method in cyclostratigraphy to assess the variation of signal intensity through depth or time. We can observe the evolution of the HP throughout a record and provide evidence for the occurrence of HP at certain intervals (Fig. 3; Supplement Material 05). An example is the TIC content in Lake Ohrid, where HP is mostly linked to interglacials (Fig. 3c). Wavelet analysis is challenging to interpret when other frequencies superimpose the HP, especially in records with a prominent contribution of high-frequency signals. The synthetic temperature record from Greenland is an example for this feature (Fig. 3h). Overall, this method is suitable for characterizing the occurrence of HP at specific intervals within a record, but straightforward quantification and comparison between different records is challenging.

Therefore, we apply an approach with correlation between original data and filtered data (see chapter 2.2 'Time series analysis'). With this method we can examine a complete record or certain parts of it and obtain one correlation coefficient value for each record (or parts of it). This facilitates comparison with records from other regions (Fig. 5; Supplement Material 07). The moving window correlation after Sageman and Hollander (1999) enables (like the wavelet analysis) the characterization of the HP signal over time. The size of the window should be selected properly; a small window leads to high fluctuations of the correlation coefficients over time, a too large one can lead to smoothing of the coefficients over a longer period of time.

4.2. Characteristics of half-precession in paleoenvironmental records

In many climate records, interglacials have a complex structure with multiple peaks and troughs in proxy values representing variable climate conditions (e.g. Lang and Wolff, 2011; Railsback et al., 2015). An example is the LR04 stack of marine benthic oxygen isotopes (Lisiecki and Raymo, 2005), where several interglacials are separated into substages (e.g. MIS 7a-e, MIS 5a-e). Albeit in these particular cases the subdivision is strongly related to precession, this example shows that proxy signal variations tend to be stronger in interglacials compared to glacials. Similar observations have been made in a lacustrine record from Lake Baikal, where interglacials can be interrupted by short cold periods (Prokopenko et al., 2006). Any proxy should be evaluated individually for its suitability to assess HP signals. Most proxies record the HP signal more accurately in interglacials, but we can distinguish them from proxies that are also capable to record HP in glacials. Even if we group these proxies, the transitions between these groups are smooth.

4.2.1. Interglacial-sensitive proxies

In general, the HP signal in all records examined in this study is more pronounced in interglacials than in glacials. However, there are some cases where the difference between the quality of HP in interglacials is particulary increased compared to glacials.

In our study, the most exceptional case of interglacial sensitivity is the TIC-content in Lake Ohrid (Figs. 3c and 4c). TIC is highly climate sensitive and reflects hydrologic variability. Its amount in Lake Ohrid's sediments is influenced by various factors such as authigenic formation of calcite in the sediments, as well karst runoff triggered by warm conditions (Francke et al., 2016; Wagner et al., 2010, 2019; Vogel et al., 2010).

Also pollen records commonly display the feature of low-variability in glacials, even if not as pronounced as in TIC (e.g. Fig. 4d). This is because certain plant species are completely absent in strong glacials (Wagner et al., 2019; Sadori et al., 2016; Tzedakis et al., 2006).

4.2.2. Proxies capable of recording HP in glacials

The low-variability in glacials is a general property within many climate sensitive proxies, and may complicate analyses of HP. To address this feature, it is necessary to use proxies that are related to amplitude variations also during glacial conditions. In context of Lake Ohrid, this is especially valid for the relative amount of quartz (Qz in Supplement Material 01) and K-concentrations (Fig. 4b). Both are indicators of detrital input (Wagner et al., 2019; Francke et al., 2016).

The wet-dry index introduced by Grant et al. (2017) is based on a sapropel/monsoon index and a dust record (Larrasoaña et al., 2003). This approach is advantageous because the record shows amplitude variations in warm and cold periods, while the variability of other records tend to not encompass both glacials and interglacials equally. Since the index is sensitive to monsoon runoff, it has a stronger connection to low latitude regions than the other examined records.

Hodell et al. (2013) described sub-Milanković cycles in a power spectrum as harmonics of the precession cycle in the Ca/Ti record. However, their study did not focus further on periods shorter than precession. Our focus on the bandwidth between 1/13–1/8.5 facilitates a more detailed investigation of HP in the Ca/Ti record.

4.3. Temporal occurrence of half-precession

The time scale quality of a record can have a relevant impact on the detectability of HP cycles. When time scales are not accurate, HP cycles may appear longer or shorter, and fall out of our filter window. We assume that the used age datasets are robust and that uncertainties in the age-depth calculations do notaffect our overall results. In addition, we address this issue setting the Taner bandpass filters from 8.5 to 13 ka, allowing for imperfect time scales with some distortion, and longer than the actual length of HP cycles (9.5–11.5 ka; Berger et al., 1997). This ensures that the HP signal is detected despite small errors in the time scales.

We observe that the HP signal is generally stronger in interglacials than in glacials. This may be due to the different responses of the proxies to environmental changes, and not an actual weakening of the HP signal in glacial periods (see chapter 4.2 Characteristics of half-precession in paleoenvironmental records'), or an increased HP influence on climate systems during interglacials. HP cycles are very distinctive in some interglacial records. Examples are MIS 7 and MIS 13 in most records of Lake Ohrid (Fig. 4a, b and 4c; Supplement Material 04), MIS 5 of the wet-dry index from the Eastern Mediterranean (Fig. 4e) and pollen from Lake Ohrid (Fig. 4d). However, depending on the selection of a proxy and its sensitivity to environmental changes, we occasionally

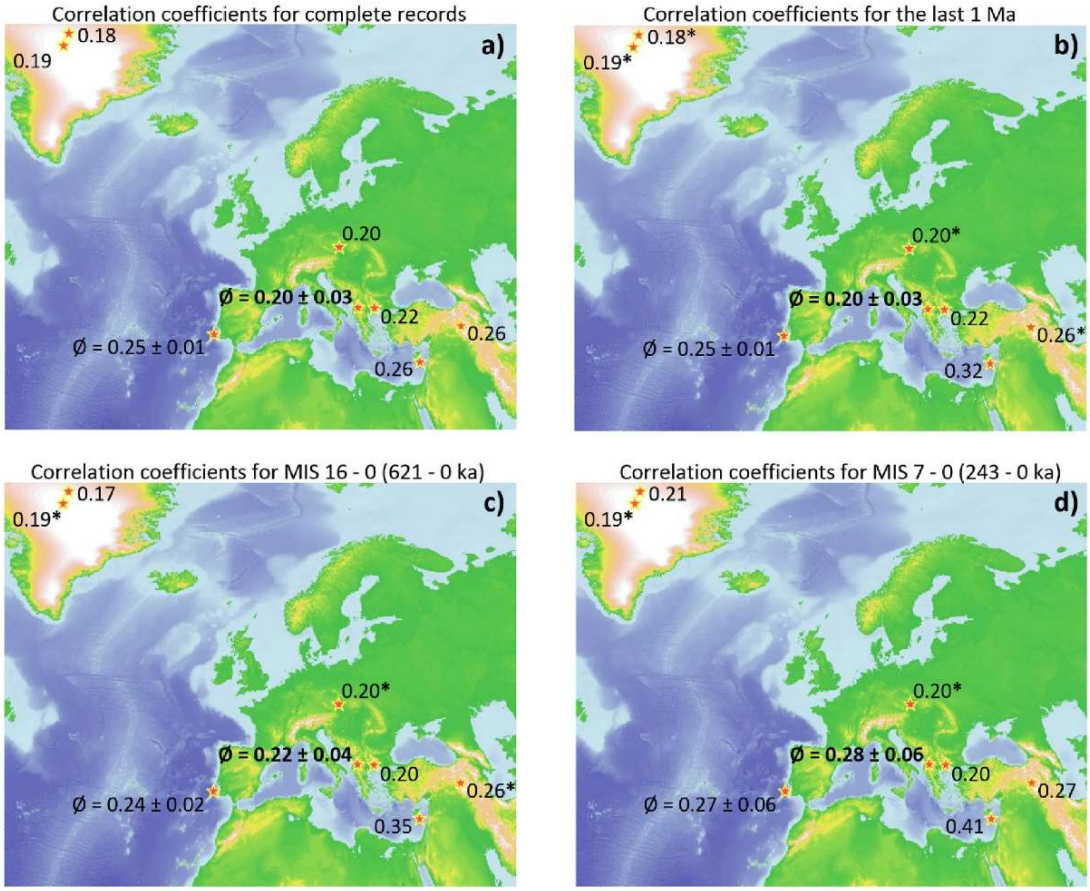

Fig. 8. Correlation coefficients as proxy for the relative contribution and clarity of the HP signal at the investigated sites in different time intervals (a–d). Lake Ohrid data is bold. Values marked with asterisks (*) are from data sets that are shorter than the time interval specified in the respective title (see Table 1 for exact time span of individual records). Average values (Ø) and standard deviations are from sites where multiple datasets are available (two records from the Iberian Margin and ten from Lake Ohrid). Note that the correlation values generally increase towards the younger intervals (from a-d; as the linear trends in Fig. 6).

recognize HP in glacials. Examples are MIS 12 in the Ca/Ti from the Iberian Margin (Fig. 4g) or MIS 16 and MIS 12 in the wet-dry index from the Eastern Mediterranean (Fig. 4e).

In addition to the variability of the HP signal between interglacials and glacials, we see a consistent trend of increasing HP signal towards the recent (Fig. 6). A possible explanation for this trend is the change from the 40-ka to the 100-ka world during the Mid-Pleistocene Transition (MPT; Shackleton and Opdyke, 1976). Since precession is modulated by eccentricity, a similar effect may be expected for the HP signal. This idea is supported by the presence of a positive correlation between HP and eccentricity (Figs. 6 and 7) in the younger part (<621 ka) of the investigated records, but the absence of such a relation between HP and obliquity (Supplement Material 08).

If assuming a relation of HP to eccentricity, one may expect a weaker expression of HP in an obliquity dominated world. Such conditions prevailed before and partly during the MPT ~1.25 to 0.7 million years ago (Pisias and Moore, 1981; Clark et al., 2006; Mudelsee and Schulz, 1997). The length of most examined records in this study does not allow assessment of HP before MPT. In the records from Lake Ohrid, the MPT is partly covered and we see an increase of HP intensity during and after the MPT. After MIS 16, the HP signal is more prominent and follows partly the E_{405} cycle while before MIS 16 (in the younger part of the MPT) the clarity of the HP signal vanishes (Fig. 6). Therefore, the HP signal in Lake Ohrid appears to be not only affected by glacial or interglacial conditions, but also by orbital eccentricity and specifically the E_{405} cycle.

4.4. Spatial occurrence of half-precession around Europe

The correlation coefficients between the paleoclimate proxy datasets and HP filters listed in Fig. 5 are an indicator of the clarity of HP signal in each record. Fig. 8a shows those values on a map of Europe and the North Atlantic. In shorter and younger time intervals, this relation persists and the gradient between the regions even increases (Fig. 8a–d and Fig. 9a–d). The r-values in Greenland remain almost equally low while values in the Eastern Mediterranean increase clearly from 0.26 to 0.41. The records from the Iberian Margin and Lake Ohrid (which are - from a spatial point of view - between the Eastern Mediterranean and Greenland), show intermediate changes in the clarity of the HP signal over time. Thus, we observe a trend of stronger HP signal in data from the southeast to weaker HP signal in the northwest. Fig. 9 illustrates this relationship with respect to latitude for four time intervals. The pattern of higher correlation coefficients in the south - and thus higher clarity of HP - is even stronger in the younger part of the records (Fig. 9d).

In Figs. 8 and 9, we use an average r-value for all sites with multiple datasets (two datasets on the Iberian Margin, ten datasets

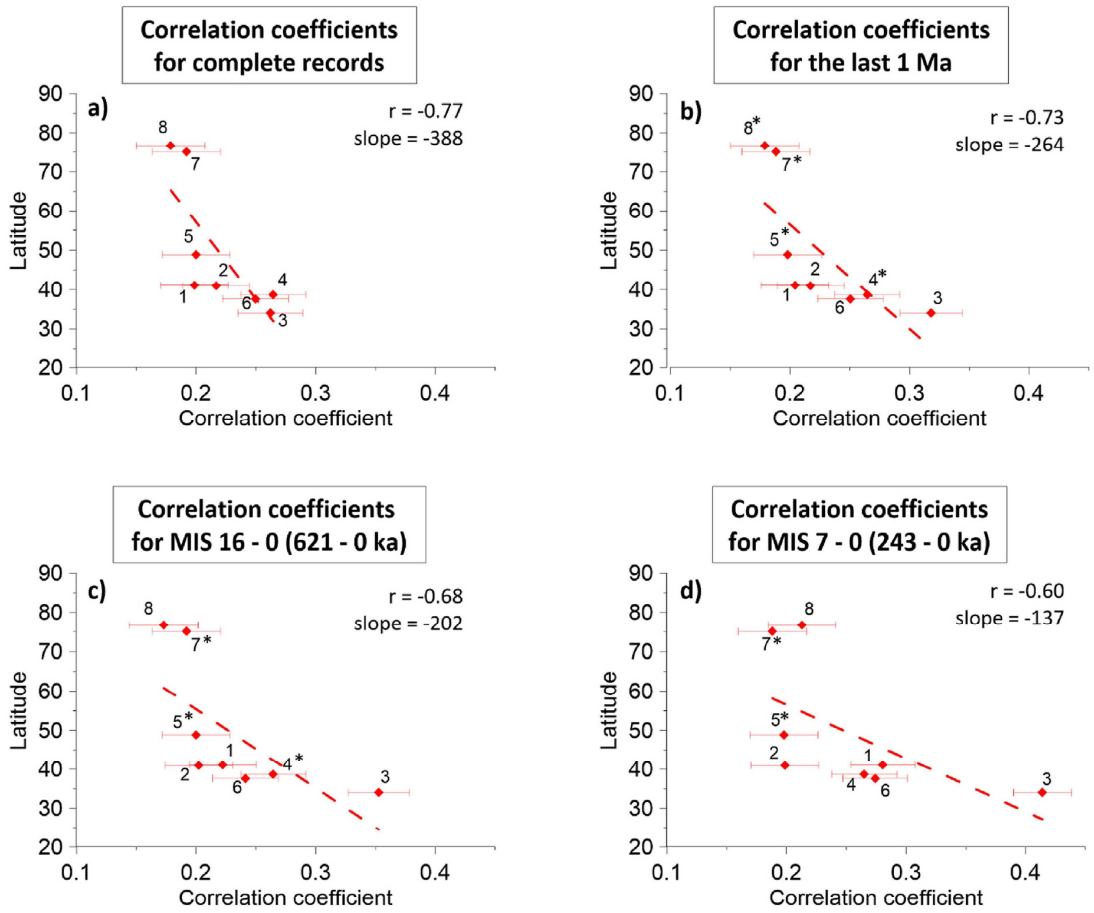

Fig. 9. Correlation coefficients between original data (black lines in Fig. 4) and bandpassed signals (thin red line in Fig. 4) as proxy for the clarity of HP cycles against latitude for the investigated sites. Time intervals as in Fig. 8. Uncertainty estimated as explained in Supplement Material 09. We use the average standard deviation for sites where multiple datasets are available (two records from the Iberian Margin and ten from Lake Ohrid). Dashed line is a linear fit with slope values given in each subplot (a–d). The relationship between latitude and clarity of HP (here correlation) is changing through time. The difference in HP clarity between the Mediterranean region and Greenland is increasing through time from a) longest time interval to d) youngest interval. Also note that data marked with asterisks (*) are from records that are shorter than the time interval specified in the respective title (see Table 1 for exact time span of individual records). 1. Lake Ohrid, Albania/North Macedonia; 2. Tenaghi Philippon, Greece; 3. ODP Site 967, Eastern Mediterranean; 4. Lake Van, Turkey; 5. Dolní Věstonice, Czech Republic; 6. IODP Site U1385 "Shackleton site", Iberian Margin; 7. NGRIP, Greenland; 8. Synthetic record, Greenland (see Table 1 for proxy details and Fig. 1 for location on the map). (For interpretation of the references to color in this figure legend, the reader is referred to the Web version of this article.)

in Lake Ohrid). Especially in records from Lake Ohrid, the range in r from 0.17 to 0.26 is relatively wide (Fig. 5). Despite this range we see an increase of average values towards the recent (Fig. 9).

Several studies demonstrated HP cycles in low latitude records (e.g. Hagelberg et al., 1994; Trauth et al., 2003). The HP signal is expected to be strongest in equatorial regions where the twice-yearly passage of the sun over the equator creates a precession harmonic at 10–12 cycles/ka (Hagelberg et al., 1994; Short et al., 1991). HP from a lacustrine record in East Africa illustrates the connection of HP cyclicity to the monsoonal system (Verschuren et al., 2009). The previous findings that HP is a mainly tropical signal is in agreement with our investigations. The closer a record is to the influence area of a monsoon system, the stronger is the HP signal. In our study, this is most evident in the ODP 967 (Grant et al., 2017) and Lake Ohrid records (Wagner et al., 2019). Towards higher latitudes the HP signal decreases gradually, but weak signals are still found in records from Greenland. High and low latitudes in the North Atlantic appear decoupled prior to the initiation of Northern Hemisphere glaciation, but strongly coupled thereafter (deMenocal et al., 1993; Hagelberg et al., 1994).

When comparing different data from different regions, several aspects like the catchment areas or regional environmental changes need to be considered. As an example, we examine the records from Lake Ohrid and the ODP 967 core from the eastern Mediterranean (Grant et al., 2017). Although both are basically a two component system (Lake Ohrid: non calcareous clay/calcareous clay (Francke et al., 2016); ODP 967: detrital input/sapropels (Grant et al., 2017), they differ by the extent of their catchment area. Local geological influences like tectonic movement in the catchment area of Lake Ohrid may affect the recording of climate signals. In comparison, the ODP core with its catchment of large parts of Africa will not be as sensitive to such small-scale events. However, in lake environments we often observe high sedimentation rates and thus, a good temporal resolution, which in turn is advantageous for the preservation of (Sub-)Milanković cycles. The same holds for terrestrial records like the loess record from Czech Republic (Supplement Material 01; Antoine et al., 2013; Fuchs et al., 2013). Due to better resolution, the HP signal is preserved very well in certain short time intervals (e.g. early MIS 5), but such records cover only a short time interval (e.g., 126–22 ka). Marine

records are often more constant regarding preservation of changes in environmental conditions over long time periods, but often have lower sedimentation rates. All of this needs to be considered when analyzing records in terms of short orbital cycles (and other high-frequency signals). Not only the type of proxy is relevant for the preservation of HP, but also the regional environmental conditions of the location from which the record originates.

4.5. Implications for the origin of half-precession in the studied region

Until now HP is poorly understood and only described in single records. Heinrich (1988) demonstrated the existence of an 11 ± 1 ka cycle based on the occurrence of ice rafted debris in marine sediments of the North Atlantic, as increased ice runoff occurred during solar radiation maxima/minima. Also Hinnov et al. (2002) proved the occurrence of HP in high latitudes and suggested a link to Dansgaard-Oeschger events. On the other hand, there are considerably more studies describing the origin of HP in equatorial regions as a result of the two insolation maxima per precession cycle (e.g. Berger et al., 1997; Laepple and Lohmann, 2009; Trauth et al., 2003). Here, we analyze HP in a suite of records in order to better understand its spatial occurrence allowing to discuss its climatic origin.

We observe a clear gradient in the intensity of HP in European and North Atlantic regions. The signal is clearest in the southeast, and may be influenced by the Asian and/or African monsoonal systems. However, the HP signal (even if significantly weaker) in the high latitudes like Greenland cannot be directly affected by the low latitude monsoon systems. Sun and Huang (2006) and also Turney et al. (2004) demonstrated that information about HP can be transferred from low to high latitudes. We suggest that when information (about HP) propagates via atmospheric and/or oceanic teleconnections, more of the information dissipates as the distance from the source of the HP signal increases. Additionally, other (orbital) signals may overprint the HP signal in high latitudes (e.g. Short et al., 1991; Hodell et al., 2013).

Alternatively, the HP signal in high latitudes may have a different mechanistic origin from the HP in low latitudes. In low latitudes the HP is a predominantly interglacial feature, possibly because the high precession amplitude during high eccentricity transports signals from one hemisphere over the equator to the other hemisphere. Contrary, in Greenland HP occurs regardless of variability between glacials and interglacials, albeit at comparably weak levels.

In Figs. 8 and 9, we demonstrate that the clarity of HP signal is stronger in the southern records and is generally increasing towards the recent. Our results suggest that the HP signal originates in the south and that this pattern is partially transported to high latitudes. We illustrate that despite a pronounced increase of the HP in the south, it is only weakly transported to the high latitudes of the Greenland records.

Assuming that the main source of the HP signal is in equatorial regions and that HP signals in high-latitude records must be transmitted from there, we see the potential of HP as an indicator for the connectivity between low- and high-latitude climate systems over time, at least in the European/North Atlantic region.

In this context our analysis shows strongest HP and connectivity of the Iberian Margin to the tropics during interglacials and especially in the high-eccentricity (high precession amplitude) interval of MIS 7 (Fig. 6). Contrary, little HP is transmitted to the Mediterranean region during the glacials, though the strongest HP signals occur in the eastern Mediterranean, where the signal is carried via the Nile River.

Kaboth-Bahr et al. (2018) suggest that the monsoonal influence on the water density structure in the Mediterranean affects the variability of the Mediterranean Outflow Water (MOW), which effectively transmits a low-latitude orbital pacing to the East Atlantic off Iberia and via atmospheric moisture transport to the European continent. In the late Quaternary, low precession amplitudes led to less severe dry phases in North Africa and thus less prominent peaks in MOW strength. If we consider the MOW as a transport mechanism for the HP signal, this is in agreement with the low HP signature in the low precession amplitude phases during MIS 14 and 11 in the Iberian Margin record (Fig. 6g). In contrast there was a phase with high MOW production caused by particularly pronounced aridity phases during MIS 6 within the E_{400}-maximum (Kaboth-Bahr et al., 2018; Trauth et al., 2009). Again, we can see a connection of the HP records from the Mediterranean to the Iberian Margin as the increased MOW probably transferred the HP signal during MIS 6 (Fig. 6e and g). This implies an astronomically forced shift of climate systems over the Mediterranean region. One prominent driver is the Nile discharge, which modulates the Mediterranean circulation and even influences the outflow of the Mediterranean Sea into the Atlantic Ocean.

5. Conclusions

The good temporal resolution and the continuity of the records in Lake Ohrid provide excellent prerequisites for cyclostratigraphic studies. In a suite of sedimentary proxies, there is recurrent evidence of HP cycles from the Mid-Pleistocene to the recent. The expression of HP cycles is generally stronger in the younger parts of the data (<MIS 16) and during interglacials. The latter may partly result from the natural behavior of proxies.

In several records from Lake Ohrid, a relationship between HP and eccentricity cycles exists. Even a connection to the long term 405-ka-eccentricity cycle is apparent after the Mid-Pleistocene Transition. However, a correlation between the HP envelope and obliquity is absent. We interpret this as a relation of HP and precession and its amplitude.

HP is present in all examined datasets between Greenland and the Eastern Mediterranean, although the proxies are dominated by different climate systems. The reasons for the appearance of the HP signal in different records may be diverse, but we see a distinct trend from weaker HP signals in the North Atlantic to a stronger signature in the Eastern Mediterranean region. The clarity of the HP signal between the Atlantic and the Mediterranean appears to be gradual, as are the transitions between the causative climate systems. We suggest that the equatorial HP signal is transported northward via different modes. Besides Nile water discharge and Mediterranean Outflow Water, the connected Monsoon systems are one major driver in this process. The sediment succession from Lake Ohrid appears to be a link between the high and low latitudes climate systems; Wagner et al. (2019) describe a connection to the African monsoon. We identify a similar influence of low latitudes on Lake Ohrid expressed as the distinctness of the HP signal in the records.

HP is a relevant part of natural climate variability - also in Europe especially in interglacials. Its probable origin in low latitudes and the possible transmission of the HP signal to high latitudes gives HP the potential to be an indicator for the interconnectivity of paleoclimate systems.

Author contribution

Zeeden, Christian Scientific support during study design. Discussion, especially for time series analysis. Writing/editing the manuscript. Prof. Dr. Voigt, Silke Scientific support and discussion, especially for spatial context of the half-precession signal. Writing/

editing the manuscript. Dr. Sardar Abadi, Mehrdad Scientific support and discussion. Writing/editing the manuscript. Dr. Wonik, Thomas Scientific support and discussion, especially in downhole logging data acquisition and interpretation.

Declaration of competing interest

The authors declare that they have no known competing financial interests or personal relationships that could have appeared to influence the work reported in this paper.

Acknowledgements

This research project was possible due to funding from the German Research Foundation (grant WO672/15). The "Scientific Collaboration on Past Speciation Conditions in Lake Ohrid" (SCOPSCO) drilling project was partly funded by grants from the International Continental Scientific Drilling Program (ICDP), the German Ministry of Higher Education and Research, the German Research Foundation, the University of Cologne, the British Geological Survey, the Italian National Institute of Geophysics and Volcanology (INGV) and the Italian National Research Council (CNR) and the governments of the republics of North Macedonia (or FYROM) and Albania. We would like to thank the whole SCOPSCO team for helpful discussions about the results. The boreholes were drilled by Drilling, Observation and Sampling of the Earth's Continental Crust, Inc. Our special thanks go to Thomas Grelle, Jan-Thorsten Blanke and Dr. Henrike Baumgarten of the Leibniz Institute for Applied Geophysics for the acquisition of the geophysical downhole logging data. We also appreciate the work of anonymous reviewers and editors.

Appendix A. Supplementary data

Supplementary data to this article can be found online at https://doi.org/10.1016/j.quascirev.2022.107413.

References

Amante, C., Eakins, B.W., 2009. ETOPO1 Arc-Minute Global Relief Model: Procedures, Data Sources and Analysis.

Antoine, P., Rousseau, D.-D., Degeai, J.-P., Moine, O., Lagroix, F., kreutzer, S., Fuchs, M., Hatté, C., Gauthier, C., Svoboda, J., Lisá, L., 2013. High-resolution record of the environmental response to climatic variations during the Last Interglacial–Glacial cycle in Central Europe: the loess-palaeosol sequence of Dolní Věstonice (Czech Republic). Quat. Sci. Rev. 67, 17–38. https://doi.org/10.1016/j.quascirev.2013.01.014.

Barker, S., Knorr, G., Edwards, R.L., Parrenin, F., Putnam, A.E., Skinner, L.C., Wolff, E., Ziegler, M., 2011. 800,000 Years of abrupt climate variability. Science 334, 347–351. https://doi.org/10.1126/science.1203580.

Baumgarten, H., Wonik, T., Tanner, D.C., Francke, A., Wagner, B., Zanchetta, G., Sulpizio, R., Giaccio, B., Nomade, S., 2015. Age–depth model of the past 630 kyr for Lake Ohrid (FYROM/Albania) based on cyclostratigraphic analysis of downhole gamma ray data. Biogeosciences 12, 7453–7465. https://doi.org/10.5194/bg-12-7453-2015.

Berger, A., Loutre, M.F., McIntyre, A., 1997. Intertropical latitudes and precessional and half-precessional cycles. Science 278, 1476–1478.

Berger, A., Loutre, M.F., Mélice, J.L., 2006. Equatorial insolation: from precession harmonics to eccentricity frequencies. Clim. Past 2, 131–136. https://doi.org/10.5194/cp-2-131-2006.

Broecker, W.S., 1998. Paleocean circulation during the Last Deglaciation: a bipolar seesaw? Paleoceanography 13, 119–121. https://doi.org/10.1029/97PA03707.

Clark, P.U., Archer, D., Pollard, D., Blum, J.D., Rial, J.A., Brovkin, V., Mix, A.C., Pisias, N.G., Roy, M., 2006. The middle Pleistocene transition: characteristics, mechanisms, and implications for long-term changes in atmospheric pCO2. Quat. Sci. Rev., Critical Quaternary Stratigraphy 25, 3150–3184. https://doi.org/10.1016/j.quascirev.2006.07.008.

Colcord, D.E., Shilling, A.M., Sauer, P.E., Freeman, K.H., Njau, J.K., Stanistreet, I.G., Stollhofen, H., Schick, K.D., Toth, N., Brassell, S.C., 2018. Sub-Milankovitch paleoclimatic and paleoenvironmental variability in East Africa recorded by Pleistocene lacustrine sediments from Olduvai Gorge, Tanzania. Palaeogeogr. Palaeoclimatol. Palaeoecol. 495, 284–291. https://doi.org/10.1016/j.palaeo.2018.01.023.

De Vleeschouwer, D., Da Silva, A.C., Boulvain, F., Crucifix, M., Claeys, P., 2012. Precessional and half-precessional climate forcing of Mid-Devonian monsoon-like dynamics. Clim. Past 8, 337–351. https://doi.org/10.5194/cp-8-337-2012.

deMenocal, P.B., Ruddiman, W.F., Pokras, E.M., 1993. Influences of high- and low-latitude processes on african terrestrial climate: Pleistocene Eolian records from equatorial Atlantic Ocean drilling Program site 663. Paleoceanography 8, 209–242. https://doi.org/10.1029/93PA02688.

Francke, A., Wagner, B., Just, J., Leicher, N., Gromig, R., Baumgarten, H., Vogel, H., Lacey, J.H., Sadori, L., Wonik, T., Leng, M.J., Zanchetta, G., Sulpizio, R., Giaccio, B., 2016. Sedimentological processes and environmental variability at Lake Ohrid (Macedonia, Albania) between 637 ka and the present. Biogeosciences 13, 1179–1196. https://doi.org/10.5194/bg-13-1179-2016.

Fuchs, M., Kreutzer, S., Rousseau, D.-D., Antoine, P., Hatté, C., Lagroix, F., Moine, O., Gauthier, C., Svoboda, J., Lisá, L., 2013. The loess sequence of Dolní Věstonice, Czech republic: a new OSL-based chronology of the last climatic cycle. Boreas 42, 664–677. https://doi.org/10.1111/j.1502-3885.2012.00299.x.

Grant, K.M., Rohling, E.J., Westerhold, T., Zabel, M., Heslop, D., Konijnendijk, T., Lourens, L., 2017. A 3 million year index for North African humidity/aridity and the implication of potential pan-African Humid periods. Quat. Sci. Rev. 171, 100–118. https://doi.org/10.1016/j.quascirev.2017.07.005.

Hagelberg, T.K., Bond, G., deMenocal, P., 1994. Milankovitch band forcing of sub-Milankovitch climate variability during the Pleistocene. Paleoceanography 9, 545–558. https://doi.org/10.1029/94PA00443.

Hays, J., Imbrie, J., Shackleton, N., 1976. Variations in the earth's orbit: pacemaker of the ice ages. Science 194, 1121–1132. https://doi.org/10.1126/science.194.4270.1121.

Heinrich, H., 1988. Origin and consequences of cyclic ice rafting in the Northeast Atlantic Ocean during the past 130,000 years. Quat. Res. 29, 142–152. https://doi.org/10.1016/0033-5894(88)90057-9.

Hinnov, L.A., 2000. New perspectives on orbitally forced stratigraphy. Annu. Rev. Earth Planet Sci. 28, 419–475. https://doi.org/10.1146/annurev.earth.28.1.419.

Hinnov, L.A., Schulz, M., Yiou, P., 2002. Interhemispheric space–time attributes of the Dansgaard–Oeschger oscillations between 100 and 0ka. Quat. Sci. Rev., Decadal-to-Millennial-Scale Climate Variability 21, 1213–1228. https://doi.org/10.1016/S0277-3791(01)00140-8.

Hodell, D., Crowhurst, S., Skinner, L., Tzedakis, P.C., Margari, V., Channell, J.E.T., Kamenov, G., Maclachlan, S., Rothwell, G., 2013. Response of Iberian Margin sediments to orbital and suborbital forcing over the past 420 ka. Paleoceanography 28, 185–199. https://doi.org/10.1002/palo.20017.

Hodell, D., Lourens, L., Crowhurst, S., Konijnendijk, T., Tjallingii, R., Jiménez-Espejo, F., Skinner, L., Tzedakis, P.C., Abrantes, F., Acton, G.D., Alvarez Zarikian, C.A., Bahr, A., Balestra, B., Barranco, E.L., Carrara, G., Ducassou, E., Flood, R.D., Flores, J.-A., Furota, S., Grimalt, J., Grunert, P., Hernández-Molina, J., Kim, J.K., Krissek, L.A., Kuroda, J., Li, B., Lofi, J., Margari, V., Martrat, B., Miller, M.D., Nanayama, F., Nishida, N., Richter, C., Rodrigues, T., Rodríguez-Tovar, F.J., Roque, A.C.F., Sanchez Goñi, M.F., Sierro Sánchez, F.J., Singh, A.D., Sloss, C.R., Stow, D.A.V., Takashimizu, Y., Tzanova, A., Voelker, A., Xuan, C., Williams, T., 2015. A reference time scale for site U1385 (Shackleton site) on the SW Iberian margin. Global Planet. Change 133, 49–64. https://doi.org/10.1016/j.gloplacha.2015.07.002.

Hooghiemstra, H., 2006. Leitfaden der Pollenbestimmung Fur Mitteleuropa und angrenzende Gebiete. H.-J. Beug. Publisher Verlag Friedrich Pfeil, Munich, 2004 (542 pp. 120 plates, 12 tables) ISBN 3 89937 043 0. J. Quat. Sci. 21, 105. https://doi.org/10.1002/jqs.915.

Kaboth-Bahr, S., Bahr, A., Zeeden, C., Toucanne, S., Eynaud, F., Jiménez-Espejo, F., Röhl, U., Friedrich, O., Pross, J., Löwemark, L., Lourens, L.J., 2018. Monsoonal forcing of European ice-sheet dynamics during the late quaternary. Geophys. Res. Lett. 45, 7066–7074. https://doi.org/10.1029/2018GL078751.

Kodama, K.P., Hinnov, L.A., 2014. Rock Magnetic Cyclostratigraphy. John Wiley & Sons.

Kutzbach, J.E., Chen, G., Cheng, H., Edwards, R.L., Liu, Z., 2014. Potential role of winter rainfall in explaining increased moisture in the Mediterranean and Middle East during periods of maximum orbitally-forced insolation seasonality. Clim. Dynam. 42, 1079–1095. https://doi.org/10.1007/s00382-013-1692-1.

Laepple, T., Lohmann, G., 2009. Seasonal cycle as template for climate variability on astronomical timescales. Paleoceanography 24. https://doi.org/10.1029/2008PA001674.

Lang, N., Wolff, E.W., 2011. Interglacial and glacial variability from the last 800 ka in marine, ice and terrestrial archives. Clim. Past 7, 361–380. https://doi.org/10.5194/cp-7-361-2011.

Larrasoaña, J.C., Roberts, A.P., Rohling, E.J., Winklhofer, M., Wehausen, R., 2003. Three million years of monsoon variability over the northern Sahara. Clim. Dynam. 21, 689–698. https://doi.org/10.1007/s00382-003-0355-z.

Laskar, J., Robutel, P., Joutel, F., Gastineau, M., Correia, A.C.M., Levrard, B., 2004. A long-term numerical solution for the insolation quantities of the Earth. Astron. Astrophys. 428, 261–285. https://doi.org/10.1051/0004-6361:20041335.

Leicher, N., Zanchetta, G., Sulpizio, R., Giaccio, B., Wagner, B., Nomade, S., Francke, A., Del Carlo, P., 2016. First tephrostratigraphic results of the DEEP site record from Lake Ohrid (Macedonia and Albania). Biogeosciences 13, 2151–2178. https://doi.org/10.5194/bg-13-2151-2016.

Li, M., Huang, C., Ogg, J., Zhang, Y., Hinnov, L., Wu, H., Chen, Z.-Q., Zou, Z., 2019. Paleoclimate proxies for cyclostratigraphy: comparative analysis using a Lower Triassic marine section in South China. Earth-Sci. Rev., Sedimentology as a Key to Understanding Earth and Life Processes 189, 125–146. https://doi.org/10.1016/j.earscirev.2019.01.011.

Liebrand, D., de Bakker, A.T.M., 2019. Bispectra of climate cycles show how ice ages are fuelled. Clim. Past 15, 1959–1983. https://doi.org/10.5194/cp-15-1959-2019.
Lionello, P., Abrantes, F., Congedi, L., Dulac, F., Gacic, M., Gomis, D., Goodess, C., Hoff, H., Kutiel, H., Luterbacher, J., Planton, S., Reale, M., Schröder, K., Struglia, M.V., Toreti, A., Tsimplis, M., Ulbrich, U., Xoplaki, E., 2012. Introduction: mediterranean climate—background information. Clim. Mediterr. Reg. https://doi.org/10.1016/B978-0-12-416042-2.00012-4. Past Future xxxv–xc.
Lisiecki, L.E., Raymo, M.E., 2005. A Pliocene-Pleistocene stack of 57 globally distributed benthic δ18O records. Paleoceanography 20. https://doi.org/10.1029/2004PA001071.
Liu, Y., Liang, X.S., Weisberg, R.H., 2007. Rectification of the Bias in the wavelet power spectrum. J. Atmos. Ocean. Technol. 24, 2093–2102. https://doi.org/10.1175/2007JTECHO511.1.
Meyers, S.R., 2019. Cyclostratigraphy and the problem of astrochronologic testing. Earth Sci. Rev. 190, 190–223. https://doi.org/10.1016/j.earscirev.2018.11.015.
Meyers, S., Malinverno, A., Hinnov, L., Zeeden, C., Liu, H., Moron, V., 2021. astrochron: A Computational Tool for Astrochronology.
Milanković, 1920. Théorie Mathématique des Phénomènes Thermiques Produits par la Radiation Solaire. Acad. Yougosl. Sci. Arts Zagreb.
Milanković, M.K., 1941. Kanon der Erdbestrahlung und seine Anwendung auf das Eiszeitenproblem. R. Serbian Acad. Spec. Publ. 133, 1–633.
Mudelsee, M., Schulz, M., 1997. The Mid-Pleistocene climate transition: onset of 100 ka cycle lags ice volume build-up by 280 ka. Earth Planet Sci. Lett. 151, 117–123. https://doi.org/10.1016/S0012-821X(97)00114-3.
North_Greenland_Ice-Core_Project_members, Andersen, K.K., Azuma, N., Barnola, J.-M., Bigler, M., Biscaye, P., Caillon, N., Chappellaz, J., Clausen, H.B., Dahl-Jensen, D., Fischer, H., Flückiger, J., Fritzsche, D., Fujii, Y., Goto-Azuma, K., Grønvold, K., Gundestrup, N.S., Hansson, M., Huber, C., Hvidberg, C.S., Johnsen, S.J., Jonsell, U., Jouzel, J., Kipfstuhl, S., Landais, A., Leuenberger, M., Lorrain, R., Masson-Delmotte, V., Miller, H., Motoyama, H., Narita, H., Popp, T., Rasmussen, S.O., Raynaud, D., Röthlisberger, R., Ruth, U., Samyn, D., Schwander, J., Shoji, H., Siggard-Andersen, M.-L., Steffensen, J.P., Stocker, T., Sveinbjörnsdottir, A.E., Svensson, A., Takata, M., Tison, J.-L., Thorsteinsson, T., Watanabe, O., Wilhelms, F., White, J., 2004. High-resolution record of the Northern Hemisphere climate extending into the last interglacial period. Nature 431, 147–151.
Pisias, N.G., Moore, T.C., 1981. The evolution of Pleistocene climate: a time series approach. Earth Planet Sci. Lett. 52, 450–458. https://doi.org/10.1016/0012-821X(81)90197-7.
Prokopenko, A.A., Hinnov, L.A., Williams, D.F., Kuzmin, M.I., 2006. Orbital forcing of continental climate during the Pleistocene: a complete astronomically tuned climatic record from Lake Baikal, SE Siberia. Quat. Sci. Rev., Critical Quaternary Stratigraphy 25, 3431–3457. https://doi.org/10.1016/j.quascirev.2006.10.002.
R Core Team, 2021. R: The R Project for Statistical Computing.
Railsback, L.B., Gibbard, P.L., Head, M.J., Voarintsoa, N.R.G., Toucanne, S., 2015. An optimized scheme of lettered marine isotope substages for the last 1.0 million years, and the climatostratigraphic nature of isotope stages and substages. Quat. Sci. Rev. 111, 94–106. https://doi.org/10.1016/j.quascirev.2015.01.012.
Rider, M., Kennedy, M., 2011. The Geological Interpretation of Well Logs. Rider-French.
Rodrigues, T., Alonso-García, M., Hodell, D.A., Rufino, M., Naughton, F., Grimalt, J.O., Voelker, A.H.L., Abrantes, F., 2017. A 1-Ma record of sea surface temperature and extreme cooling events in the North Atlantic: a perspective from the Iberian Margin. Quat. Sci. Rev. 172, 118–130. https://doi.org/10.1016/j.quascirev.2017.07.004.
Rohling, E.J., Marino, G., Grant, K.M., 2015. Mediterranean climate and oceanography, and the periodic development of anoxic events (sapropels). Earth Sci. Rev. 143, 62–97. https://doi.org/10.1016/j.earscirev.2015.01.008.
Rossignol-Strick, M., 1985. Mediterranean Quaternary sapropels, an immediate response of the African monsoon to variation of insolation. Palaeogeogr. Palaeoclimatol. Palaeoecol. 49, 237–263. https://doi.org/10.1016/0031-0182(85)90056-2.
Sadori, L., Koutsodendris, A., Panagiotopoulos, K., Masi, A., Bertini, A., Combourieu-Nebout, N., Francke, A., Kouli, K., Joannin, S., Mercuri, A.M., Peyron, O., Torri, P., Wagner, B., Zanchetta, G., Sinopoli, G., Donders, T.H., 2016. Pollen-based paleoenvironmental and paleoclimatic change at Lake Ohrid (south-eastern Europe) during the past 500 ka. Biogeosciences 13, 1423–1437. https://doi.org/10.5194/bg-13-1423-2016.
Sageman, B.B., Hollander, D.J., 1999. Cross correlation of paleoecological and geochemical proxies: a holistic approach to the study of past global change. Spec. Pap. Geol. Soc. Am. 332, 365–384. https://doi.org/10.1130/0-8137-2332-9.365.
Schemmel, F., Niedermeyer, E.M., Schwab, V.F., Gleixner, G., Pross, J., Mulch, A., 2016. Plant wax δD values record changing Eastern Mediterranean atmospheric circulation patterns during the 8.2 kyr B.P. climatic event. Quat. Sci. Rev. 133, 96–107. https://doi.org/10.1016/j.quascirev.2015.12.019.
Scholz, C.A., Johnson, T.C., Cohen, A.S., King, J.W., Peck, J.A., Overpeck, J.T., Talbot, M.R., Brown, E.T., Kalindekafe, L., Amoako, P.Y.O., Lyons, R.P., Shanahan, T.M., Castañeda, I.S., Heil, C.W., Forman, S.L., McHargue, L.R., Beuning, K.R., Gomez, J., Pierson, J., 2007. East African megadroughts between 135 and 75 thousand years ago and bearing on early-modern human origins. Proc. Natl. Acad. Sci. Unit. States Am. 104, 16416–16421.
Shackleton, N.J., Opdyke, N.D., 1976. Oxygen-Isotope and Paleomagnetic Stratigraphy of Pacific Core V28-239 Late Pliocene to Latest Pleistocene. https://doi.org/10.1130/MEM145-p449.
Short, D.A., Mengel, J.G., Crowley, T.J., Hyde, W.T., North, G.R., 1991. Filtering of milankovitch cycles by earth's geography. Quat. Res. 35, 157–173. https://doi.org/10.1016/0033-5894(91)90064-C.
Stocker, T.F., Johnsen, S.J., 2003. A minimum thermodynamic model for the bipolar seesaw. Paleoceanography 18. https://doi.org/10.1029/2003PA000920.
Stockhecke, M., Kwiecien, O., Vigliotti, L., Anselmetti, F.S., Beer, J., Çağatay, M.N., Channell, J.E.T., Kipfer, R., Lachner, J., Litt, T., Pickarski, N., Sturm, M., 2014a. Chronostratigraphy of the 600,000 year old continental record of Lake Van (Turkey). Quat. Sci. Rev. 104, 8–17. https://doi.org/10.1016/j.quascirev.2014.04.008. Special Issue: Results from the PALEOVAN Drilling Project: a 600,000 year long continental archive in the Near East.
Stockhecke, M., Sturm, M., Brunner, I., Schmincke, H.-U., Sumita, M., Kipfer, R., Cukur, D., Kwiecien, O., Anselmetti, F.S., 2014b. Sedimentary evolution and environmental history of Lake Van (Turkey) over the past 600 000 years. Sedimentology 61, 1830–1861. https://doi.org/10.1111/sed.12118.
Sun, J., Huang, X., 2006. Half-precessional cycles recorded in Chinese loess: response to low-latitude insolation forcing during the Last Interglaciation. Quat. Sci. Rev. 25, 1065–1072. https://doi.org/10.1016/j.quascirev.2005.08.004.
Taner, M.T., 1992. Attributes revisited (Technical Report). Rock Solid Images, Inc.
Thomson, J., Nixon, S., Summerhayes, C.P., Schönfeld, J., Zahn, R., Grootes, P., 1999. Implications for sedimentation changes on the Iberian margin over the last two glacial/interglacial transitions from (230Thexcess)0 systematics. Earth Planet Sci. Lett. 165, 255–270. https://doi.org/10.1016/S0012-821X(98)00265-9.
Torrence, C., Compo, G.P., 1998. A practical guide to wavelet analysis. Bull. Am. Meteorol. Soc. 79, 61–78. https://doi.org/10.1175/1520-0477(1998)079<0061:APGTWA>2.0.CO;2.
Trauth, M.H., Deino, A.L., Bergner, A.G.N., Strecker, M.R., 2003. East African climate change and orbital forcing during the last 175 kyr BP. Earth Planet Sci. Lett. 206, 297–313. https://doi.org/10.1016/S0012-821X(02)01105-6.
Trauth, M.H., Larrasoaña, J.C., Mudelsee, M., 2009. Trends, rhythms and events in Plio-Pleistocene African climate. Quat. Sci. Rev. 28, 399–411. https://doi.org/10.1016/j.quascirev.2008.11.003.
Turney, C.S.M., Kershaw, A.P., Clemens, S.C., Branch, N., Moss, P.T., Keith Fifield, L., 2004. Millennial and orbital variations of El Niño/Southern Oscillation and high-latitude climate in the last glacial period. Nature 428, 306–310. https://doi.org/10.1038/nature02386.
Tzedakis, P.C., Hooghiemstra, H., Pälike, H., 2006. The last 1.35 million years at Tenaghi Philippon: revised chronostratigraphy and long-term vegetation trends. Quat. Sci. Rev., Critical Quaternary Stratigraphy 25, 3416–3430. https://doi.org/10.1016/j.quascirev.2006.09.002.
Ulfers, A., Zeeden, C., Wagner, B., Krastel, S., Buness, H., Wonik, T., 2022. Borehole logging and seismic data from Lake Ohrid (North Macedonia/Albania) as a basis for age-depth modelling over the last one million years. Quat. Sci. Rev. 276, 107295. https://doi.org/10.1016/j.quascirev.2021.107295.
Ünal-İmer, E., Shulmeister, J., Zhao, J.-X., Tonguç Uysal, I., Feng, Y.-X., Duc Nguyen, A., Yüce, G., 2015. An 80 kyr-long continuous speleothem record from Dim Cave, SW Turkey with paleoclimatic implications for the Eastern Mediterranean. Sci. Rep. 5, 13560. https://doi.org/10.1038/srep13560.
Verschuren, D., Sinninghe Damsté, J.S., Moernaut, J., Kristen, I., Blaauw, M., Fagot, M., Haug, G.H., 2009. Half-precessional dynamics of monsoon rainfall near the East African Equator. Nature 462, 637–641. https://doi.org/10.1038/nature08520.
Vogel, H., Wagner, B., Zanchetta, G., Sulpizio, R., Rosén, P., 2010. A paleoclimate record with tephrochronological age control for the last glacial-interglacial cycle from Lake Ohrid, Albania and Macedonia. J. Paleolimnol. 44, 295–310. https://doi.org/10.1007/s10933-009-9404-x.
Wagner, B., Vogel, H., Francke, A., Friedrich, T., Donders, T., Lacey, J.H., Leng, M.J., Regattieri, E., Sadori, L., Wilke, T., Zanchetta, G., Albrecht, C., Bertini, A., Combourieu-Nebout, N., Cvetkoska, A., Giaccio, B., Grazhdani, A., Hauffe, T., Holtvoeth, J., Joannin, S., Jovanovska, E., Just, J., Kouli, K., Kousis, I., Koutsodendris, A., Krastel, S., Lagos, M., Leicher, N., Levkov, Z., Lindhorst, K., Masi, A., Melles, M., Mercuri, A.M., Nomade, S., Nowaczyk, N., Panagiotopoulos, K., Peyron, O., Reed, J.M., Sagnotti, L., Sinopoli, G., Stelbrink, B., Sulpizio, R., Timmermann, A., Tofilovska, S., Torri, P., Wagner-Cremer, F., Wonik, T., Zhang, X., 2019. Mediterranean winter rainfall in phase with African monsoons during the past 1.36 million years. Nature 573, 256–260. https://doi.org/10.1038/s41586-019-1529-0.
Wagner, B., Vogel, H., Zanchetta, G., Sulpizio, R., 2010. Environmental change within the Balkan region during the past ca. 50 ka recorded in the sediments from lakes Prespa and Ohrid. Biogeosciences 7, 3187–3198. https://doi.org/10.5194/bg-7-3187-2010.
Wagner, B., Wilke, T., Krastel, S., Zanchetta, G., Sulpizio, R., Reicherter, K., Leng, M.J., Grazhdani, A., Trajanovski, S., Francke, A., Lindhorst, K., Levkov, Z., Cvetkoska, A., Reed, J.M., Zhang, X., Lacey, J.H., Wonik, T., Baumgarten, H., Vogel, H., 2014. The SCOPSCO drilling project recovers more than 1.2 million years of history from Lake Ohrid. Sci. Drill. 17, 19–29. https://doi.org/10.5194/sd-17-19-2014.
Wanner, H., Brönnimann, S., Casty, C., Gyalistras, D., Luterbacher, J., Schmutz, C., Stephenson, D.B., Xoplaki, E., 2001. North Atlantic oscillation – concepts and studies. Surv. Geophys. 22, 321–381. https://doi.org/10.1023/A:1014217317898.
Weedon, G.P., 2003. Time-Series Analysis and Cyclostratigraphy: Examining Stratigraphic Records of Environmental Cycles. Cambridge University Press.
Zeeden, C., Kaboth, S., Hilgen, F.J., Laskar, J., 2018. Taner filter settings and automatic correlation optimisation for cyclostratigraphic studies. Comput. Geosci. 119, 18–28. https://doi.org/10.1016/j.cageo.2018.06.005.

3. Summary and conclusion

As part of two drilling campaigns of the International Continental Scientific Drilling Program (ICDP), several geophysical borehole measurements were carried out by the Leibniz Institute for Applied Geophysics (LIAG) in two lakes. The acquired data was used to answer stratigraphic and paleoclimatic research questions, including the establishment of robust age-depth models and the construction of continuous lithological profiles.

The investigated lakes are Lake Towuti on Sulawesi (Indonesia), which is approximately 1 million years old, and Lake Ohrid on the Balkan Peninsula (North Macedonia/Albania), which dates back to 1.36 million years.

Lake Towuti

In the Towuti Drilling Project (TDP), the age of the lake is still not entirely determined. Only one tephra layer in the lower third of the lacustrine sequence was dated to 797.3 ± 1.6 ka using the $^{40}Ar/^{39}Ar$-method. The publication on Lake Towuti included in this thesis presents the first continuous age-depth model of the lake sediments. Assuming that eccentricity is the main driver of orbitally induced changes in sedimentary composition, we performed cyclostratigraphic analysis on the magnetic susceptibility data from borehole measurements. This method enables the calculation of sedimentation rate (SR), and its variation, such as increased SR during diatom blooms. Our age-depth model is ''anchored'' to the previously mentioned tephra layer, covers 77 % of Lake Towuti's lacustrine facies, and ranges from 903 ± 11 ka (~84 mblf) to 131 ± 67 ka (~19 mblf). In addition, an artificial lithology log of the sediment sequences was constructed from a series of borehole data using cluster analysis. The results are consistent with core descriptions and sections with core loss are described through artificial lithology. This is particularly relevant in the lower section of the borehole, as core loss was highest here.

Thus, not only the questions relevant to this publication were addressed and successfully answered, but also an important contribution to the achievement of the objectives of the TDP was made.

Lake Ohrid

The age determination method used within the SCOPSCO (Scientific Collaboration on Past Speciation Conditions in Lake Ohrid) project is a novelty, since it completely avoids the use of sediment core material. Lake Ohrid is well suited for this purpose, as a comparison of the natural gamma radiation from borehole measurements with the global LR04 benthic stack reference data shows high similarity.

Seismic data provide the basis for linking of the three investigated drilling sites 'DEEP', 'Pestani' and 'Cerava'. Prominent marker horizons in these data were tracked with the goal of transferring age information from DEEP to both other sites. This provided the starting point for further analyses to determine the age of the Pestani and Cerava records. Using correlation to the global LR04 benthic stack reference record and cyclostratigraphic approaches, each independently, we estimated the SR of the individual sites. The different calculation methods for SR at DEEP exhibit similar results. The average SR determined by correlation to the global reference curve is 34.8 cm/ka, while the SR determined by cyclostratigraphy is 35.8 cm/ka. However, the limits of the cyclostratigraphic methods are evident at the other locations and the results for the SRs differ significantly (Pestani), or cannot be calculated (Cerava). The limits are determined by the fact that orbital cycles are not optimally archived at these locations. Nevertheless, age-depth models could be generated using the correlative approach for Pestani and Cerava as well.

The different logging parameters were used to generate complete lithological profiles for all three drill locations using cluster analysis. A comparison of the results is only possible with the published core description of the upper ~250 mblf of DEEP. The similarity of the artificial profile and the lithological description is high at DEEP. Hence, cluster analysis is suited to reflect the lithology. At all sites, the results of the cluster analysis are integrated into the developed age-depth model. With this step, the determination about what kind of material was deposited in which time interval is accomplished. At all three locations, the change between warm and cold climate conditions is evident in the artificial lithological profiles. All of this information was obtained without investigating the core material and provides an important contribution for further research in the SCOPSCO project.

Half-precession signals in Lake Ohrid and in the European realm

Driven by curiosity of the origin of visually-present half-precession (HP) cycles in parts of the Lake Ohrid logging data, the data from Lake Ohrid were compared with other proxy data in and around Europe regarding the presence and intensity of (HP) cycles. As can be concluded from previous studies, sediments from Lake Ohrid offer excellent conditions for cyclostratigraphic investigations. In addition to the borehole data, sediment core data from the SCOPSCO-project was now included. The comparison data from Europe involve widely dissimilar proxies. For instance, marine cores from the Mediterranean Sea and the Iberian Margin off the coast of Portugal, terrestrial sedimentary archives distributed across Europe, and data from the Greenland ice are included in the analyses. It has been considered to include archives with the longest possible time span to obtain a representation of the HP over the last one million years. In all the archives/locations mentioned, HP can be observed, but exhibits varying degrees of clarity. It is particularly pronounced in the south(east)ern records, decreases toward the north, and is almost undetectable in Greenland. The reason for this may be the equatorial origin of the signal. The further away from the low latitudes, the weaker is the signal. However, it is suggested that a variety of atmospheric/ oceanographic processes may transmit the signal to higher latitudes. If confirmed, the HP signal may be seen as an indicator for connectivity between low and high latitude climate systems. In particular, the African Monsoon, the Nile River, and the outflow of the Mediterranean Sea through the Strait of Gibraltar take on important roles in the publication presented in this thesis.

Regarding the temporal evolution of the HP signal, we can state that the intensity increases during the last 1 Ma especially in the younger part (<621 ka). Furthermore, we observe an increase in the signal clarity during interglacial periods. Some proxies show no variability in glacials and thus are unable to record short orbital cycles in some parts. It should be noted that some proxies show a correlation of the HP signal to both the 100 ka and 405 ka cycles of eccentricity. The origin of these features require further investigation.

Consequently, the HP signal is not only observed in (sub-)tropical sedimentary archives, but could be transmitted to higher latitudes through different mechanisms. The essential factor in this context is how interconnected the (paleo-)climate systems were in the past.

Perspectives

The publication about HP is a further step towards a better understanding of this signal. Nevertheless, much effort will be necessary to fully understand the origin and evolution of HP over longer time periods. Even geophysical downhole logging can be used in this case, provided that the ratio of vertical resolution of the individual sensors in the borehole probes to the accumulation rate in the sediment archive is sufficient to record these signals. The spatial relationships of HP can be addressed through the inclusion of additional datasets. Especially (sub)tropical data will play an important role, as several publications suggest that the HP signal is of low latitude origin. Marine sediment archives are yet in the focus of HP investigations. While open marine sedimentary systems usually have a lower accumulation rate compared to lacustrine deposits and HP cycles may not be detectable by downhole logging equipment, studies on marine sediment core can lead to success. Devices such as MSCL and/or XRF loggers can provide the desired resolution. The potential of marine cores is that these often extend beyond the Pleistocene, allowing assessment of HP in the deeper past.

The publications presented here address the reconstruction of paleoclimatic conditions in lake sediments. For this purpose, mainly geophysical downhole measurements and to some extent also seismic data were analyzed. Despite the fact that borehole measurements have been used for industrial purposes since the early 20th century, their use in paleoclimatology, especially for age determination, is relatively young. As these methods evolve, age-depth models will be more precise and available more quickly, possibly immediately after a drilling campaign. Nevertheless, classical methods for age estimations (tephra-, magneto-, bio-stratigraphy) on the sediment core will still be necessary to complement the borehole data (and vice versa).

Geophysical downhole logging will continue to increase in importance with more advanced data analyses. Using a suite of downhole logging data, sediment properties and the variability of these data, sedimentation processes can be explained even when the cores have not been opened yet or are not present at all.

The topics covered in this dissertation cover a wide area, but the focus is on geophysical borehole data and their cyclostratigraphic analysis. The downhole measurement methods were further developed and established in the paleo-geoscientific community. The advantages are

obvious when considering, for example, the short time taken for the results to be available, or the quality/continuity of the recorded data. It was demonstrated that borehole data have the potential to successfully answer a wide range of paleoclimatic questions and for this reason should be closely integrated into future drilling projects.

4. Zusammenfassung und Schlussfolgerung

Im Rahmen zweier Bohrkampagnen des International Continental Scientific Drilling Program (ICDP) wurden in zwei Seen mehrere geophysikalische Bohrlochmessungen vom Leibniz Institut für Angewandte Geophysik (LIAG) durchgeführt. Die gewonnenen Daten wurden benutzt um stratigraphische und paläoklimatische Fragestellungen zu beantworten, unter anderem um robuste Alters-Tiefen-Modelle zu erstellen und kontinuierliche lithologische Profile der Sedimente zu konstruieren.

Bei den Seen handelt es sich um den etwa 1 Millionen Jahre alten Lake Towuti auf Sulawesi (Indonesien) und den 1.36 Millionen Jahre alten Lake Ohrid auf der Balkanhalbinsel (Nordmazedonien/Albanien).

Lake Towuti

Im Towuti Drilling Projekt (TDP) ist das Alter des Sees bis heute nicht vollständig geklärt. Lediglich eine Tephra-Lage im unteren Drittel der lakustrinen Sequenz wurde mit der $^{40}Ar/^{39}Ar$-Methode auf 797.3 ± 1.6 ka datiert. Die in dieser Arbeit eingebundene Publikation zu Lake Towuti enthält das erste kontinuierliche Alters-Tiefen-Modell der Seesedimente. Unter der Annahme, dass die Exzentrizität hauptsächlich für orbital induzierte Veränderungen der Sedimentzusammensetzung verantwortlich ist, haben wir die magnetische Suszeptibilität aus den Bohrlochmessungen zyklostratigraphisch analysiert. Diese Methode ermöglicht die Berechnung der Sedimentationsrate (SR), und Veränderungen, wie z.B. eine erhöhte SR während Wachstumsphasen von Diatomeen. Unser Alters-Tiefen-Modell wurde an die oben erwähnte Tephra-Lage ‚eingehängt', deckt 77 % der lakustrinen Fazies von Lake Towuti ab und erstreckt sich von 903 ± 11 ka (~84 mblf) bis 131 ± 67 ka (~19 mblf). Zusätzlich wurde aus einer Reihe von Bohrlochdaten mittels Clusteranalyse ein künstliches lithologisches Profil der Sedimentsequenzen konstruiert. Die Ergebnisse stimmen mit den Kernbeschreibungen überein und Abschnitte mit Kernverlusten werden durch die künstliche Lithologie beschrieben. Dies ist besonders im unteren Bereich der Bohrung von Bedeutung, da hier die größten Kernverluste auftraten.

Es wurden somit nicht nur die für die Publikation relevanten Fragenstellungen bearbeitet und erfolgreich beantwortet, sondern auch ein wichtiger Beitrag für die Erreichung der Ziele des TDP geliefert.

Lake Ohrid

Die im Rahmen des SCOPSCO Projekts (Scientific Collaboration on Past Speciation Conditions in Lake Ohrid) angewandte Methode zur Bestimmung des Alters ist ein Novum, da hierfür komplett auf die Verwendung von Kernmaterial verzichtet wurde. Lake Ohrid ist hierfür sehr gut geeignet, da ein Vergleich der im Bohrloch gemessenen, natürlichen Gamma-Strahlung mit der globalen $\delta^{18}O$-Referenzkurve große Ähnlichkeit zeigt.

Seismische Daten liefern die Grundlage für die Verbindung der drei untersuchten Bohrlokationen ‚DEEP', ‚Pestani' und ‚Cerava'. Markante Horizonte in diesen Daten wurden mit dem Ziel verfolgt, Altersinformation von DEEP zu den beiden anderen Lokationen zu transferieren. Damit war die Basis für weitere Analysen zur Altersbestimmung an Pestani und Cerava gelegt. Mittels Korrelation zur globalen ‚LR04 benthic stack' Referenz und zyklostratigraphischer Methoden wurden jeweils unabhängig voneinander die SR der einzelnen Sites bestimmt. Die unterschiedlichen Wege zur Berechnung der SR bei DEEP zeigen ähnliche Ergebnisse. So beträgt die durchschnittlich bestimmte SR durch die Korrelation zur globalen Referenzkurve 34.8 cm/ka, die zyklostratigraphisch bestimmte ist 35.8 cm/ka. Jedoch zeigen sich an den anderen Lokationen die Grenzen der zyklo-stratigraphischen Methoden und die Ergebnisse für die SR weichen voneinander ab (Pestani), bzw. sind nicht berechenbar (Cerava). Die Grenzen werden dadurch bestimmt, dass orbitale Zyklen an diesen Lokationen nicht optimal archiviert sind. Nichtsdestotrotz konnten mittels der korrelativen Methode auch für Pestani und Cerava Alters-Tiefen-Modelle erstellt werden.

Aus den verschiedenen Bohrlochparametern wurde für alle drei Bohrlokationen mittels Clusteranalyse ein komplettes lithologisches Profil erstellt. Ein Abgleich der Ergebnisse ist nur mit der veröffentlichten Kernbeschreibung der oberen ~250 mblf von DEEP möglich. Hier ist die Ähnlichkeit des künstlichen Profils und der lithologischen Beschreibung sehr hoch. Die Clusteranalyse ist somit geeignet die Lithologie wiederzugeben. An allen Lokationen werden die Ergebnisse der Clusteranalyse in das entwickelte Alters-Tiefen-Modell integriert. Durch diesen

Schritt kann eine Aussage getroffen werden, welche Art von Material zu welchem Zeitpunkt abgelagert wurde. An allen drei Lokationen ist der Wechsel zwischen Warm- und Kaltzeiten in den künstlichen lithologischen Profilen erkennbar. Alle diese Erkenntnisse wurde ohne Sichtung des Kernmaterials erlangt und liefern einen wichtigen Beitrag für weitere Arbeiten im SCOPSCO-Projekt.

Halb-Präzessionssignale im Ohridsee und im europäischen Raum

Ausgehend von der Frage nach dem Ursprung der visuell sichtbaren Halb-Präzessions(HP)-Zyklen in Teilen der Daten aus dem Ohridsee wurden diese mit anderen Proxydaten in und um Europa hinsichtlich des Vorhandenseins und der Intensität von HP verglichen. Wie aus den vorherigen Studien ersichtlich, bieten die Sedimente im Lake Ohrid hervorragende Bedingungen für zyklostratigraphische Untersuchungen. Ergänzend zu den Bohrlochdaten wurden nun auch Kerndaten aus dem SCOPSCO-Projekt hinzugezogen. Bei den europäischen Vergleichsdaten handelt es sich um sehr unterschiedliche Proxies: Es sind beispielsweise marine Kerne aus dem Mittelmeer und dem ‚Iberian Margin' vor der Küste Portugals, über Europa verteilte terrestrische Sedimentarchive bis hin zu Daten aus dem Grönland-Eis in die Analysen eingebunden. Es wurde darauf geachtet zeitlich möglichst lange Archive zu benutzen, um ein Bild der HP über die letzten eine Millionen Jahre zu bekommen. In allen genannten Archiven/Lokationen ist HP zu beobachten, weist jedoch unterschiedliche Deutlichkeit auf. Es ist besonders deutlich in den süd(öst)lichen Daten ausgeprägt, nimmt Richtung Norden ab und ist in Grönland quasi nicht mehr nachweisbar. Der Grund hierfür könnte im äquatorialen Ursprung des Signals liegen. Je weiter von den niedrigen Breiten entfernt, desto schwächer ist das Signal. Es wird jedoch vorgeschlagen, dass unterschiedliche atmosphärische/ozeanographische Prozesse das Signal in höhere Breiten transportieren können. Wenn sich dies bestätigt, könnte das HP-Signal als Indikator für die Konnektivität zwischen den Klimasystemen der niedrigen und der hohen Breiten gesehen werden. Besonders der afrikanische Monsun, der Nil und der Ausfluss des Mittelmeers durch die Straße von Gibraltar nehmen in der hier präsentierten Publikation eine wichtige Rolle ein.

Über die zeitliche Entwicklung des HP-Signals können wir sagen, dass die Intensität während der letzten 1 Ma vor allem im jüngeren Teil (<621 ka) zunimmt. Außerdem beobachten wir eine

Zunahme des Signals in interglazialen Perioden. Einige Proxies zeigen keine Variabilität in Glazialen und sind daher nicht in der Lage, kurze orbitale Zyklen in bestimmten Abschnitten aufzuzeichnen. Außerdem ist festzuhalten, dass einige Proxies einen Zusammenhang des HP-Signals sowohl zum 100 ka als auch zum 405 ka Zyklus der Exzentrizität aufweisen. Der Ursprung dieser Merkmale bedarf weiterer Untersuchungen.

Das HP-Signal ist also nicht nur in (sub-)tropischen Sedimentarchiven zu beobachten, sondern könnte durch verschiedene Mechanismen in höhere Breiten transportiert werden. Dabei ist entscheidend wie stark die (Paläo-)Klimasysteme miteinander verbunden sind.

Perspektiven

Mit der Publikation zur HP wurde ein weiterer Schritt zum besseren Verständnis dieses Signals gemacht. Dennoch wird weiterhin viel Forschung nötig sein, um die Hintergründe der Entstehung und der Evolution der HP über längere Zeiträume vollständig zu verstehen. Auch hierbei können Bohrlochmessungen zum Einsatz kommen, vorausgesetzt, dass das Verhältnis aus vertikaler Auflösung der einzelnen Sensoren in den Bohrlochsonden zur Akkumulationsrate im Sedimentkörper ausreichend ist, um diese Signale aufzuzeichnen. Die räumlichen Zusammenhänge der HP können mit der Hinzunahme weiterer Datensätze beantwortet werden. Hierbei werden v.a. (sub)tropische Daten eine Rolle spielen, da in einigen Publikationen angenommen wird, dass es sich beim HP-Signal um ein Signal handelt, welches in niedrigen Breiten entsteht. Marine Sedimentarchive rücken derzeit in den Fokus der Untersuchungen zu HP. Zwar haben marine Sedimentsysteme im Vergleich zu lakustrinen Ablagerungen meist eine niedrigere Akkumulationsrate und HP-Zyklen sind möglicherweise nicht durch Bohrlochmessgeräte nachweisbar, jedoch können Untersuchungen an marinen Sedimentkernen trotzdem erfolgreich sein. Hierbei können Geräte wie MSCL und/oder XRF-Logger die gewünschte Auflösung liefern. Das Potenzial mariner Kerne besteht darin, dass diese oft über das Pleistozän hinausreichen und somit eine Beurteilung der HP in der tieferen Vergangenheit erlauben.

Die hier vorgestellten Publikationen befassen sich mit der Rekonstruktion paläoklimatischer Bedingungen in Seesedimenten. Dafür wurden hauptsächlich geophysikalische Bohrlochmessungen und z. T. auch seismische Daten verwendet. Auch wenn Bohrlochmessungen

schon seit dem frühen 20. Jhd. für industrielle Zwecke genutzt werden, ist deren Verwendung in der Paläoklimatologie, im speziellen für die Altersbestimmung, relativ neu. Mit der Weiterentwicklung dieser Methoden werden die Alters-Tiefen-Modelle zukünftig präziser und zügiger, möglicherweise direkt im Anschluss an eine Bohrkampagne, vorhanden sein. Trotzdem werden klassische Methoden zur Altersbestimmung (Tephra-, Magneto-, Biostratigraphie) am Sedimentkern weiterhin nötig sein um die Bohrlochdaten zu komplementieren (und umgekehrt). Geophysikalische Bohrlochmessungen werden mit fortschrittlicheren Datenanalysen weiter an Bedeutung zunehmen. Mit Hilfe einer Reihe von Bohrlochmessdaten, Sedimenteigenschaften und der Variabilität dieser Daten können Sedimentationsprozesse erklärt werden, auch wenn die Bohrkerne noch nicht geöffnet wurden oder nicht vorhanden sind.

Die in dieser Dissertation behandelten Themen umfassen ein weites Gebiet, jedoch liegt der Fokus auf geophysikalischen Bohrlochdaten und deren zyklostratigraphischer Analyse. Die Methodik der Bohrlochmessungen wurde in der paläogeowissenschaftlichen Community weiter ausgebaut und gefestigt. Die Vorteile liegen auf der Hand, wenn man z.B. die Schnelligkeit, mit der die Ergebnisse vorliegen, berücksichtigt, oder die Qualität/Kontinuität der aufgezeichneten Daten. Es hat sich gezeigt, dass Bohrlochdaten das Potential haben, einen Großteil von paläoklimatischen Fragestellungen erfolgreich zu beantworten und aus diesem Grund in zukünftigen Bohrprojekten eng eingebunden werden sollten.

5. Data policy

The data basis for the '2.1 Peer-reviewed publication (Lake Towuti)' and '2.2 Peer-reviewed publication (Lake Ohrid)' is attached electronically to this thesis**.** Most of the data used in '2.3 Peer-reviewed publication (Half-precession in Lake Ohrid and Europe)' is publically available or was provided on request from corresponding authors.

6. Author contributions to publications

All authors mentioned in this chapter have poof read the respective manuscript and gave advice for improvements. Finally, all authors agreed to the submission of the respective manuscript.

Title: Cyclostratigraphy and paleoenvironmental inference from downhole logging of sediments in tropical Lake Towuti, Indonesia

Name	Contribution
Ulfers, Arne	Interpretation of the geological/geophysical datasets, performing all analyses (cluster analysis/cyclostratigraphy) and writing the major part of the manuscript.
Hesse, Katja	Pre-processing geophysical downhole logging data. Advisor in technical aspects of geophysical borehole measurements.
Dr. Zeeden, Christian	Scientific support and discussion, especially for cyclostratigraphic investigations.
Prof. Dr. Russell, James M.	Scientific support and discussion, especially for regional geology, sedimentology and the paleoenvironmental context.
Dr. Vogel, Hendrik	Scientific support and discussion, especially on sedimentation processes and interpretation of the pre-lacustrine facies.
Prof. Dr. Bijaksana, Satria	Scientific support and discussion, especially in aspects of regional geology and Indonesian hydroclimate.
Dr. Wonik, Thomas	Scientific support and discussion, especially in downhole logging data acquisition and interpretation.

Title: Borehole logging and seismic data from Lake Ohrid (North Macedonia/Albania) as a basis for age-depth modelling over the last one million years

Name	Contribution
Ulfers, Arne	Interpretation of the geological/geophysical datasets, performing all analyses (cluster analysis/cyclostratigraphy) and writing the major part of the manuscript.
Dr. Zeeden, Christian	Scientific support and discussion, especially for cyclostratigraphic investigations.
Prof. Dr. Wagner, Bernd	Scientific support and discussion, especially for regional geology and sedimentology in Lake Ohrid.
Prof. Dr. Krastel, Sebastian	Provision and pre-processing of seismic data. Discussion and support interpreting seismic survey.
Dr. Buness, Hermann	Time-depth conversion of seismic data. Support for chapter 2.2 Data processing.
Dr. Wonik, Thomas	Scientific support and discussion, especially in downhole logging data acquisition and interpretation.

Title: Half-precession signals in Lake Ohrid (Balkan) and their spatio-temporal relations to climate records from the European realm

Name	Contribution
Ulfers, Arne	Interpretation of the geological/geophysical datasets, performing all analyses (time series analysis) and writing major parts of the manuscript.
Dr. Zeeden, Christian	Scientific support during study design. Discussion, especially for time series analysis. Writing/editing the manuscript.
Prof. Dr. Voigt, Silke	Scientific support and discussion, especially for spatial context of the half-precession signal. Writing/editing the manuscript.
Dr. Sardar Abadi, Mehrdad	Scientific support and discussion. Writing/editing the manuscript.
Dr. Wonik, Thomas	Scientific support and discussion, especially in downhole logging data acquisition and interpretation.

7. References

(References of publications are listed therein)

Aldrian, E., Dwi Susanto, R., 2003. Identification of three dominant rainfall regions within Indonesia and their relationship to sea surface temperature. International Journal of Climatology 23, 1435–1452. https://doi.org/10.1002/joc.950

An, Z., 2000. The history and variability of the East Asian paleomonsoon climate. Quaternary Science Reviews 19, 171–187. https://doi.org/10.1016/S0277-3791(99)00060-8

Anderson, D.M., 2001. Attenuation of millennial-scale events by bioturbation in marine sediments. Paleoceanography 16, 352–357. https://doi.org/10.1029/2000PA000530

Baumgarten, H., Wonik, T., 2015. Cyclostratigraphic studies of sediments from Lake Van (Turkey) based on their uranium contents obtained from downhole logging and paleoclimatic implications. Int J Earth Sci (Geol Rundsch) 104, 1639–1654. https://doi.org/10.1007/s00531-014-1082-x

Baumgarten, H., Wonik, T., Tanner, D.C., Francke, A., Wagner, B., Zanchetta, G., Sulpizio, R., Giaccio, B., Nomade, S., 2015. Age–depth model of the past 630 kyr for Lake Ohrid (FYROM/Albania) based on cyclostratigraphic analysis of downhole gamma ray data. Biogeosciences 12, 7453–7465. https://doi.org/10.5194/bg-12-7453-2015

Berger, A., 1988. Milankovitch Theory and climate. Reviews of Geophysics 26, 624–657. https://doi.org/10.1029/RG026i004p00624

Berger, A., Loutre, M.F., Laskar, J., 1992. Stability of the Astronomical Frequencies Over the Earth's History for Paleoclimate Studies. Science. https://doi.org/10.1126/science.255.5044.560

Berger, A., Loutre, M.F., McIntyre, A., 1997. Intertropical Latitudes and Precessional and Half-Precessional Cycles. Science 278, 1476–1478.

Berger, A., Loutre, M.F., Mélice, J.L., 2006. Equatorial insolation: from precession harmonics to eccentricity frequencies. Climate of the Past 2, 131–136. https://doi.org/10.5194/cp-2-131-2006

Brewer, T.S., Harvey, P.K., Lovell, M.A., Haggas, S., Williamson, G., Pezard, P., 1998. Ocean floor volcanism: constraints from the integration of core and downhole logging measurements. Geological Society, London, Special Publications 136, 341–362. https://doi.org/10.1144/GSL.SP.1998.136.01.28

Buecker, C., Jarrard, R.D., Wonik, T., Brink, J., 2000. Analysis of downhole logging data from CRP-2/2A, Victoria Land Basin, Antarctica: a multivariate statistical approach. Terra Antartica 7, 299–310.

Burchfiel, B.C., Nakov, R., Dumurdzanov, N., Papanikolaou, D., Tzankov, T., Serafimovski, T., King, R.W., Kotzev, V., Todosov, A., Nurce, B., 2008. Evolution and dynamics of the Cenozoic tectonics of the South Balkan extensional system. Geosphere 4, 919–938. https://doi.org/10.1130/GES00169.1

Cohen, A.S., 2012. Scientific drilling and biological evolution in ancient lakes: lessons learned and recommendations for the future. Hydrobiologia 682, 3–25. https://doi.org/10.1007/s10750-010-0546-7

Costa, K.M., Russell, J.M., Vogel, H., Bijaksana, S., 2015. Hydrological connectivity and mixing of Lake Towuti, Indonesia in response to paleoclimatic changes over the last 60,000years.

Palaeogeography, Palaeoclimatology, Palaeoecology 417, 467–475. https://doi.org/10.1016/j.palaeo.2014.10.009

De Deckker, P., 2016. The Indo-Pacific Warm Pool: critical to world oceanography and world climate. Geoscience Letters 3, 20. https://doi.org/10.1186/s40562-016-0054-3

De Vleeschouwer, D., Da Silva, A.C., Boulvain, F., Crucifix, M., Claeys, P., 2012. Precessional and half-precessional climate forcing of Mid-Devonian monsoon-like dynamics. Climate of the Past 8, 337–351. https://doi.org/10.5194/cp-8-337-2012

Ellis, D.V., Singer, J.M., 2007. An Overview of Well Logging, in: Ellis, D.V., Singer, J.M. (Eds.), Well Logging for Earth Scientists. Springer Netherlands, Dordrecht, pp. 1–15. https://doi.org/10.1007/978-1-4020-4602-5_1

Erickson, S.N., Jarrard, R.D., 1998. Velocity-porosity relationships for water-saturated siliciclastic sediments. Journal of Geophysical Research: Solid Earth 103, 30385–30406. https://doi.org/10.1029/98JB02128

Francke, A., Wagner, B., Just, J., Leicher, N., Gromig, R., Baumgarten, H., Vogel, H., Lacey, J.H., Sadori, L., Wonik, T., Leng, M.J., Zanchetta, G., Sulpizio, R., Giaccio, B., 2016. Sedimentological processes and environmental variability at Lake Ohrid (Macedonia, Albania) between 637 ka and the present. Biogeosciences 13, 1179–1196. https://doi.org/10.5194/bg-13-1179-2016

Friese, A., Bauer, K., Glombitza, C., Ordoñez, L., Ariztegui, D., Heuer, V.B., Vuillemin, A., Henny, C., Nomosatryo, S., Simister, R., Wagner, D., Bijaksana, S., Vogel, H., Melles, M., Russell, J.M., Crowe, S.A., Kallmeyer, J., 2021. Organic matter mineralization in modern and ancient ferruginous sediments. Nat Commun 12, 2216. https://doi.org/10.1038/s41467-021-22453-0

Friese, A., Kallmeyer, J., Axel Kitte, J., Montaño Martínez, I., Bijaksana, S., Wagner, D., the ICDP Lake Chalco Drilling Science Team and the ICDP Towuti Drilling Science Team, 2017. A simple and inexpensive technique for assessing contamination during drilling operations. Limnology and Oceanography: Methods 15, 200–211. https://doi.org/10.1002/lom3.10159

Goudge, T.A., Russell, J.M., Mustard, J.F., Head, J.W., Bijaksana, S., 2017. A 40,000 yr record of clay mineralogy at Lake Towuti, Indonesia: Paleoclimate reconstruction from reflectance spectroscopy and perspectives on paleolakes on Mars. GSA Bulletin 129, 806–819. https://doi.org/10.1130/B31569.1

Haffner, G.D., Hehanussa, P.E., Hartoto, D., 2001. The biology and physical processes of large lakes of Indonesia: Lakes Matano and Towuti. The Great Lakes of the World. Food-web, Health and Integrity. Backhuys Publishers, Leiden 183192.

Hall, R., Wilson, M.E.J., 2000. Neogene sutures in eastern Indonesia. Journal of Asian Earth Sciences 18, 781–808. https://doi.org/10.1016/S1367-9120(00)00040-7

Hamilton, W.B., 1979. Tectonics of the Indonesian Region. U.S. Government Printing Office.

Hasberg, A.K.M., Bijaksana, S., Held, P., Just, J., Melles, M., Morlock, M.A., Opitz, S., Russell, J.M., Vogel, H., Wennrich, V., 2019. Modern sedimentation processes in Lake Towuti, Indonesia, revealed by the composition of surface sediments. Sedimentology 66, 675–698. https://doi.org/10.1111/sed.12503

Hendon, H.H., 2003. Indonesian Rainfall Variability: Impacts of ENSO and Local Air–Sea Interaction. Journal of Climate 16, 1775–1790. https://doi.org/10.1175/1520-0442(2003)016<1775:IRVIOE>2.0.CO;2

Herbert, T.D., de Boer, P.L., Smith, D.G., 1994. Reading orbital signals distorted by sedimentation: models and examples. Orbital forcing and cyclic sequences 19, 483–507.

Hilgen, F.J., Krijgsman, W., Langereis, C.G., Lourens, L.J., Santarelli, A., Zachariasse, W.J., 1995. Extending the astronomical (polarity) time scale into the Miocene. Earth and Planetary Science Letters 136, 495–510. https://doi.org/10.1016/0012-821X(95)00207-S

Hinnov, L.A., 2018. Chapter One - Cyclostratigraphy and Astrochronology in 2018, in: Montenari, M. (Ed.), Stratigraphy & Timescales, Cyclostratigraphy and Astrochronology. Academic Press, pp. 1–80. https://doi.org/10.1016/bs.sats.2018.08.004

Hinnov, L.A., Schulz, M., Yiou, P., 2002. Interhemispheric space–time attributes of the Dansgaard–Oeschger oscillations between 100 and 0ka. Quaternary Science Reviews, Decadal-to-Millennial-Scale Climate Variability 21, 1213–1228. https://doi.org/10.1016/S0277-3791(01)00140-8

Hoffmann, N., Reicherter, K., Fernández-Steeger, T., Grützner, C., 2010. Evolution of ancient Lake Ohrid: a tectonic perspective. Biogeosciences 7, 3377–3386. https://doi.org/10.5194/bg-7-3377-2010

Imbrie, J., Berger, A., Shackleton, N.J., 1993. Role of orbital forcing: a two-million-year perspective, in: Dahlem Workshop on Global Changes in the Perspective of the Past. pp. 263–277.

Imbrie, J., Imbrie, K.P., 1979. Ice Ages: Solving the Mystery. Harvard University Press, Cambridge, Massachusetts.

Jozja, N., Neziraj, A., 1998. Geological heritage conservation of the Ohrid Lake. GEOLOGICA BALCANICA 28, 91–96.

Kadarusman, A., Miyashita, S., Maruyama, S., Parkinson, C.D., Ishikawa, A., 2004. Petrology, geochemistry and paleogeographic reconstruction of the East Sulawesi Ophiolite, Indonesia. Tectonophysics, Continental Margins of the Pacific Rim 392, 55–83. https://doi.org/10.1016/j.tecto.2004.04.008

Koeberl, C., Milkereit, B., Overpeck, J.T., Scholz, C.A., Amoako, P.Y.O., Boamah, D., Danuor, S., Karp, T., Kueck, J., Hecky, R.E., King, J.W., Peck, J.A., 2007. An international and multidisciplinary drilling project into a young complex impact structure: The 2004 ICDP Bosumtwi Crater Drilling Project—An overview. Meteoritics & Planetary Science 42, 483–511. https://doi.org/10.1111/j.1945-5100.2007.tb01057.x

Laskar, J., Joutel, F., Boudin, F., 1993. Orbital, precessional, and insolation quantities for the Earth from-20 Myr to+ 10 Myr. Astronomy and Astrophysics 270, 522–533.

Laskar, J., Robutel, P., Joutel, F., Gastineau, M., Correia, A.C.M., Levrard, B., 2004. A long-term numerical solution for the insolation quantities of the Earth. A&A 428, 261–285. https://doi.org/10.1051/0004-6361:20041335

Lehmusluoto, P., Machbub, B., Terangna, N., Rusmiputro, S., Achmad, F., Boer, L., Brahmana, S.S., Priadi, B., Setiadji, B., Sayuman, O., 1995. National inventory of the major lakes and reservoirs in Indonesia. Expedition Indodanau Technical Report, Edita Oy.

Leicher, N., Giaccio, B., Zanchetta, G., Wagner, B., Francke, A., Palladino, D.M., Sulpizio, R., Albert, P.G., Tomlinson, E.L., 2019. Central Mediterranean explosive volcanism and tephrochronology during the last 630 ka based on the sediment record from Lake Ohrid. Quaternary Science Reviews 226, 106021. https://doi.org/10.1016/j.quascirev.2019.106021

Lindhorst, K., Gruen, M., Krastel, S., Schwenk, T., 2012. Hydroacoustic Analysis of Mass Wasting Deposits in Lake Ohrid (FYR Macedonia/Albania), in: Yamada, Y., Kawamura, K., Ikehara, K., Ogawa, Y., Urgeles, R., Mosher, D., Chaytor, J., Strasser, M. (Eds.), Submarine Mass Movements and Their Consequences, Advances in Natural and Technological Hazards Research. Springer Netherlands, Dordrecht, pp. 245–253. https://doi.org/10.1007/978-94-007-2162-3_22

Lindhorst, K., Krastel, S., Reicherter, K., Stipp, M., Wagner, B., Schwenk, T., 2015. Sedimentary and tectonic evolution of Lake Ohrid (Macedonia/Albania). Basin Research 27, 84–101. https://doi.org/10.1111/bre.12063

Lisiecki, L.E., Raymo, M.E., 2005. A Pliocene-Pleistocene stack of 57 globally distributed benthic δ18O records. Paleoceanography 20. https://doi.org/10.1029/2004PA001071

Lovell, M.A., Harvey, P.K., Jackson, P.D., Brewer, T.S., Williamson, G., Williams, C.G., 1998. Interpretation of core and log data—integration or calibration? Geological Society, London, Special Publications 136, 39–51.

Matzinger, A., Spirkovski, Z., Patceva, S., Wüest, A., 2006. Sensitivity of Ancient Lake Ohrid to Local Anthropogenic Impacts and Global Warming. jglr 32, 158–179. https://doi.org/10.3394/0380-1330(2006)32[158:SOALOT]2.0.CO;2

Melles, M., Brigham-Grette, J., Minyuk, P.S., Nowaczyk, N.R., Wennrich, V., DeConto, R.M., Anderson, P.M., Andreev, A.A., Coletti, A., Cook, T.L., Haltia-Hovi, E., Kukkonen, M., Lozhkin, A.V., Rosén, P., Tarasov, P., Vogel, H., Wagner, B., 2012. 2.8 Million Years of Arctic Climate Change from Lake El'gygytgyn, NE Russia. Science 337, 315–320. https://doi.org/10.1126/science.1222135

Meyers, S., 2017. Cracking the palaeoclimate code. Nature 546, 219–220. https://doi.org/10.1038/nature22501

Meyers, S.R., Sageman, B.B., Hinnov, L.A., 2001. Integrated Quantitative Stratigraphy of the Cenomanian-Turonian Bridge Creek Limestone Member Using Evolutive Harmonic Analysis and Stratigraphic Modeling. Journal of Sedimentary Research 71, 628–644. https://doi.org/10.1306/012401710628

Milanković, M.K., 1941. Kanon der Erdbestrahlung und seine Anwendung auf das Eiszeitenproblem. Royal Serbian Academy Special Publication 133, 1–633.

Monnier, C., Girardeau, J., Maury, R.C., Cotten, J., 1995. Back-arc basin origin for the East Sulawesi ophiolite (eastern Indonesia). Geology 23, 851–854.

Morlock, M.A., Vogel, H., Nigg, V., Ordoñez, L., Hasberg, A.K.M., Melles, M., Russell, J.M., Bijaksana, S., the TDP Science Team, 2019. Climatic and tectonic controls on source-to-sink processes in the tropical, ultramafic catchment of Lake Towuti, Indonesia. J Paleolimnol 61, 279–295. https://doi.org/10.1007/s10933-018-0059-3

O'Sullivan, P., Reynolds, C.S., 2004. The Lakes Handbook, Volume 1: Limnology and Limnetic Ecology. John Wiley & Sons.

Popovska, C., Bonacci, O., 2007. Basic data on the hydrology of Lakes Ohrid and Prespa. Hydrological Processes 21, 658–664. https://doi.org/10.1002/hyp.6252

Prokopenko, A.A., Hinnov, L.A., Williams, D.F., Kuzmin, M.I., 2006. Orbital forcing of continental climate during the Pleistocene: a complete astronomically tuned climatic record from Lake Baikal, SE Siberia. Quaternary Science Reviews, Critical Quaternary Stratigraphy 25, 3431–3457. https://doi.org/10.1016/j.quascirev.2006.10.002

Quirein, J.A., Gardner, J.S., Watson, J.T., 1982. Combined natural gamma ray spectral/litho-density measurements applied to complex lithologies, in: SPE Annual Technical Conference and Exhibition. OnePetro.

Reicherter, K., Hoffmann, N., Lindhorst, K., Krastel, S., Fernandez-Steeger, T., Grützner, C., Wiatr, T., 2011. Active basins and neotectonics: Morphotectonics of the Lake Ohrid Basin (FYROM and Albania). Zeitschrift der Deutschen Gesellschaft für Geowissenschaften 162, 217–234. https://doi.org/10.1127/1860-1804/2011/0162-0217

Rider, M., Kennedy, M., 2011. The Geological Interpretation of Well Logs. Rider-French.

Russell, J., Bijaksana, S., 2012. The Towuti Drilling Project: Paleoenvironments, Biological Evolution, and Geomicrobiology of a Tropical Pacific Lake. Sci. Dril. 14, 68–71. https://doi.org/10.5194/sd-14-68-2012

Russell, J.M., Bijaksana, S., Vogel, H., Melles, M., Kallmeyer, J., Ariztegui, D., Crowe, S., Fajar, S., Hafidz, A., Haffner, D., Hasberg, A., Ivory, S., Kelly, C., King, J., Kirana, K., Morlock, M., Noren, A., O'Grady, R., Ordonez, L., Stevenson, J., von Rintelen, T., Vuillemin, A., Watkinson, I., Wattrus, N., Wicaksono, S., Wonik, T., Bauer, K., Deino, A., Friese, A., Henny, C., Imran, Marwoto, R., Ngkoimani, L.O., Nomosatryo, S., Safiuddin, L.O., Simister, R., Tamuntuan, G., 2016. The Towuti Drilling Project: paleoenvironments, biological evolution, and geomicrobiology of a tropical Pacific lake. Scientific Drilling 21, 29–40. https://doi.org/10.5194/sd-21-29-2016

Russell, J.M., Vogel, H., Bijaksana, S., Melles, M., Deino, A., Hafidz, A., Haffner, D., Hasberg, A.K.M., Morlock, M., von Rintelen, T., Sheppard, R., Stelbrink, B., Stevenson, J., 2020. The late quaternary tectonic, biogeochemical, and environmental evolution of ferruginous Lake Towuti, Indonesia. Palaeogeography, Palaeoclimatology, Palaeoecology 556, 109905. https://doi.org/10.1016/j.palaeo.2020.109905

Russell, J.M., Vogel, H., Konecky, B.L., Bijaksana, S., Huang, Y., Melles, M., Wattrus, N., Costa, K., King, J.W., 2014. Glacial forcing of central Indonesian hydroclimate since 60,000 y B.P. Proceedings of the National Academy of Sciences 111, 5100–5105. https://doi.org/10.1073/pnas.1402373111

Sheppard, R.Y., Milliken, R.E., Russell, J.M., Dyar, M.D., Sklute, E.C., Vogel, H., Melles, M., Bijaksana, S., Morlock, M.A., Hasberg, A.K.M., 2019. Characterization of Iron in Lake Towuti sediment. Chemical Geology 512, 11–30. https://doi.org/10.1016/j.chemgeo.2019.02.029

Short, D.A., Mengel, J.G., Crowley, T.J., Hyde, W.T., North, G.R., 1991. Filtering of Milankovitch cycles by earth's geography. Quaternary Research 35, 157–173. https://doi.org/10.1016/0033-5894(91)90064-C

Stage, M., 1999. Signal analysis of cyclicity in Maastrichtian pelagic chalks from the Danish North Sea. Earth and Planetary Science Letters 173, 75–90. https://doi.org/10.1016/S0012-821X(99)00213-7

Stein, R., 1990. Organic carbon content/sedimentation rate relationship and its paleoenvironmental significance for marine sediments. Geo-Marine Letters 10, 37–44. https://doi.org/10.1007/BF02431020

Stelbrink, B., Stöger, I., Hadiaty, R.K., Schliewen, U.K., Herder, F., 2014. Age estimates for an adaptive lake fish radiation, its mitochondrial introgression, and an unexpected sister

group: Sailfin silversides of the Malili Lakes system in Sulawesi. BMC Evol Biol 14, 94. https://doi.org/10.1186/1471-2148-14-94

Ulfers, A., Hesse, K., Zeeden, C., Russell, J.M., Vogel, H., Bijaksana, S., Wonik, T., 2021. Cyclostratigraphy and paleoenvironmental inference from downhole logging of sediments in tropical Lake Towuti, Indonesia. J Paleolimnol 65, 377–392. https://doi.org/10.1007/s10933-020-00171-9

Ulfers, A., Zeeden, C., Wagner, B., Krastel, S., Buness, H., Wonik, T., 2022. Borehole logging and seismic data from Lake Ohrid (North Macedonia/Albania) as a basis for age-depth modelling over the last one million years. Quaternary Science Reviews 276, 107295. https://doi.org/10.1016/j.quascirev.2021.107295

Vogel, H., Russell, J.M., Cahyarini, S.Y., Bijaksana, S., Wattrus, N., Rethemeyer, J., Melles, M., 2015. Depositional modes and lake-level variability at Lake Towuti, Indonesia, during the past ~29 kyr BP. J Paleolimnol 54, 359–377. https://doi.org/10.1007/s10933-015-9857-z

Vogel, H., Wessels, M., Albrecht, C., Stich, H.-B., Wagner, B., 2010. Spatial variability of recent sedimentation in Lake Ohrid (Albania/Macedonia). Biogeosciences 7, 3333–3342. https://doi.org/10.5194/bg-7-3333-2010

Vuillemin, A., Friese, A., Alawi, M., Henny, C., Nomosatryo, S., Wagner, D., Crowe, S.A., Kallmeyer, J., 2016. Geomicrobiological Features of Ferruginous Sediments from Lake Towuti, Indonesia. Frontiers in Microbiology 7.

Wagner, B., Lotter, A.F., Nowaczyk, N., Reed, J.M., Schwalb, A., Sulpizio, R., Valsecchi, V., Wessels, M., Zanchetta, G., 2009. A 40,000-year record of environmental change from ancient Lake Ohrid (Albania and Macedonia). J Paleolimnol 41, 407–430. https://doi.org/10.1007/s10933-008-9234-2

Wagner, B., Reicherter, K., Daut, G., Wessels, M., Matzinger, A., Schwalb, A., Spirkovski, Z., Sanxhaku, M., 2008. The potential of Lake Ohrid for long-term palaeoenvironmental reconstructions. Palaeogeography, Palaeoclimatology, Palaeoecology, Lake systems: sedimentary archives of climate change and tectonics 259, 341–356. https://doi.org/10.1016/j.palaeo.2007.10.015

Wagner, B., Vogel, H., Francke, A., Friedrich, T., Donders, T., Lacey, J.H., Leng, M.J., Regattieri, E., Sadori, L., Wilke, T., Zanchetta, G., Albrecht, C., Bertini, A., Combourieu-Nebout, N., Cvetkoska, A., Giaccio, B., Grazhdani, A., Hauffe, T., Holtvoeth, J., Joannin, S., Jovanovska, E., Just, J., Kouli, K., Kousis, I., Koutsodendris, A., Krastel, S., Lagos, M., Leicher, N., Levkov, Z., Lindhorst, K., Masi, A., Melles, M., Mercuri, A.M., Nomade, S., Nowaczyk, N., Panagiotopoulos, K., Peyron, O., Reed, J.M., Sagnotti, L., Sinopoli, G., Stelbrink, B., Sulpizio, R., Timmermann, A., Tofilovska, S., Torri, P., Wagner-Cremer, F., Wonik, T., Zhang, X., 2019. Mediterranean winter rainfall in phase with African monsoons during the past 1.36 million years. Nature 573, 256–260. https://doi.org/10.1038/s41586-019-1529-0

Wagner, B., Vogel, H., Zanchetta, G., Sulpizio, R., 2010. Environmental change within the Balkan region during the past ca. 50 ka recorded in the sediments from lakes Prespa and Ohrid. Biogeosciences 7, 3187–3198. https://doi.org/10.5194/bg-7-3187-2010

Wagner, B., Wilke, T., Francke, A., Albrecht, C., Baumgarten, H., Bertini, A., Combourieu-Nebout, N., Cvetkoska, A., D'Addabbo, M., Donders, T.H., Föller, K., Giaccio, B., Grazhdani, A., Hauffe, T., Holtvoeth, J., Joannin, S., Jovanovska, E., Just, J., Kouli, K.,

Koutsodendris, A., Krastel, S., Lacey, J.H., Leicher, N., Leng, M.J., Levkov, Z., Lindhorst, K., Masi, A., Mercuri, A.M., Nomade, S., Nowaczyk, N., Panagiotopoulos, K., Peyron, O., Reed, J.M., Regattieri, E., Sadori, L., Sagnotti, L., Stelbrink, B., Sulpizio, R., Tofilovska, S., Torri, P., Vogel, H., Wagner, T., Wagner-Cremer, F., Wolff, G.A., Wonik, T., Zanchetta, G., Zhang, X.S., 2017. The environmental and evolutionary history of Lake Ohrid (FYROM/Albania): interim results from the SCOPSCO deep drilling project. Biogeosciences 14, 2033–2054. https://doi.org/10.5194/bg-14-2033-2017

Wagner, B., Wilke, T., Krastel, S., Zanchetta, G., Sulpizio, R., Reicherter, K., Leng, M.J., Grazhdani, A., Trajanovski, S., Francke, A., Lindhorst, K., Levkov, Z., Cvetkoska, A., Reed, J.M., Zhang, X., Lacey, J.H., Wonik, T., Baumgarten, H., Vogel, H., 2014. The SCOPSCO drilling project recovers more than 1.2 million years of history from Lake Ohrid. Scientific Drilling 17, 19–29. https://doi.org/10.5194/sd-17-19-2014

Watzin, M.C., Puka, V., Naumoski, T.B., 2002. Lake Ohrid and its watershed: state of the environment report. Hydrobiological Institute.

Weedon, G.P., 2003. Time-Series Analysis and Cyclostratigraphy: Examining Stratigraphic Records of Environmental Cycles. Cambridge University Press.

Wicaksono, S.A., Russell, J.M., Bijaksana, S., 2015. Compound-specific carbon isotope records of vegetation and hydrologic change in central Sulawesi, Indonesia, since 53,000 yr BP. Palaeogeography, Palaeoclimatology, Palaeoecology 430, 47–56. https://doi.org/10.1016/j.palaeo.2015.04.016

Wilke, T., Hauffe, T., Jovanovska, E., Cvetkoska, A., Donders, T., Ekschmitt, K., Francke, A., Lacey, J.H., Levkov, Z., Marshall, C.R., Neubauer, T.A., Silvestro, D., Stelbrink, B., Vogel, H., Albrecht, C., Holtvoeth, J., Krastel, S., Leicher, N., Leng, M.J., Lindhorst, K., Masi, A., Ognjanova-Rumenova, N., Panagiotopoulos, K., Reed, J.M., Sadori, L., Tofilovska, S., Van Bocxlaer, B., Wagner-Cremer, F., Wesselingh, F.P., Wolters, V., Zanchetta, G., Zhang, X., Wagner, B., 2020. Deep drilling reveals massive shifts in evolutionary dynamics after formation of ancient ecosystem. Science Advances 6. https://doi.org/10.1126/sciadv.abb2943

Wilke, T., Wagner, B., Van Bocxlaer, B., Albrecht, C., Ariztegui, D., Delicado, D., Francke, A., Harzhauser, M., Hauffe, T., Holtvoeth, J., Just, J., Leng, M.J., Levkov, Z., Penkman, K., Sadori, L., Skinner, A., Stelbrink, B., Vogel, H., Wesselingh, F., Wonik, T., 2016. Scientific drilling projects in ancient lakes: Integrating geological and biological histories. Global and Planetary Change 143, 118–151. https://doi.org/10.1016/j.gloplacha.2016.05.005

Wonik, T., Olea, R.A., 2007. Borehole Logging, in: Knödel, K., Lange, G., Voigt, H.-J. (Eds.), Environmental Geology: Handbook of Field Methods and Case Studies. Springer, Berlin, Heidelberg, pp. 431–474. https://doi.org/10.1007/978-3-540-74671-3_13

Yan, X.-H., Ho, C.-R., Zheng, Q., Klemas, V., 1992. Temperature and Size Variabilities of the Western Pacific Warm Pool. Science.

Zolitschka, B., Anselmetti, F., Ariztegui, D., Corbella, H., Francus, P., Ohlendorf, C., Schäbitz, F., the PASADO Scientific Drilling Team, 2009. The Laguna Potrok Aike Scientific Drilling Project PASADO (ICDP Expedition 5022). Sci. Dril. 8, 29–34. https://doi.org/10.5194/sd-8-29-2009

E R K L Ä R U N G

Ich erkläre hiermit, dass ich mich bisher keiner Doktorprüfung im Mathematisch-Naturwissenschaftlichen Bereich unterzogen habe.

Frankfurt am Main, den ….....

Unterschrift

Versicherung

Ich erkläre hiermit, dass ich die vorgelegte Dissertation über

Cyclostratigraphic and lithological characteristics of lacustrine sediments obtained from geophysical downhole measurements and seismic data – Lake Ohrid (North Macedonia/Albania) and Lake Towuti (Indonesia)

selbständig angefertigt und mich anderer Hilfsmittel als der in ihr angegebenen nicht bedient habe, insbesondere, dass alle Entlehnungen aus anderen Schriften mit Angabe der betreffenden Schrift gekennzeichnet sind.

Ich versichere, die Grundsätze der guten wissenschaftlichen Praxis beachtet, und nicht die Hilfe einer kommerziellen Promotionsvermittlung in Anspruch genommen zu haben.

Frankfurt am Main, den .....

(Unterschrift)